

The Pennsylvania State University  
The Graduate School  
Intercollege Graduate Program in Neuroscience

**RBM8A IS REQUIRED FOR NORMAL CORTICAL DEVELOPMENT**

A Dissertation in  
Neuroscience  
by  
Colleen McSweeney

© 2017 Colleen McSweeney

Submitted in Partial Fulfillment  
of the Requirements  
for the Degree of

Doctor of Philosophy

December 2017

The dissertation of Colleen McSweeney was reviewed and approved\* by the following:

Yingwei Mao  
Associate Professor of Biology  
Dissertation Advisor  
Chair of Committee

David Vandenberg  
Professor of Biobehavioral Health

Bernhard Lüscher  
Professor of Biology, Biochemistry, and Molecular Biology

Gong Chen  
Professor of Biology  
Verne M. Willaman Chair in Life Sciences

Kevin Alloway  
Professor of Neural and Behavioral Sciences  
Program Chair

\*Signatures are on file in the Graduate School

## ABSTRACT

The formation of the nervous system requires a balance between proliferation, differentiation and migration of neural progenitors, resulting in a neural network that mediates both behaviors and autonomic functions. Here, we identified an exon junction complex protein, RBM8a, as a positive regulator of embryonic neural progenitor cell proliferation and differentiation. We determined that RBM8a knockdown (using *in utero* electroporation) leads to increased migration of neural progenitor cells (NPCs) to the cortical plate (CP), depletion of the NPC pool, and a decrease in the number of cells in the DNA synthesis phase of the cell cycle. Conversely, RBM8a overexpression leads to decreased migration of NPCs to the CP, expansion of the progenitor pool, and increased proliferation. In order to further explore the role of RBM8a in neurogenesis, we developed a conditional knockout mouse. We selectively knocked out RBM8a in neural stem cells, and the resulting mice exhibited microcephaly, early postnatal lethality, and altered distribution of neurons in the neocortex. We then assessed the novel role of RBM8a in the development of GABAergic interneurons in the cortex. We discovered that in addition to the profound phenotypes observed in mice with reduced expression of RBM8a in excitatory neurons previously described in (Mao et al., 2015), *Nes-cre;RBM8a<sup>fl/+</sup>* mice show a significant decrease in the density of parvalbumin (PV)<sup>+</sup> and neuropeptide Y (NPY)<sup>+</sup> interneurons in the cortex, and PV<sup>+</sup>, NPY<sup>+</sup> and somatostatin (SST)<sup>+</sup> cells are abnormally distributed throughout the cortical layers. To determine the mechanism underlying this phenotype, we injected EdU into pregnant dams when the pups are E17 to label and quantitate the number of proliferating cells in the medial ganglionic eminence, where interneuron progenitors reside. We found a significant decrease in the number of cells in the S phase of the cell cycle. However, we did not observe any change in the number or distribution of Edu<sup>+</sup>/Nkx2.1<sup>+</sup> progenitors (which become cortical interneurons). This indicates that the changes

in interneuron number and distribution seen in adolescent mice (P17) are likely due to defects in proliferation migration of Nkx2.1<sup>+</sup> progenitors from the GE to the cortex, or changes in cell fate. We then utilized Nkx2.1-cre mice to determine if the interneuron deficits were due to intrinsic changes in the progenitors, or due to cues received from other altered cell types. We determined that knockout of RBM8a in interneuron progenitors alone led to some changes in their distribution, but this effect was significantly less profound as when compared to the deletion of RBM8a from all neural stem cells (NSCs). Therefore, we concluded that the phenotype is likely caused by some changes in intrinsic properties of Nkx2.1<sup>+</sup> interneuron progenitors, but conceivably could also be due to changes in extrinsic cues from excitatory neurons and other cell types.

To determine if pyramidal cells of the cortex have normal electrophysiological properties, we conducted spontaneous postsynaptic currents from putative pyramidal cells in the somatosensory cortex of Nes-cre;RBM8a<sup>fl/+</sup> mice and RBM8a<sup>fl/+</sup> controls. Pyramidal cells of knockout mice show a significant decrease in the spontaneous inhibitory postsynaptic current (sIPSC) frequency, but no changes in sIPSC amplitude, or spontaneous excitatory postsynaptic current (sEPSC) frequency or amplitude. This suggests that there are functional deficits in the presynaptic, but not postsynaptic neurons. Deficits could include reduced activity of presynaptic interneurons, reduced number of synapses, or a lower vesicle release probability. Given our findings that these mice have fewer PV<sup>+</sup> and NPY<sup>+</sup> cells, we posit that cortical interneurons are releasing normal amounts of GABA, indicating that the change in frequency results from the decrease in interneuron number. However, more experiments need to be completed to clarify this point, including but not limited to evaluating miniature IPSCs (mIPSCs) and mEPSCs.

Analyses of the transcriptome of mice with decreased RBM8a expression, and SH-SY5Y cells with RBM8a overexpressed indicated that RBM8a modulates many developmental

pathways, such as the extracellular matrix (ECM) pathway, growth factor signaling and Notch signaling. Additionally, our findings indicate that RBM8a is a moderate regulator of alternative splicing, and regulates transcripts with characteristics predisposing them to degradation via NMD (intron in the 3' UTR, long 3' UTR etc.). We further assessed the mechanisms behind the observed phenotypes by quantitative western blotting of synaptic and developmental pathway proteins to determine if any were differentially expressed in RBM8a mutants vs. controls. We identified decreased expression of the GluA1 subunit of AMPA receptors and  $\beta 3$  subunit of GABA<sub>A</sub> receptors in P17 whole brain lysate, and interestingly a 50% reduction in Notch1 NICD (Notch1 intracellular domain) expression. These results could explain the deficits observed in the knockout mice, however further research is needed to conclusively support this statement. Taken together, these data indicate a critical role for RBM8a in interneuron development, and establish that perturbation of this gene leads to profound developmental defects of the cerebral cortex.

## TABLE OF CONTENTS

List of Figures .....	ix
List of Tables .....	xi
List of Abbreviations.....	xii
Acknowledgements.....	xiv
Chapter 1 Background .....	1
1.1 Cortical Development .....	1
1.1.1 Cell Cycle Regulation .....	3
1.1.2 Determination of stemness .....	4
1.1.3 Neurogenesis .....	6
1.1.4 Interneuron Development.....	7
1.1.5 Disruptions in neurogenesis .....	9
1.2 RNA Stability and Neurodevelopment .....	11
1.3 RNA Surveillance Mechanisms .....	12
1.4 Clinical Phenotypes Caused by RBM8a .....	14
1.5 EJC Proteins and Neurodevelopment.....	15
Chapter 2 Materials and Methods .....	17
2.1 Materials.....	17
2.1.1 Antibodies used in this study.....	17
2.2 Methods.....	20
2.2.1 Mice.....	20
2.2.2 Immunohistochemistry .....	21
2.2.3 Organ Measurements.....	22
2.2.4 Western Blot.....	23
2.2.5 Cell Culture .....	23
2.2.6 In utero electroporation .....	24
2.2.7 RNAseq.....	24
2.2.8 DNA construct, Transfection and Lentivirus production .....	27
2.2.9 Slice Electrophysiology.....	28
2.2.10 Mouse Behavior .....	28
Chapter 3 RBM8a is a positive regulator of embryonic NPC proliferation.....	30
3.1 Introduction.....	30
3.2 RBM8a is highly expressed during embryonic development .....	30
3.3 RBM8a regulates the distribution of cells in the cortex.....	32
3.4 RBM8a is a positive regulatory of embryonic neural proliferation .....	35
3.5 RBM8a regulates cell cycle exit and neural progenitor differentiation .....	38
3.6 Conclusion .....	41
Chapter 4 RBM8a haploinsufficiency leads to microcephaly and early postnatal lethality ....	42

4.1 Introduction.....	42
4.2 Generation and Verification of knockout mouse .....	42
4.3 RBM8a haploinsufficiency causes microcephaly .....	44
4.4 Organ deficits in the cKO mice are specific to the nervous system.....	45
4.5 RBM8a haploinsufficiency causes disorganized cortical layers .....	47
4.6 Conclusion .....	48
 Chapter 5 RBM8a is required for normal cortical interneuron development .....	 50
5.1 Introduction.....	50
5.2 RBM8a cKO altered number and distribution of PV+ interneurons in the cortex.....	50
5.3 RBM8a cKO modulated the distribution of SST + interneuron in the cortex.....	52
5.4 The effect of RBM8a cKO on NPY+ interneurons.....	55
5.5 RBM8a haploinsufficiency does not change the number or distribution of Nkx2.1+ progenitors in the GE .....	57
5.6 RBM8a Haploinsufficiency modulates GABAergic input onto pyramidal cells .....	60
5.7 RBM8a haploinsufficiency in Nkx2.1+ progenitors leads to a muted distribution phenotype and no change in cell number .....	61
5.8 RBM8a haploinsufficiency modulates GABAergic and glutamatergic receptor expression and Notch1 signaling.....	64
5.9 RBM8a haploinsufficiency modulates the Notch Pathway.....	64
5.10 Conclusion .....	68
 Chapter 6 RBM8a modulates neurodevelopmental pathways and partially regulates alternative splicing and targets of NMD .....	 69
6.1 Introduction.....	69
6.2 RBM8a regulates genes involved in neurological and psychiatric disease.....	69
6.3 RBM8a regulates genes involved in developmental functions and signaling pathways.....	73
6.4 RBM8a is a moderate regulator of alternative splicing.....	76
6.5 RBM8a haploinsufficiency modulates primarily protein coding transcripts .....	78
6.6 RBM8a haploinsufficiency in vivo mediates developmental functions.....	82
6.7 Transcriptome of RBM8a cKO mice during embryonic development .....	85
6.8 Cortical RNAs regulated by RBM8a at E12 mediate degradation pathways.....	88
6.9 Conclusion .....	90
 Chapter 7 RBM8a modulates anxiety and other neuropsychiatric behaviors .....	 91
7.1 Introduction.....	91
7.2 RBM8a expression does not affect locomotion .....	91
7.3 RBM8a mediates anxiety behaviors.....	93
7.4 RBM8a knockdown but not overexpression affects learning and memory .....	93
7.5 RBM8a knockdown does not affect anti-depressive behaviors .....	94
7.6 RFP expression in the dentate gyrus indicates successful injection of the virus .....	95
7.7 Conclusion .....	96
 Chapter 8 Discussion .....	 97

8.1 RBM8a is a positive regulator of neural progenitor cell proliferation .....	97
8.2 Using RNAseq to identify RBM8a's role in developmental functions, NMD regulation and alternative splicing .....	99
8.3 RBM8a haploinsufficiency leads to microcephaly and altered distribution and number of cortical interneurons .....	102
8.4 In utero mechanisms behind the abnormal interneuron distribution and number .....	103
8.5 Molecular mechanisms regulating interneuron development .....	105
Appendix Differentially expressed RNAs that are potential NMD targets.....	110
References.....	116

## LIST OF FIGURES

Figure 1-1: Schematic illustrating asymmetric and symmetric division during neurogenesis.....	2
Figure 1-2: Schematic illustrating the orientation of mitotic spindles.....	5
Figure 1-3: Illustration of interneuron subtypes and where they originate from .....	8
Figure 1-4: Schematic illustrating how RBM8a regulates the balance between self-renewal and differentiation during asymmetric division.....	10
Figure 1-5: Schematic illustrating how the cell uses the EJC to identify mRNAs with PTCs.....	13
Figure 3-1. RBM8a expression in the embryonic brain.....	32
Figure 3-2. RBM8a controls the balance between proliferation and differentiation .....	34
Figure 3-3. RBM8a knockdown results in decreased proliferation .....	36
Figure 3-4: RBM8a overexpression leads to increased proliferation.....	37
Figure 3-5 RBM8a regulates cell cycle exit.....	39
Figure 3-6: RBM8a overexpression leads to decreased cell cycle exit.....	40
Figure 4-1: RBM8a is successfully knocked out in cells expressing cre .....	43
Figure 4-2: RBM8a haploinsufficiency modulates brain size.....	44
Figure 4-3: RBM8a haploinsufficiency leads to microcephaly and profound cortical deficits.....	46
Figure 4-4: RBM8a haploinsufficiency leads to microcephaly and profound cortical deficits.....	48
Figure 5-1: RBM8a regulates the number, distribution and size of PV+ interneurons.....	52
Figure 5-3: RBM8a regulates the number, distribution and size of NPY+.....	56
58	
Figure 5-4: RBM8a haploinsufficiency decreases the proliferation of cells in the ganglionic eminence (GE).....	58
Figure 5-5: RBM8a haploinsufficiency does not affect the number or distribution of Nkx2.1 progenitors.....	59

Figure 5-6: Putative Pyramidal Cells in the somatosensory cortex have decreased GABA amplitude.....	61
Figure 5-8: RBM8a cKO mice have altered expression of GABRB3 and GlurR1 receptors, but not GAD67 .....	66
67	
Figure 5-9: RBM8a mediates Notch1 NICD expression .....	67
Figure 6-1. RBM8a regulates protein coding genes that are risk genes for neurological and neuropsychiatric disease.....	71
Figure 6-2: RBM8a overexpression regulates transcripts involved in developmental pathways.....	74
Figure 6-3: RBM8a regulates RNAs targeted by NMD and is a moderate regulator of alternative splicing .....	77
Figure 6-4: RBM8a modulates developmental functions at P17 .....	80
Figure 6-5: RBM8a modulates mostly protein coding transcripts and is a moderate regulator of alternative splicing at P17 .....	81
Figure 6-6: Transcripts mediated by RBM8a at P17 regulate developmental pathways .....	84
87	
Figure 6-7: RBM8a modulates different functions in different brain areas at E12, but consistently regulates cell proliferation .....	87
Figure 6-8: Cortical RNAs mediated by RBM8a at E12 regulate a variety of pathways involved in immune response, addiction and cell death.....	89
Figure 7-1: Expression pattern of RBM8a in the adult mouse. Taken from the Allen Brain Atlas Expression Database.....	92
Figure 7-2: RBM8a expression does not affect locomotion .....	92
Figure 7-3: RBM8a modulates anxiety behaviors .....	93
Figure 7-4: RBM8a knockdown affects learning and memory.....	94
Figure 7-5: RBM8a knockdown does not affect the anti-depressive phenotype .....	95

**LIST OF TABLES**

Table 2-1: Primary antibodies used in this study .....	17
Table 2-2: Primer sequences used for genotyping .....	18
Table 2-3: Buffers and Reagents used in this study .....	19
Table 6-2: Functional Clusters of RBM8a downstream genes (genes can be in multiple categories) .....	75
Table 6-3: RBM8a mediated alternative splicing genes significantly overlap with ASD risk genes.....	77
Table 6-4: RBM8a mediated potential NMD targets significantly overlap with risk genes for neurological and psychiatric disease .....	78
Table 6-5: Alternative splicing protein coding RNAs list .....	82

## LIST OF ABBREVIATIONS

5HT3aR	Serotonin Receptor 3A
A3SS	Alternative 3' Splice Site
A5SS	Alternative 5' Splice Site
AD	Alzheimer's Disease
AS	Alternative Splicing
ASD	Autism Spectrum Disorder
Atxn1	Ataxin 1
BP	Basal Progenitor
BrdU	5'-Bromo-2'-Deoxyuridine
CC3	Cleaved Caspase 3
CDK5	Cyclin Dependent Kinase 5
CGE	Caudal Ganglionic Eminence
cKO	Conditional Knockout Mouse
CNV	Copy Number Variation
CP	Cortical Plate
CR	Calretinin
CUX1	Homeobox Protein Cut-Like 1
DCX	Doublecortin
ECM	Extracellular Matrix
EdU	5-Ethynyl-2-Deoxyuridine
EJC	Exon Junction Complex
EPSP	Excitatory Post Synaptic Potential
FoxP2	Forkhead Box Protein P2
GFAP	Glial Fibrillary Acidic Protein
GFP	Green Fluorescent Protein
ID	Intellectual Disability
INP	Intermediate Neural Progenitor
IZ	Intermediate Zone
Kif1 $\alpha$	Kinesin Family Member 1a
MGE	Medial Ganglionic Eminence
MTOC	Microtubule Organizing Complex
MXE	Mutually Exclusive Exons
NeuN	RNA binding protein, fox-1 homolog ( <i>C. Elegans</i> ) 3, Rbfox3
NICD	Notch Intracellular Domain
Nkx2.1	Nk2 Homeobox 1
NMD	Nonsense Mediated mRNA Decay
NPC	Neural Progenitor Cell
NPY	Neuropeptide Y
OE	Overexpression
ORF	Open Reading Frame
PCR	Polymerase Chain Reaction
PH3	Phospho-Histone H3
PTC	Pre-termination Codon
PV	Parvalbumin
RBM8a	RNA Binding Motif 8a
RFP	Red Fluorescent Protein

RG	Radial Glia
RGP	Radial Glial Progenitor
RI	Retained Intron
SCZ	Schizophrenia
SE	Skipped Exon
SOX2	Sex Determining Region Y-Box 2
SST	Somatostatin
SVZ	Subventricular Zone
TAR	Thrombocytopenia with Absent Radius
TLE4	Transducin Like Enhancer of Split 4
Tuj1	Neuron Specific Class 3 $\beta$ -tubulin
VEGFR3	Vascular Endothelial Growth Factor Receptor 3
VIP	Vasoactive Intestinal Polypeptide
VZ	Ventricular Zone
WT	Wild Type

## ACKNOWLEDGEMENTS

The path to a PhD can be quite difficult and stressful, and I would like to acknowledge those who have been instrumental to my graduate journey. First, I would like to thank my thesis advisor, Dr. Yingwei Mao. Dr. Mao is an excellent scientist, and has taught me so much about experimental design, analysis, interpretation and presentation. These skills will be vital to my future as a scientist, and I thank him for all he has taught me. I would also like to thank my thesis committee, Dr. Bernhard Lüscher, Dr. David Vandenberg and Dr. Gong Chen, and my fellowship mentor Dr. Troy Ott. They have guided me and taught me so much during my graduate career, and I am immensely thankful for their guidance and expertise. I also would like to thank my lab mates Yijing Zou and Fengping Dong. Yijing and Fengping have taught me so much on their expertise, and answered so many questions I had about new techniques. Not only that, but they are a joy to be around, and made my graduate journey a great experience. They are excellent scientists, and excellent people. I am thankful to have them as colleagues, and as friends. I would also like to thank Dr. Donghua Zou, Dr. Long Liu, Dr. Dazhi Deng, Dr. Chongdong Jian, and Dr. Xiaolei Shi for their all their assistance in the lab and on my project, and for sharing their stories and Chinese culture with me.

Additionally, I would like to thank all my friends who have supported me during this time. I would like to especially thank my CMIND colleagues for their feedback on my project, and advice and support they have always generously given. In particular, I want to thank my friends Sarah Jefferson, Chrissy Hamilton, Mengyung Feng, Lucilla Pizzo, Dr. Nicole Crowley, Jennifer Legault, Derek Nye and Aditya Pisupati for their wonderful friendship during graduate school. You have always supported me, and never cease to make me laugh and have a good time. Great friends make academic success possible, and I would not have made it without you guys!

I want to thank my family. My parents have always advocated for me, and worked tirelessly to support me academically, mentally and emotionally. Without all their help during my childhood, I would not have had the solid academic foundation I did. They taught me so much on how to study, achieve your dreams and most importantly how to be a good person. They are amazing people, and I am blessed to be their daughter.

I would also like to thank my sister Laurie. She has had many medical struggles throughout her life, and has persisted to achieve her dreams. She is a wonderful and inspiring special education teacher, and her perseverance has always motivated me. Her struggles with Tourette Syndrome inspired me to go into Neuroscience, and I am in awe of her work with children with special needs. I will always try to help solve the molecular causes of psychiatric disease, but people like her are the true miracle workers, who support those living with autism and intellectual disability, and guides them to success.

Finally, I want to thank my boyfriend Josh. He has tirelessly supported me these past years, and always knows how to make me laugh and ease my fears. The last few years of graduate school have been difficult, and he has been my rock. I am so thankful to have met him.

And last but not least, I want to thank my cat Penny for her endless supply of cuddles when I am tired and stressed!

## Chapter 1

### Background

#### 1.1 Cortical Development

The development of the nervous system requires a balance between the proliferation and maintenance of a pool of neural progenitors (NPCs), and the differentiation/migration of NPCs to the cortical and subcortical regions of the brain. The successful development of the rodent brain specifically, requires that the appropriate number of cells remain in the stem cell state, while a designated number of cells differentiate and migrate at a specific time in development. Cortical development begins with the generation of radial glial cells around embryonic day 9/10 (E9/10). Prior to this step, neuroepithelial cells (NECs) occupy the neural plate and neural tube. These cells undergo symmetric division, generating two NECs, during a phase known as pre-neurogenesis (McConnell, 1995; Rakic, 2007). At the onset of neurogenesis, these NECs transition into radial glia (RG). These radial glial cells undergo asymmetric division, in which after division, one cell maintains its stemness (RG), while the other cell, termed basal progenitor (BP), begins to differentiate and migrate. When the BP reaches the intermediate zone (IZ), it then undergoes symmetric division, where it generates two identical daughter cells (Gray et al., 1988; Grove and Fukuchi-Shimogori, 2003; Haubensak et al., 2004; Kornack and Rakic, 1995; Luskin et al., 1988; Mione et al., 1997; Miyata et al., 2001, 2004; Noctor et al., 2008; Price and Thurlow, 1988; Reid et al., 1997). This mechanism of symmetric division (pre-neurogenesis) followed by asymmetric division, then repeated symmetric division, ensures that the stem cell pool (that will give rise to the entirety of the nervous system) is maintained, while the remaining cells set down the foundation for the brain. In the cortex, the region of the brain where NPCs reside is the ventricular zone (VZ) and sub-ventricular zone (SVZ). As cells begin to differentiate, they

migrate on the radial glia to their final resting place, in an inside out manner (in vertebrates). That is the deeper layers of the cortex will be formed before the more superficial layers. The whole process of proliferation, differentiation and migration of neural progenitor cells is known as neurogenesis (Figure 1-1). When this process is perturbed, as in the case with RBM8a haploinsufficiency, it results in changes in cell number and distribution, which manifests in phenotypes such as microcephaly and macrocephaly, which in turn results in changes in behavior and physiology.

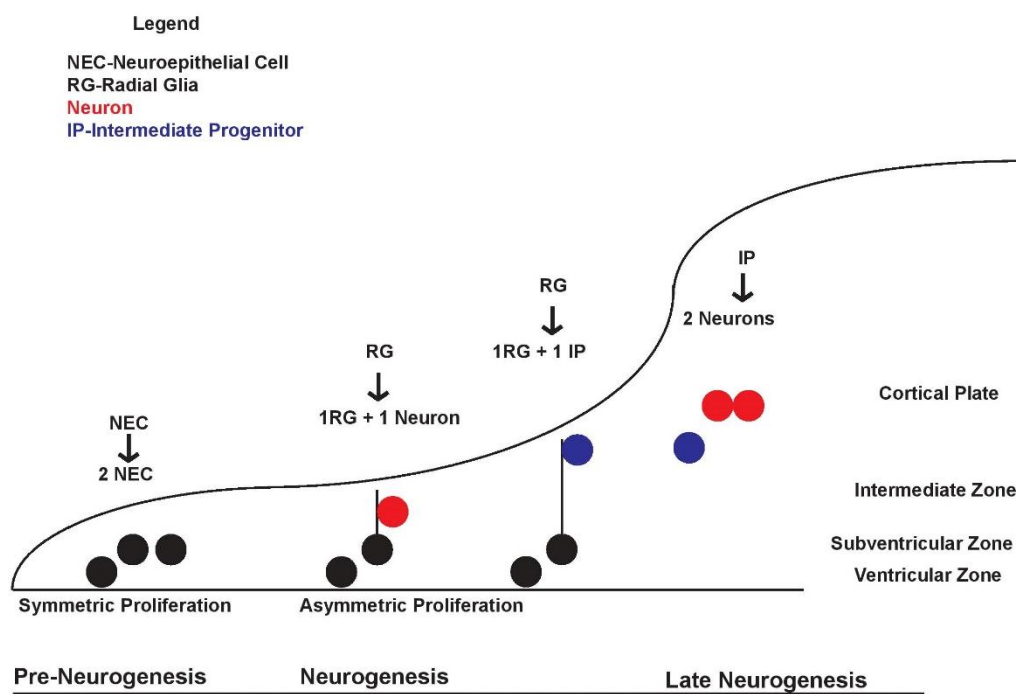


**Figure 1-1: Schematic illustrating asymmetric and symmetric division during neurogenesis.**

Modified from (Paridaen and Huttner, 2014). During pre-neurogenesis NECs divide symmetrically to create two identical daughter NECs. At the onset of neurogenesis, RG undergo asymmetric division to create two different daughter cells, typically 1 RG and 1 neuron. As neurogenesis continues, the RG divide in the IZ and create 1RG and 1 IP. During late neurogenesis, the IPs divide to create two neurons at the CP.

### 1.1.1 Cell Cycle Regulation

The process of neurogenesis is tightly regulated, and relies heavily on the cell cycle. The cell cycle is the process in which a cell undergoes DNA replication and cell division to make two daughter cells. The cell cycle consists of the following phases: G1 (gap 1), S (DNA synthesis), G2 (gap 2), and M (mitosis). The cell cycle is regulated by CDKs or cyclin dependent kinases. These kinases help the cell transition between phases, and specific CDKs are expressed at specific phases of the cell cycle. Specifically, CDK4, 6 and 2 are active during G1, CDK2 is active during S phase, and CDK1 is active during G2 and M phase (Evans et al., 1983; Morgan, 1995; Norbury and Nurse, 1992; Pines, 1991, 1995; Vermeulen et al., 2003). These CDKs regulate the cell cycle by monitoring cell cycle checkpoints. Cell cycle checkpoints are regulatory mechanisms that identify errors in the cell cycle. If an error is detected, CDK activity will change, which stops the cell cycle so the error can be repaired. When these checkpoints are non-functional, errors in DNA synthesis can persist, which can lead to cancer, developmental abnormalities, or other defects (Malumbres and Barbacid, 2009).

The centrosome is another important player in regulating the cell cycle. The centrosome is an organelle that acts as the microtubule organizing center (MTOC) during the cell cycle (Euteneuer and McIntosh, 1981). During the cell cycle, the successful division of a cell results in two identical daughter cells. After DNA replication, the chromosomes are required to line up on the bipolar apparatus, where the spindle fibers then pull them away to their respective daughter cell. This process relies on intact centrosome function (Giansanti et al., 2001; Hornick et al., 2011; Mazia, 1987; Yamashita et al., 2007). Errors in this process can result in polyploidy (excess of chromosomes in the daughter cell) or unequal number of daughter cells (Brinkley, 2001; Hinchcliffe and Sluder, 2001; Orr-Weaver and Weinberg, 1998). The centrosome also helps determine spindle polarity, which is dictated by the number of centrosomes at the beginning of

mitosis (Carroll et al., 1999; Hinchcliffe and Sluder, 2001; Lingle et al., 1998; Maiato and Logarinho, 2014; Pihan et al., 1998). Cell cycle regulation is critical for neural development, because asymmetric division, which corticogenesis relies on, is regulated by parameters dictated by the cell cycle, such as spindle polarity and cell division. When cell division is perturbed, for example, it can change the number of cells in the nervous system, their cell fate, and their location in the brain. These changes result in developmental deficits that can lead to lethality or developmental syndromes.

### **1.1.2 Determination of stemness**

The normal development of the brain requires that symmetric and asymmetric divisions create the correct number of NPCs to maintain the progenitor pool, while also guaranteeing enough BPs begin the process of differentiation and migration. To ensure this, molecular cues exist both within the cell (gene expression) and outside of the cell (the environment) to guide it through this process. In the development of the cortex, neurogenesis relies on asymmetric division, which produces a stem cell and a cell that will terminally differentiate. This is in contrast to symmetric mitotic division, which results in two identical daughter cells. In mammals, this asymmetric division can be regulated in multiple ways. One way is via numb inheritance. During asymmetric division, one daughter cell will inherit more numb protein. This protein inhibits notch and leads to the production of a neuron (Shen et al., 2002).

Asymmetric division can also be regulated by the orientation of the mitotic spindles. The mitotic spindles are responsible for pulling apart the chromosomes of the daughter cells during cell division (specifically metaphase). Therefore, these spindles regulate cell division, and determine the position and identity of the daughter cells (Kaltschmidt et al., 2000; Morin and Bellaiche, 2011; Morrison and Kimble, 2006). During asymmetric division, cleavage planes are

usually within  $30^\circ$  of the apicobasal axis. This orientation is consistent through both proliferative and neurogenic phases (Konno et al., 2008). If this spindle orientation is altered, it can result in altered asymmetric division, which results in changes in cell fate and migration (Figure 1-2).

Magoh haploinsufficiency is a prime example of how changes in the orientation of mitotic spindles can result in deficits in asymmetric division. Magoh haploinsufficiency results in microcephaly, and leads to increased cell division along the horizontal plane. Cells that divide horizontally, are destined to become basal daughter cells, and post-mitotic neurons. Cells that divide obliquely remain as radial glia (Sun and Hevner, 2014). Therefore, increased horizontal division leads to increased ectopic neuron differentiation (Silver et al., 2010). There needs to be a balance in asymmetric division, to maintain the stem cell pool while still generating neurons. Changes in mitotic spindle orientation is therefore critically important for maintaining the balance of stemness and terminal differentiation during asymmetric division.

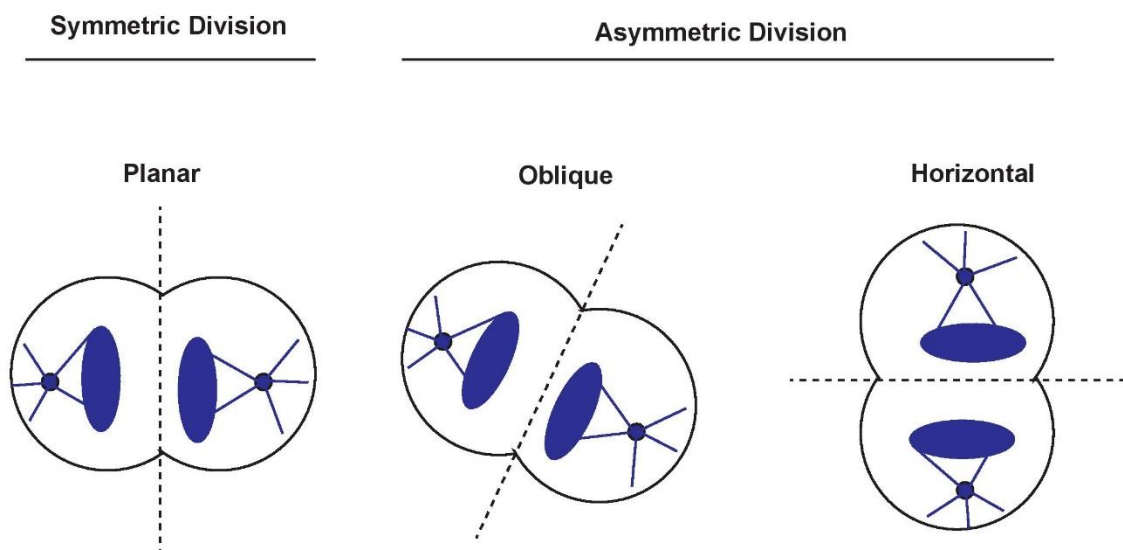


**Figure 1-2: Schematic illustrating the orientation of mitotic spindles.**

The blue circle represents the centrosome, and the blue lines are the mitotic spindles. Adapted from (Paridaen and Huttner, 2014). The plane on which the cells divide (planar, oblique, horizontal) determine the fate of the daughter cells. During symmetric division, the cells divide with a planar orientation, resulting in two identical daughter cells. Horizontal division leads to basal progenitors and post-mitotic neurons, while oblique division leads to RG.

### 1.1.3 Neurogenesis

Before neurogenesis begins NECs occupy the neural tube and neural plate. Once neurogenesis begins, around E10.5, NECs begin to downregulate genes such as Par3, N-cadherin and tight junctions, in the ventricular zone (Aaku-Saraste et al., 1996; Campbell and Gotz, 2002; Gotz, 2003; Gotz and Huttner, 2005; Huttner and Brand, 1997; Kriegstein and Gotz, 2003; Paridaen and Huttner, 2014; Taverna et al., 2014; Wodarz and Huttner, 2003). This downregulation leads to cells being “less epithelial like” and gaining some astroglial properties, such as increased expression of vimentin and S100 $\beta$ . However, these cells, called radial glia, still share some properties with NECs in that they connect to the apical surface and have an apical localization of the centrosome (important for asymmetric division) (Campbell and Gotz, 2002; Chenn et al., 1998; Gotz, 2003; Gotz and Huttner, 2005; Hartfuss et al., 2001; Kriegstein and Gotz, 2003; Paridaen and Huttner, 2014; Taverna et al., 2014). After the radial glia undergo asymmetric division, the BP migrates up the processes of the RG. When it reaches the IZ, it undergoes symmetric division to make two BP. The BP will continue to migrate and concurrently differentiate until it reaches its final destination, where it receives a stop signal from reelin that prompts the BP (though now differentiated) to dissociate from the radial glia (D’Arcangelo, 2005; Fatemi et al., 1999; Lee and D’Arcangelo, 2016; Nadarajah and Parnavelas, 2002). In mammals, the cortex forms in an inside out fashion, with the deep layers of the cortex forming prior to the superficial layers. Migrating and differentiating neurons travel up the RG through already formed cortices to reach their final destination. At the end of neurogenesis, the RG terminate their association with the ventricle, and migrate toward the cortical surface, where they typically undergo gliogenesis and become astrocytes (Campbell and Gotz, 2002; Gotz and Huttner, 2005; Paridaen and Huttner, 2014; Taverna et al., 2014). During corticogenesis, cortical layers form at specific times, starting with layer 6 at E12, and ending with gliogenesis starting at around E17.

For this reason, if neurogenesis is delayed, it can result in the malformation, or absence of cortical layers. For instance, if neural differentiation is delayed at E12, and cells only begin to differentiate and migrate at E13, then layer 6 of the cortex would be missing. This leads to decreased cortical thickness and cell numbers. This phenomenon is observed in the mouse model of Magoh haploinsufficiency, and results in decreased cortical thickness (Silver et al., 2010).

#### **1.1.4 Interneuron Development**

During corticogenesis, different neuron types (excitatory vs. inhibitory) arise from different embryonic brain regions and have different migration patterns. Excitatory cells arise from dividing RG cells in the VZ (dorsal, pallial telencephalon) and migrate up RG processes to form the cortex. Inhibitory interneurons, however, arise from the ganglionic eminences (subpallium), and undergo a tangential migration to the cortex, where they eventually reside and interact with the excitatory neurons (DeDiego et al., 1994; Wonders and Anderson, 2006). Cortical interneurons can also be divided into subtypes based on gene expression patterns, electrophysiological properties and morphology. Expression pattern subtypes include parvalbumin (PV), somatostatin (SST), neuropeptide Y (NPY), calretinin (CR) and 5HT3aR (VIP+ and non-VIP+). Cells can also exist in multiple subtypes. For example, a large portion of SST+ cells are also NPY+. SST+ and PV+ interneurons make up about 60% of the cortex, and arise primarily from Nkx2.1+ progenitors in the medial ganglionic eminence (MGE) (Gonchar and Burkhalter, 1997; Kawaguchi and Kubota, 1997).. The CGE also gives rise to CR+ bipolar cells (dorsal) and 5HT3aR+ cells (Rudy et al., 2011). NPY+ interneurons can originate from both the MGE and dorsal CGE (Anderson et al., 2001; Butt et al., 2008; Nery et al., 2002, 2003; Tremblay et al., 2016; Valcanis and Tan, 2003; Wichterle et al., 2001; Wonders and Anderson,

2006). Cortical interneurons also form in an inside out fashion, so that cells in deeper layers will migrate first, followed by cells in the superficial layers.

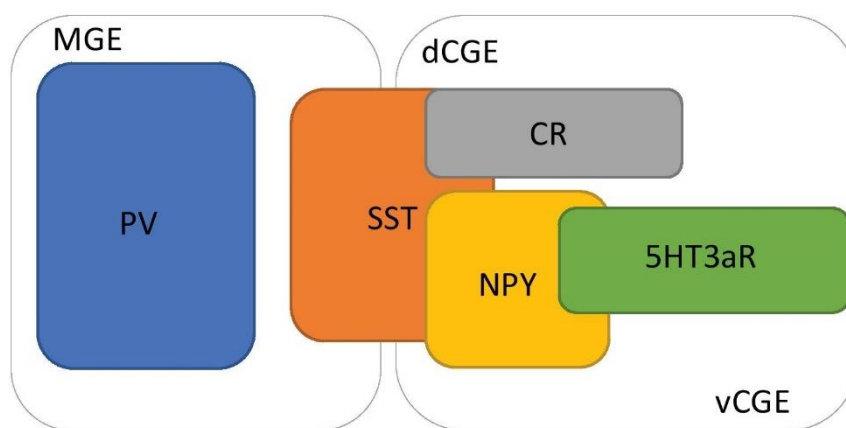


**Figure 1-3: Illustration of interneuron subtypes and where they originate from**

Modified from (Wonders and Anderson, 2006). The majority of interneuron progenitors arise from the MGE, including PV<sup>+</sup> interneurons (most populous subtype), and a sub population of SST<sup>+</sup> interneurons. A sub population of SST<sup>+</sup> interneurons can also be CR<sup>+</sup> or NPY<sup>+</sup>. SST and CR<sup>+</sup> interneurons arise from the dCGE, while SST<sup>+</sup> and NPY<sup>+</sup> interneurons arise from the vCGE. 5HT3aR<sup>+</sup> interneurons arise from the CGE.

Different interneuron subtypes also have different electrophysiological properties and morphology. PV<sup>+</sup> cells can be split up into fast-spiking basket cells, and fast-spiking chandelier cells (also known as axo-axonic). Though both fast-spiking, basket cells have a greater latency to fire, and chandelier cells have a higher frequency of firing compared to basket cells (DeFelipe et al., 2013; Inan and Anderson, 2014; Meyer et al., 2002; Monyer and Markram, 2004). SST<sup>+</sup> cells can be subdivided into Martinotti and non-Martinotti cells. The difference is that Martinotti cells have an axonal plexus in layer 1 (L1) that targets dendrites, whereas non-Martinotti cells do not (Monyer and Markram, 2004; Tremblay et al., 2016). Martinotti cells are present in L2/3 and L5/6, and arborize in L1. The arbors then interact with the dendrites of neurons in the same layer. L4 non-martinotti cells target PV interneurons, which may lead to disinhibition of pyramidal cells (which are typically inhibited by PV interneurons) (Tremblay et al., 2016). SST<sup>+</sup> cells differ

from other interneurons in that their electrophysiological properties allow EPSP (excitatory post synaptic potential) summation. SST+ cells therefore have the unique capability to facilitate excitatory inputs (Tremblay et al., 2016). One single burst from a presynaptic cell is sufficient to make a SST+ cell fire, whereas a PV + cell would require high synchronous firing from multiple presynaptic cells to trigger an action potential (Tremblay et al., 2016).

### **1.1.5 Disruptions in neurogenesis**

Since neurogenesis is responsible for generating the entirety of the nervous system, when it is perturbed it results in profound deficits. Neurogenesis is like a seesaw, a balance between the stem cell and neuron states. Imbalance in either direction will lead to developmental defects (Figure 1-4). For example, if the balance is shifted toward the stem cell phase, it will result in overexpansion of the stem cell pool and decreased differentiation. This can lead to microcephaly, where the brain is significantly smaller than normal, while the body size is intact. One potential reason for this to occur is because too few NPCs have differentiated into neurons and migrated to form the cortex. Instead they remain as progenitors. This balance is regulated by many genes. One regulator is MCPH. Humans with mutations (single nucleotide polymorphisms [SNPs] and frame shift mutations) in this gene exhibit microcephaly, and as a result, mild mental retardation (Alderton et al., 2006; Darvish et al., 2010; Garshasbi et al., 2006; Gruber et al., 2011; Jackson et al., 2002; Neitzel et al., 2002). Another microcephaly gene is CDK5RAP2. When an in-frame mutation in exon 4 of CDK5RAP2 occurs in mice (genomic inversion of exon 4), it results in the predominant expression of an alternative isoform. This results in microcephaly, a thin cortex, and decreased size of the superficial cortical layers. These deficits are caused by decreased proliferation of NPCs. Interestingly, the deficits in proliferation seem to be caused by impaired centrosome function, and mitotic spindle orientation during proliferation (Lizarraga et al., 2010).

It is important to note that shifting the balance toward stem cell phase doesn't necessarily mean there is more proliferation. Instead, it indicates that the cells are remaining in the stem cell fate instead of differentiating into neurons. Conversely, mutations in PTEN in mice lead to macrocephaly (large brain), caused by increased proliferation, shortened cell cycle and decreased apoptosis (Groszer et al., 2001).

Another example of genes that regulate this balance between a stem cell state and a differentiated state is the gene RBM8a (RNA binding motif 8A), also known as Y14. When RBM8a is overexpressed, it leads to increased proliferation, and prevents cell cycle exit and differentiation (Zou et al., 2015). This leads to an expanded stem cell pool in the ventricular/subventricular zone (VZ/SVZ), and fewer neurons in the cortical plate. Alternatively, when RBM8a is knocked down, it results in decreased proliferation of NPCs, increased cell cycle exit, and precocious differentiation. This results in a depleted stem cell pool, and an excess of neurons in the cortical plate (Zou et al., 2015). Due to RBM8a's clear role in regulating neurogenesis, my dissertation work will focus on this gene and how it is vital to the development of the nervous system (Figure 1-4).

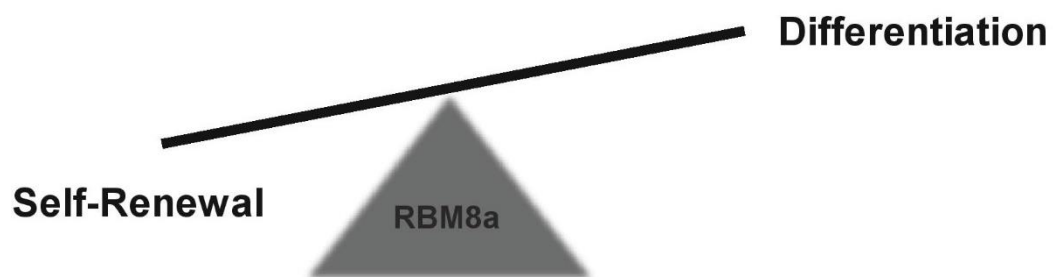


**Figure 1-4: Schematic illustrating how RBM8a regulates the balance between self-renewal and differentiation during asymmetric division.**

Too much RBM8a tips the balance towards self-renewal, leading to an over-expansion of the stem cell pool and decreased differentiation of neurons. Decreased expression of RBM8a tips the balance toward differentiation, leading to ectopic neuron differentiation and depletion of the stem cell pool.

## 1.2 RNA Stability and Neurodevelopment

RNA stability includes an RNA's predisposition to degradation via different RNA surveillance pathways, enhancers and lincRNAs (long noncoding RNAs) that modulate RNA expression, as well as alternative splicing of mRNAs. RNA degradation and alternative splicing have profound effects on gene expression, and have been linked to neurodevelopment, specifically neurological disease. DISC1 (Disrupted in Schizophrenia 1) is a gene well known to be associated with psychiatric disease. This gene plays vital roles in neuronal proliferation and differentiation, and when perturbed can result in schizophrenia, depression, bipolar disorder and more (Mao et al., 2009; Nakata et al. 2009). Additionally, lincRNA Gomafu was found to modulate DISC1 alternative splicing. Gomafu is important for brain development, and could possibly modulate development by regulating the alternative splicing of other genes (Barry et al., 2014).

Another set of proteins that are vital to neurodevelopment, and has a role in RNA stability are the neuroligin proteins. These synaptic adhesion proteins are located on the post-synaptic neuron and help facilitate the interaction of two neurons at the synapse. There are many neuroligin isoforms, and different splice variants have been associated with psychiatric disease and developmental abnormalities. Mutations in Neuroligin 2 (NL2), for example is associated with schizophrenia (Sun et al., 2011). When the isoform NL2 and NL2A is expressed, it causes changes in receptor clustering at the synapse, leading to enlargement of VGAT and vGLUT1 puncta (Chih et al., 2006). Expression of these isoforms also causes cells to lose the ability to induce GABAergic presynaptic terminals (Chih et al., 2006). Therefore, alternative splicing of Neurexins prevents neuroligins from associating with GABAergic synapses, which alters

neuronal circuits. Interestingly, alternative splicing of Neurexins (found on pre-synaptic neurons, and interact with neuroligins) to exclude splice site 4, lead to altered interaction of neurexins and neuroligins (Chih et al., 2006).

Surveillance mechanisms such as nonsense mediated mRNA decay (NMD) can also regulate gene expression and alternative splicing. One prominent protein involved in NMD and alternative splicing, is Exon Junction Complex (EJC) factor RBM8a.

### **1.3 RNA Surveillance Mechanisms**

Although RBM8a is clearly implicated in neurogenesis, it is most well-known for its role in nonsense mediated mRNA decay (NMD). NMD is a surveillance mechanism that identifies and tags mRNAs with pre-termination codons (PTCs) for degradation. This mechanism ensures that faulty mRNAs are not fully translated into nonfunctional proteins. This mechanism relies on the exon junction complex (EJC) to help identify mRNAs with PTCs. The EJC is comprised of four proteins, RBM8a, Magoh, BTZ, and EIF4AIII. This tetramer is deposited at exon-exon junctions after splicing. As the mRNA is being translated, the ribosome senses EJCs downstream from the stop codon. As there are no exons after the stop codon, when the ribosome reaches a stop codon, it should not sense any more EJCs downstream. In the presence of a PTC, when the ribosome reaches the stop codon, EJCs will remain downstream of the ribosome. This signals to the ribosome that the stop codon is premature and the ribosome then recruits the SURF complex to interact with the EJC to tag the mRNA via UPF1 mediated phosphorylation for degradation (Hosoda, 2006; Isken and Maquat, 2008; Isken et al., 2008; Kashima et al., 2006; Ohnishi et al., 2003; Wittmann et al., 2006) (Figure 1-5).

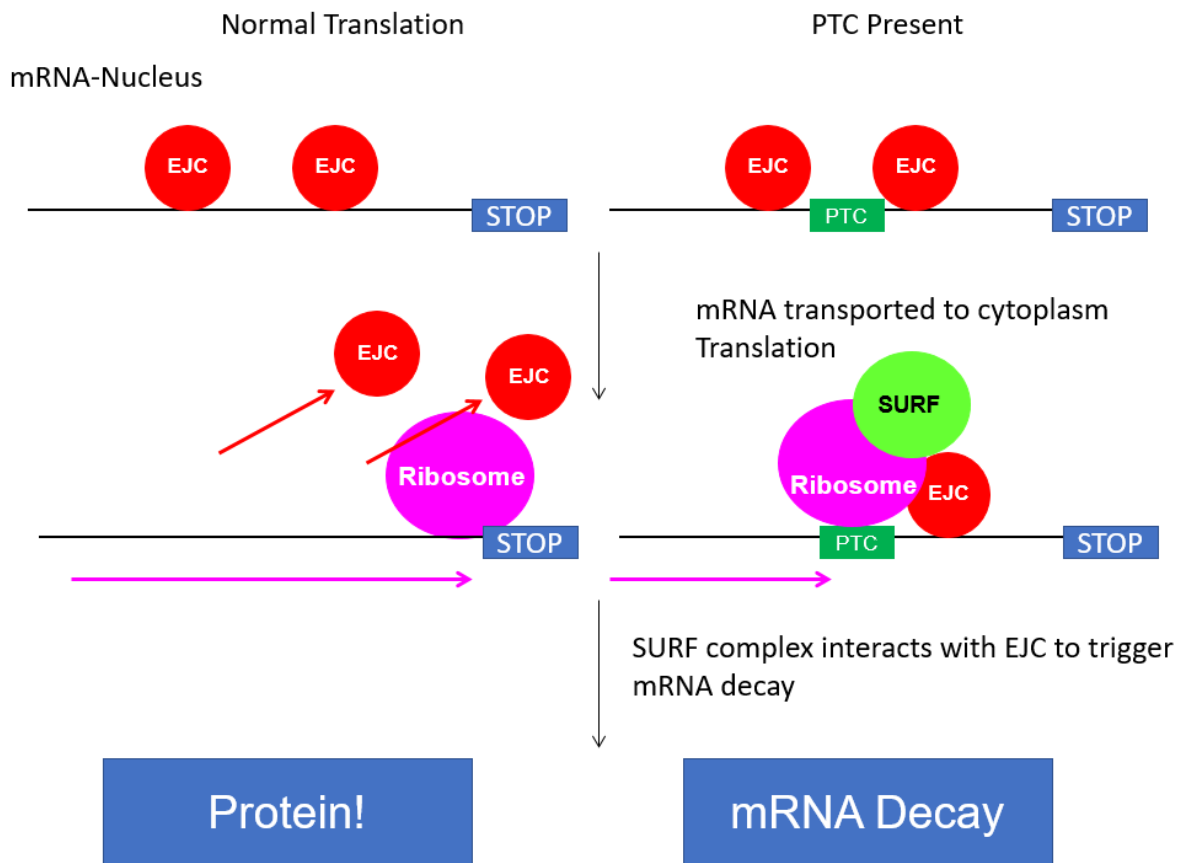


**Figure 1-5: Schematic illustrating how the cell uses the EJC to identify mRNAs with PTCs**

During normal translation, EJCs are deposited on exon-exon junctions after splicing. When the ribosomes translate the mRNA, they displace the EJC as they reach the exon-exon junction. When the ribosome reaches a stop codon, typically there will be no more EJCs downstream of the stop codon. When a PTC is present, once the ribosome reaches the PTC, it will still sense EJCs downstream. This indicates to the ribosome that it has reached a PTC as opposed to a natural stop codon. The cell then recruits the SURF complex which interacts with the EJC to tag the mRNA for degradation via Upf1 phosphorylation.

NMD also regulates a subset of RNAs that display special characteristics and lack PTCs. These characteristics include a long 3'UTR, an exon-exon junction >50 nucleotides downstream of a stop codon, long upstream open reading frame (ORF) and introns in the 3' UTR. RNAs with introns in the 3'UTR usually introduce a stop codon, or a frameshift which leads to a PTC downstream, causing the RNA to be tagged for degradation (Behm-Ansmant and Izaurralde,

2006; Chang et al., 2007; Isken and Maquat, 2007, 2008; Kervestin and Jacobson, 2012; Peccarelli and Kebaara, 2014). Typically, NMD is identified when the ribosome reaches a stop codon and there is still an EJC downstream. In the case of an intron in the 3'UTR, this occurs when in some cases not all the exons are translated. This leaves both exon(s) and intron(s) downstream, which can also trigger NMD. An example of this is the human HLA 6.09 gene, in which the last exon is not translated (Nagy and Maquat, 1998).

#### **1.4 Clinical Phenotypes Caused by RBM8a**

RBM8a mutations have been implicated in a variety of clinical phenotypes. Compound mutations in RBM8a have been found to cause TAR syndrome (Thrombocytopenia with Absent Radius syndrome). This disorder is characterized primarily by low blood platelet counts (thrombocytopenia), and missing radii bones. Additional features of TAR patients include short ulnas, low megakaryocyte numbers, axial root of the kidney, renal and heart defects, agenesis of the corpus callosum, and hypoplasia of the cerebellum (Greenhalgh et al., 2002; Homans et al., 1988; Menghsol et al., 2003; Skorka et al., 2005). In a case study conducted by (Skorka et al., 2005), the patient with TAR syndrome exhibited partial seizures, psychomotor retardation, and cerebral dysgenesis.

The specific genetics of TAR syndrome were found to include a microdeletion of around 200bp in the 1q21.1 region of the genome (including RBM8a) on one inherited chromosome, and a low frequency non coding SNP in RBM8a on the other inherited chromosome 1 (rs139428292 or rs201779890) (Albers et al., 2012; Tassano et al., 2015).

In addition to the TAR clinical phenotype, RBM8a is also associated with various neuropsychiatric disease cases. RBM8a is located in the 1q21.1 region of the genome, which is

highly associated with neuropsychiatric diseases as a result of copy number variations (CNVs) (both duplication and deletions) (Bernier et al., 2015; Brunetti-Pierri et al., 2008; Dolcetti et al., 2013; Mefford et al., 2008). Additionally, *de novo* mutations in RBM8a have been associated with autism spectrum disorders (ASD) (Iossifov et al., 2012). One unpublished case in particular was recently discovered, in which a 4-year-old boy was found to have a mutation in the 5'UTR of RBM8a, thought to be causative of his ASD. This case was brought to our attention when the family was encouraged to email us in order to better understand RBM8a. In this dissertation, the role of RBM8a in the nervous system is explored, however, RBM8a is expressed throughout the body, and when perturbed using other cre (not neural specific), other phenotypes emerge. One such phenotype is when the floxed mice are crossed with Prx1 (limb bud cre). The resulting progeny have smaller radii and ulna, reminiscent of TAR syndrome patients (data not shown).

## 1.5 EJC Proteins and Neurodevelopment

Recent research in mice has implicated the core EJC proteins in neurogenesis and neurodevelopment. First, Magoh haploinsufficiency was reported to result in small body size, decreased cortical thickness, and microcephaly (McMahon et al., 2014; Silver et al., 2010). Mechanistically, these phenotypes were found to result from premature neuron differentiation, decreased intermediate progenitors (IPs) and increased apoptosis (Silver et al., 2010). This resulted from prolonged prometaphase, leading to delayed progression of mitosis (McMahon et al., 2014; Pilaz et al., 2016; Silver et al., 2010).

Additionally, RBM8a haploinsufficiency (using forebrain specific Emx1-cre) was found to also cause microcephaly, premature neuronal differentiation, and disorganized cortical layers. These mice had decreased NSCs and IPs, and the cells were observed to have increased cell cycle exit (Mao et al., 2015). Similar to Magoh and RBM8a, Eif4A3 haploinsufficiency also results in

microcephaly, decreased cortical thickness, NSC depletion and increased neuronal differentiation (Mao et al., 2016).

Another core EJC protein *Casc3* (BTZ, MLN51), was associated with less severe developmental phenotypes when mutated. Homozygous null mice were embryonic lethal, indicating that *Casc3* is required for viability. However, heterozygous mice did not show severe deficits like *Magoh* and *RBM8a* mutations. These mice had thin cortices, but did not have display any alterations in apoptosis or premature neuron differentiation (Mao et al., 2017).

My dissertation aims to further investigate the role of *RBM8a* in neurodevelopment to relate these developmental changes (microcephaly, early postnatal lethality) to behavior and RNA stability. Clearly *RBM8a* is immensely important for the development of the nervous system. However, to date it is not known why *RBM8a* haploinsufficiency results in lethality. Prior research has established the key role for RNA stability in neurodevelopment, and there is a significant body of work on *RBM8a*'s role in NMD (Bhuvanagiri et al., Aug 27; Brogna and Wen, 2009; Gehring et al., 2003; Isken and Maquat, 2008; Kervestin and Jacobson, 2012). It is my goal to link these two roles of *RBM8a*, developmental and RNA stability, as a potential mechanism behind pathologies involving *RBM8a* mutations.

## Chapter 2

### Materials and Methods

#### 2.1 Materials

##### 2.1.1 Antibodies used in this study

Table 2-1: Primary antibodies used in this study

Antibody	Species	Dilution		Vendor (Catalog #)
		IHC	WB	
BrdU	Mouse	1/250		DAKO (M074401-8)
GFP	Chicken	1/1000		Aves labs (NC9510598)
Ki67	Rabbit	1/100		Lab vision (RB90431P1)
Tuj1	Mouse	1/100		Covance (PRB-435P)
Nlgn1	Mouse		1/500	NeuromAB
Rest	Rabbit		1/500	Abcam ab21635
TLE4	Rabbit		1/500	Santa Cruz sc-9125
KIF1a	Mouse		1/500	BD bioscience
B-actin	Mouse		1/4000	Santa Cruz sc-81178
RBM8a	Mouse		1/500	Santa Cruz sc-32312
Atxn1	Mouse		1/500	NeuromAB
RFP	Rabbit	1/250		Genscript (A00682-40)

CDK5	Rabbit		1/500	Santa Cruz sc-750
DCX	Goat	1/250		Santa Cruz sc-8066
B-catenin	Rabbit		1/500	Santa Cruz sc-7199
NeuN	Rabbit	1/100		Millipore ABN78
GFAP	Mouse	1/250		540N1A1
PV	Rabbit	1/250		Abcam ab11427
SST	Rat	1/250		Millipore MAB354
NPY	Rabbit	1/250		Abcam ab180809
Nkx2.1	Rabbit	1/250		Santa Cruz sc-13040
Calbindin	Rabbit	1/250		Millipore AB1778
VEGFR3	Goat	1/2000		R and D Systems AF743
CC3	Rabbit	1/500		Cell Signaling 96615
PH3	Rabbit	1/100		Millipore 06-570
Sox2	Goat	1/200		Santa Cruz sc-17320
Nestin	Chicken	1/100		Santa Cruz disc.
Notch1 (NICD)	Mouse		1/500	BD Pharmingen (552466)
mGluR1	Mouse		1/500	NeuromAB N355/1
Cux1	Rabbit	1/300		Santa Cruz sc-13024
Foxp2	Goat	1/300		Santa Cruz sc-21069

Table 2-2: Primer sequences used for genotyping

Gene/Size (bp)	Forward Primer	Reverse Primer
Cre/100	5' GCGAAGATTTGCCATGGAT 3'	5' CCTGTCGCGTTTCCTAGACT 3'
Ai9 WT/297	5' AAGGGAGCTGCAGTGGAGTA 3'	5' CCGAAAATCTGTGGGAAGTC 3'

Ai9 mutant/196	5' CTGTTCTGTACGGCATGG 3'	5' GGCATTAAAGCAGCGTATCC 3'
5' loxp/156 (WT), 308 (KO)	5' GCGAAGATTCGCCATGGAT 3'	5' CCTGTCGCGTTTCCTAGACT 3'
5' long arm/4700	5' ACCTGGGTAATTTAGCAAGACT 3'	5' CGAAGTTATATTAAGGGTTCCGGATC 3'
3' long arm/3756	5' TCTTCTGAGGGGATCAATTCTC 3'	5' GCCTGTAGCAGCAATAGCCT 3'

Table 2-3: Buffers and Reagents used in this study

Buffer/Reagent	Recipe
Stacking Gel Solution (4x)	Tris (pH 6.8), HCl, SDS, Water
Lower Gel Solution	Tris (pH 8.8), HCl, SDS, Water
10x Phosphate-Buffered Saline (PBS)	1.37M NaCl, 27mM KCl, 100mM Na <sub>2</sub> HPO <sub>4</sub> , 18mM KH <sub>2</sub> PO <sub>4</sub>
Artificial Cerebrospinal Fluid (ACSF)	119mM NaCl, 26.2 mM NaHCO <sub>3</sub> , 2.5mM KCl, 1mM NaH <sub>2</sub> PO <sub>4</sub> , 1.3mM MgCL <sub>2</sub> , 10mM glucose
Phospho Buffer Saline Tween (PBST)	Add 0.3% Tween-20 to 1X PBS
Blocking Solution	5% Donkey Serum in 0.3% PBST

Reagent	Vendor (Catalog #)
Acrylamide-Bisacrylamide Solution 30% (37:5:1)	VWR (97064-750)
APS	Aqua Solutions (SKU#A5188-500G)
Dreamtaq buffer (10X)	Thermo Fisher Scientific (B71)
Dreamtaq taq polymerase	Thermo Fisher Scientific (EP0713)
25mM dNTP	Bio Basic Canada (DD0057)

Agarose	Med Supply Partners (62-1001-1)
Prolong Gold Antifade	Thermo Fisher Scientific (P36930)
BrdU	Sigma (B5002-100mg)
Click-iT EdU Alexa Fluor 488 Imaging Kit	Thermo Fisher Scientific (C10337)
Para formaldehyde (16% PFA in methanol)	BD (BD H0500-4LP)

## 2.2 Methods

### 2.2.1 Mice

#### *In utero electroporation*

Wild type male and female C57/BL6N mice were obtained from Taconic C57BL/6 N male mice were housed 2–4 mice per cage in a room with a light/dark cycle at 12 h interval (lights on at 7:00 am), and provided *ad libitum* access to food and water. All procedures on mice were reviewed and approved by The Pennsylvania State University IACUC committee, under IACUC protocol, 44057, to Yingwei Mao.

#### *Conditional knockout mice*

Mice were separated by sex (2-5 mice per cage) in a room with a light/dark cycle at 12hr intervals. The knockout strategy was designed using the cre-loxp system of PGKneolox2DTA vector (Soriano, 1997). To make the targeting construct, a 4.5 kb 5' homologous region to the exon 2 was subcloned into the SacII and NotI sites in the vector. LoxP sites flanked exons 2, 3 and 4, and a neomycin-resistance cassette (PGK-neo) was at the downstream of Exon 4. PGKneo is flanked by flpe recombinase recognition sites (FRT). A 2.7 kb 3' homologous region was subcloned at NheI and EcoRV sites of the vector. To generate RBM8a conditional knockout

mice, the linearized targeting construct was electroporated into embryonic stem (ES) cells derived from C57BL/6J/129S6 hybrid line. Two targeted ES clones were identified from 196 G418-resistant clones. The positive clones were identified by long-range PCR using 5' primer pair (ACCTGGGTAATTTAGCAAGACT and CGAAGTTATATTAAGGGTTCCGGATC) to examine 5' recombination and 3' primer pairs (TCTTCTGAGGGGATCAATTCTC and GCCTGTAGCAGCAATAGCCT). Correct embryonic stem cells were injected into blastocysts of C57BL/6J mice at the Transgenic Core of University of Rochester Medical School, and the chimeras were crossed with C57BL/6J mice to obtain germ line transmission. The resulting progeny were then crossed with Actin-Flipase mice to remove the Neo cassette (used for selection) (JAX stock #003800, C57BL/6J) (Rodriguez et al., 2000). The mice were then backcrossed to create homozygous floxed mice without the Neo cassette. These mice were then crossed with Nes-Cre (Jackson lab # 003771), a neural stem cell specific cre line (C57BL/6J background, backcrossed 6 generations), to selectively delete RBM8a in neural stem cells. Chimera mice were backcrossed with C57BL/6J mice for a minimum of three generations.

### **2.2.2 Immunohistochemistry**

Postnatal brains were collected on postnatal day 17 (the last day where I could guarantee 100% survival of the cKO mice. Mice were anesthetized with avertin (2.5% avertin), and perfused with artificial cerebrospinal fluid (119mM NaCl, 26.2mM NaHCO<sub>3</sub>, 2.5 mM KCl, 1mM NaH<sub>2</sub>PO<sub>4</sub>, 1.3 mM MgCl<sub>2</sub>, 10 mM glucose) until the liver was clear of blood. Then the mice were briefly perfused with 4% paraformaldehyde (PFA). The brain was then dissected out, and post-fixed in 4% PFA for a minimum of 24hrs at 4°C. The brains were then sliced on the vibratome in 70 µm thick slices. Slices were stored in 6 well plates filled with PBS and sodium azide in 4° C. For immunohistochemistry, slices were rinsed 3 times in PBS for 5 min while

gently rocked at room temperature (RT). Then slices were blocked and permeabilized using 5% donkey serum in 0.3% PBST (1x PBST 8g NaCl, 0.2g KCl, 1.44g NaH<sub>2</sub>PO<sub>4</sub>, 0.24 g KH<sub>2</sub>PO<sub>4</sub>, 3mL Tween-20, fill to 1L). During the blocking step, slices were gently rocked at RT. Next, slices were incubated in primary antibody diluted in 5% donkey serum in 0.3% PBST. Slices were shaken gently at RT O/N. See Table 1 for a list of primary antibodies. The next day, slices were washed 3 times in PBS, then incubated for 1hr with the secondary antibody of the appropriate species, conjugated with either Alexa Flour 488 or 555. Samples were rocked gently at RT and covered with foil to protect them from the light. Slices were then washed with PBS with 1/1000 DAPI and ToPro for 15 min at RT, then washed two more times with PBS for 5 min. Slices were then plated on mount slides with prolong gold anti-fade. Fluorescent images were captured using a Zeiss LSM 5 confocal microscope or a Zeiss Axio Observer with ApoTome.2 LSM 880 microscope (cell size images). Images were quantified using ImageJ. Cell number were quantified using the Cell Counter plugin, and DAPI cell number was calculated using the ITCN plugin. For cell distribution analyses, the cortex was divided in to 6 equal sextets, and the number of cells in each sextet was counted. For all analyses, 3 biological replicates were used for the experimental and control group, and three slices were used for each biological replicate.

### **2.2.3 Organ Measurements**

Organs were dissected out immediately after sacrifice, and the excess liquid was dabbed onto a Kim wipe. The weigh boat was tared and the organ was placed on the weigh boat to determine the weight in grams. The organ weight was normalized to the total weight of the mouse to determine the percentage of body weight that the organ occupied.

#### **2.2.4 Western Blot**

Immunoblots were performed as previously described (Zou et al., 2015). The total proteins were prepared from whole cell extracts from whole mouse brains at postnatal day 17 using 500  $\mu$ l RIPA cell lysis buffer (10 mM Tris-HCl (pH 8.0), 140 mM NaCl, 1 mM EDTA, 1% TritonX-100, and 0.1% SDS, 1 mM  $\beta$ -glycerophosphate, 1 mM Na<sub>3</sub>VO<sub>4</sub>, 2  $\mu$ g/ml aprotinin, 1 mM PMSF, 130  $\mu$ M bestatin). The tissue was homogenized, then placed on ice for 20 min with vortexing every 2 minutes. The samples were then centrifuged at 4°C for 20 min. The supernatant from each sample was collected and stored in aliquots at -80°C. For each sample, the protein concentration was determined by Bradford assay (ThermoFisher Scientific). 20-50 $\mu$ g of cell lysate were resolved by 8-12% SDS-polyacrylamide gel electrophoresis, and were transferred to nitrocellulose membranes using BIORAD SYSTEM. The blots were blocked with 5% milk in TBST (10 mM Tric-HCl, pH 8.0, 150 mM NaCl, 0.5% Triton X-100) for 1hr at RT. Blots were then incubated with primary antibody in 5% milk in TBST overnight at 4°C, with shaking. Samples were then washed 3X in TBST for 10 min each, then incubated in LICOR secondary antibody diluted in 5% milk (see secondary antibody table). Blots were then washed 4x in PBST for 10 min each, then Immunoreactivity was detected using the LI-COR Odyssey imaging system according to the company's instructions.

#### **2.2.5 Cell Culture**

Mouse CAD and human 293T SH-SY5Y cells were cultured using DMEM containing 10% FBS, L-Glutamine, and penicillin/streptomycin, Primary NPCs were isolated from E14 mouse embryos and cultured as described in (Mao et al., 2009). The cortex from 6-8 mouse brains at E14 were dissected out and trypsinized in 0.5% trypsin and DNase at 37°C for no more

than 5 min. 0.2% Trypsin inhibitor was added to stop trypsinization and tissues were shattered into single cells by pipetting. After removal of trypsin solution, cells were seeded in fibronectin coated plates with NPC medium (DMEM F-12/1% Penn-Strep/1% L-glutamine/1% N-2 supplement/bFGF (10-20ng/ml)). To induce NPC differentiation, FGF2 was removed from the culture medium and 1 $\mu$ M retinoic acid/1% FBS was added to the medium for 7 days.

### **2.2.6 *In utero* electroporation**

The pregnant female mouse was anesthetized by intraperitoneal (i.p.) injection of avertin (800  $\mu$ l/40 g) and Buprenorphine (0.05 mg/kg). The anesthetized female was put on the sterile warm pad at 37 °C and eye ointment was applied to prevent their eyes from drying. Control or RBM8a shRNA constructs together with an enhanced GFP (EGFP)-expressing plasmid (final concentration, 2  $\mu$ g/ $\mu$ l; pCAGIG-Venus) at a 2:1 ratio were injected into the lateral ventricle of the embryonic brains at E13. In the overexpression experiments, vector or human WT-RBM8a plasmid was electroporated into E14 embryonic brains. The electric pulses were delivered through the brain of the embryos (5 pulses of 30–45 V). After electroporation, embryos were put back to original position. The mother mice were sutured and returned to animal facility for recovery. BrdU (100 mg/kg) was i.p. injected into mice 2 h before sacrifice. Brains at E16 were removed and post-fixed in 4 % paraformaldehyde at 4 °C for overnight.

### **2.2.7 RNAseq**

#### *Cells (chapter 2)*

SH-SY5Y cells stably expressing RBM8a or a control vector were created as described in the previous section, and the total RNA was purified from the cells using TRIzol reagent. To

preserve the noncoding RNAs, we used RiboZero Kit (Invitrogen) to remove the ribosomal RNA and RNAs were used for construction of a sequencing library using the Illumina TruSeq Stranded total RNA Kit (NIH NHLBI Sequencing Core). One lane of  $50 \times 50$  paired-end reads were generated by the Illumina HiSeq 2500 platform at the NHLBI DNA Sequencing and Genomics Core (DSGC) and mapped to the human genome (UCSC build hg19) using Tophat (Trapnell et al., 2012). Gene type information for each gene was obtained from GRCh37.75 annotation (Quinlan and Hall, 2010). Cuffdiff (<http://cufflinks.cbc.umd.edu/>) was used with the reference genomes to identify the differentially expressed genes and isoforms (Trapnell et al., 2012). The fold change for each gene was determined by dividing the FPKM for each gene in the overexpression sample, by the FPKM of the control sample. The cutoff of genes considered to be differentially expressed was a q-value of 0.05 or less, and either greater than a 1.5 fold upregulation or less than a 0.67 fold downregulation.

#### *Brain tissue*

Brains were extracted from cKO and control mice at P17 or E12. For the P17 dataset the whole brain was used, and for the E12 datasets, the brains were divided into the cortex and hindbrain/midbrain. The total RNA was purified from the cells using TRIzol reagent. To preserve the noncoding RNAs, we used RiboZero Kit (Invitrogen) to remove the ribosomal RNA and RNAs were used for construction of a sequencing library using the Illumina TruSeq Stranded total RNA Kit (NIH NHLBI Sequencing Core). One lane of  $50 \times 50$  paired-end reads were generated by the Illumina HiSeq 2500 platform at the NHLBI DNA Sequencing and Genomics Core (DSGC) and mapped to the human genome (UCSC build hg19) using Tophat (Trapnell et al., 2012). Gene type information for each gene was obtained from GRCh37.75 annotation (Quinlan and Hall, 2010). Cuffdiff (<http://cufflinks.cbc.umd.edu/>) was used with the reference genomes to identify the differentially expressed genes and isoforms (Trapnell et al., 2012). The

fold change for each gene was determined by dividing the FPKM for each gene in the overexpression sample, by the FPKM of the control sample. The cutoff of genes considered to be differentially expressed was a p-value of 0.05 or less, and either greater than a 1.5-fold upregulation or less than 0.67-fold downregulation. We then repeated the functional analysis using a different cutoff point for differentially expressed genes. The new cutoff, was defined as a q-value of 0.05 or less and a fold change of 2x up or down (for a stricter analysis).

#### *Cross-reference with disease databases*

The list of differentially expressed genes was cross-referenced with databases consisting of genes known to be associated with various neurological disease. The number of genes present in both datasets was determined, and a hypergeometric analysis was used to identify the statistical probability that the genes in common were due to chance (data presented had a  $p < 0.05$ ). The list of common genes generated in the cross-reference with disease databases was then input in to DAVID gene functional classification tool (functional annotation cluster). DAVID identified what signaling pathways and what functional categories were significantly affected (Fisher exact test) based on the number of genes in the pathway located in the dataset.

#### *Alternative splicing analysis*

For the alternative splicing analysis, all bam files created by TopHat (version 2.0.6) (Trapnell et al., 2009) were merged into a single file using samtools (version 1.1) (Li et al., 2009). The total number of reads that support the individual variants associated with each of the predicted functional alternative splicing events were determined using the MISO (Mixture of Isoform) package (version 0.5.3) (Katz et al., 2010) using events annotated as of 26 June 2013. Significant differentially spliced events were determined by requiring a Bayes' factor  $>10$  and  $\Delta\psi >0.2$  in a comparison of cherry and RBM8a. Each event was required to pass the default MISO minimum read coverage thresholds.

### *NMD analysis*

Transcripts targeted by NMD were determined by cross-referencing the list of differentially expressed RNAs with the hg19 annotation. Targets were identified as targeted by NMD if they had a 3' UTR greater than or equal to 1250 bp, an intron in the 3' UTR, or an exon junction greater than 50 nt downstream of a stop codon.

### **2.2.8 DNA construct, Transfection and Lentivirus production**

Human RBM8a cDNA was PCR amplified and cloned into the lentiviral vector pLV-3FLAG3HA-T2A-GFP as previously described (Alachkar et al., 2013) and pTRIPZ-mCherry to generate the fusion gene, pTRIPZ-mCherry-RBM8a. The sequences for shRNAs targeting mouse RBM8a are as follows: control shRNA: 5'-CGGCTGAAACAAGAGTT GG-3'; shRNA-1: 5'-GCGGACCTTGTGT TTATATTT-3'; shRNA-2: 5'-CCATGACAAATTCG CTGAATA -3'; in lentiviral pLKO.1 vector (Sigma). Transfection was performed according to a published protocol using polyethylenimine (Longo et al., 2013). Mouse CAD cells were plated in a 24-well plate on coverslips. Control or RBM8a shRNAs (0.5 µg) were co-transfected with a GFP reporter (0.1 µg). To determine the knockdown effect of RBM8a, cells were fixed in 4 % paraformaldehyde 48 h post transfection and stained with RBM8a antibody. To generate stable SH-SY5Y cell line, pTRIPZ-mCherry or pTRIPZ-mCherry-RBM8a were co-transfected with psPAX2, pCMV-VSVG, into 293 T cells using PEI method. VSVG-pseudotyped lentiviruses were collected 48 after transfection and concentrated by ultracentrifugation at 36,000 rpm for 90 min (Mao and Lee, 2005). The lentiviruses expressing pTRIPZ-mCherry or pTRIPZ-mCherry-RBM8a were co-infected with virus expressing rtTA in SH-SY5Y cells at multiplicity of infection (MOI) =20. Stable clones were selected by puromycin selection.

### 2.2.9 Slice Electrophysiology

Whole-cell patch-clamp electrophysiology was conducted as published previously (Crowley et al., 2016; Pleil et al., 2015). Briefly, mice were anesthetized with 1-2% isoflurane anesthesia and rapidly decapitated. Brains were removed and immediately placed in ice-cold oxygenated (95% O<sub>2</sub>/5% CO<sub>2</sub>) high-sucrose artificial cerebrospinal fluid (aCSF) (containing the following, in mM: 194 sucrose, 20 NaCl, 4.4 KCl, 2 CaCl<sub>2</sub>, 1 MgCl<sub>2</sub>, 1.2 NaH<sub>2</sub>PO<sub>4</sub>, 10.0 glucose, and 26.0 NaHCO<sub>3</sub>). 300μM cortical slices containing the somatosensory cortex were prepared on a Leica VT1200s vibratome, and immediately placed in oxygenated heated (30°C) aCSF (containing the following, in mM: 124 NaCl, 4.4 KCl, 2 CaCl, 1.2 MgSO<sub>4</sub>, 1 NaPO<sub>4</sub>, 10 glucose, 26 NaHCO<sub>3</sub>) where they were allowed to recover for at least one hour. Recording electrodes (3–7 MΩ) were pulled from thin-walled borosilicate glass capillaries with a Flaming-Brown Micropipette Puller. Pyramidal neurons were selected based on morphology and general location. Spontaneous excitatory post synaptic currents (sEPSCs) and inhibitory post-synaptic currents (sIPSCs) were recorded in the same neurons at a holding potential of -55mV (sEPSCs) and +10mV (sIPSCs) using a cesium-methansulfonate based intracellular solution (containing the following, in mM: 135 cesium methansulfonate, 10 KCl, 1 MgCl<sub>2</sub>, 0.2 EGTA, 2 QX-314, 4 MgATP, 0.3 GTP, 20 phosphocreatine, pH 7.3, 285-290 mOsmol). Signals were digitized at 10 kHz and filtered at 6 kHz using a Multiclamp 700B amplifier and analyzed using Clampfit 10.3 software (Molecular Devices, Sunnyvale, CA).

### 2.2.10 Mouse Behavior

#### *Open Field Test*

The open field test was conducted as previously described in (McSweeney and Mao, 2015). Mice were placed individually in a novel open field (opaque acrylic box, 40x40x40cm) in a brightly lit room for 5 min. A video camera recorded the movement of the mice, and total distance travelled, duration, and frequency of entries into the center (13.3x13.3cm) was recorded using Ethovision XT software. The open field apparatus was cleaned with 70% ethanol between trials, and thoroughly dried.

#### *Forced Swim Test*

The forced swim test was conducted as previously reported in (McSweeney and Mao, 2015). Mice were gently placed in a bucket of room temperature water, ensuring their head was not submerged. Mice were observed for 6 min using Ethovision XT, the amount of time spent floating (immobility of 11%) vs swimming was assessed. After 6 min, the mice were removed and dried using a paper towel.

#### *Contextual Fear Conditioning*

Contextual fear conditioning was conducted as previously reported in (Shoji et al., 2014; Zou et al., 2016). On the first day of fear conditioning, the mice were individually placed in the fear conditioning apparatus for 5 min to explore and acclimate. The day after the acclimation session, they were placed in the testing chamber and received three tone stimuli at 58 second intervals. The tone lasted 20 seconds and was at 85 dB and 2.8 kHz. The tone co-terminated with a 0.55mA foot shock. The mouse was immediately removed after the last foot shock. 24 hours after the training period the mice were placed back in the fear conditioning apparatus for 4 min for a memory recall test. There was no tone or shock during this session. The amount of time freezing was measured using sensors at the bottom of the apparatus. Between mice the apparatus was cleaned using 70% ethanol and allowed to dry.

## Chapter 3

### **RBM8a is a positive regulator of embryonic NPC proliferation**

In this study Yingwei Mao and Donghua Zou completed the *in utero* electroporation experiments. This study was published in Neural Development (Zou et al., 2015).

#### **3.1 Introduction**

RBM8a has been shown to be important for RNA regulation through its role in NMD, but increasing evidence has indicated it may have an important role in development. Other EJC proteins, such as Magoh, have been shown to be critical for normal neural development, and Magoh haploinsufficiency leads to microcephaly, disorganized cortices and aberrant asymmetric division (Silver et al., 2010). Since RBM8a forms a heterodimer with Magoh and because Magoh is critically important for normal brain development, it is likely that RBM8a also plays a role in development of the nervous system. In addition, RBM8a has been independently linked to developmental abnormalities, including TAR syndrome and rare cases of ASD. Therefore, we hypothesized that RBM8a plays an important role in neural development, and when perturbed may result in these clinical phenotypes. To test this hypothesis, we utilized *in utero* electroporation of mouse embryos to modulate RBM8a expression during corticogenesis and observe corresponding effects on cortex development.

#### **3.2 RBM8a is highly expressed during embryonic development**

First, we sought to determine whether RBM8a is actively expressed during embryonic brain development of mice. To test this, brain lysates of mice of different developmental stages

(E9 – adulthood) were collected, and tested for RBM8a expression using western blot (Figure 3-1A). RBM8a expression was highest from E10-E13, and decreased with development to relatively low expression in adulthood. Next, we probed western blots for Tuj1 (differentiated neuronal marker), Sox2 (neural stem cell marker), and  $\beta$ -actin (load control). Interestingly, the decrease in RBM8a expression coincided with the increase in Tuj1 expression and decrease of Sox2 expression, reminiscent of neural differentiation (Figure 3-1A). This lead us to conclude that downregulation of RBM8a likely occurs when a cell differentiates from a NPC to a neuron. To further test this hypothesis, we cultured E14 NPCs from WT mice and collected lysates from cells pre-and post-differentiation *in vitro*. Pre-differentiated cells showed high RBM8a and Sox2 and low Tuj1 expression. Upon differentiation, RBM8a expression dramatically decreased, while Tuj1 expression was upregulated and Sox2 expression was slightly downregulated (Figure 3-1B). Thus, RBM8a expression decreases upon differentiation of NPCs. We then confirmed these results using immunohistochemistry of brain sections. RBM8a co-localized with the neural stem cell marker, nestin, but not with the immature neuronal marker, doublecortin (DCX) (Figure 3-1C-D). Thus, RBM8a is selectively expressed in stem cells and perhaps early neural progenitor cells.

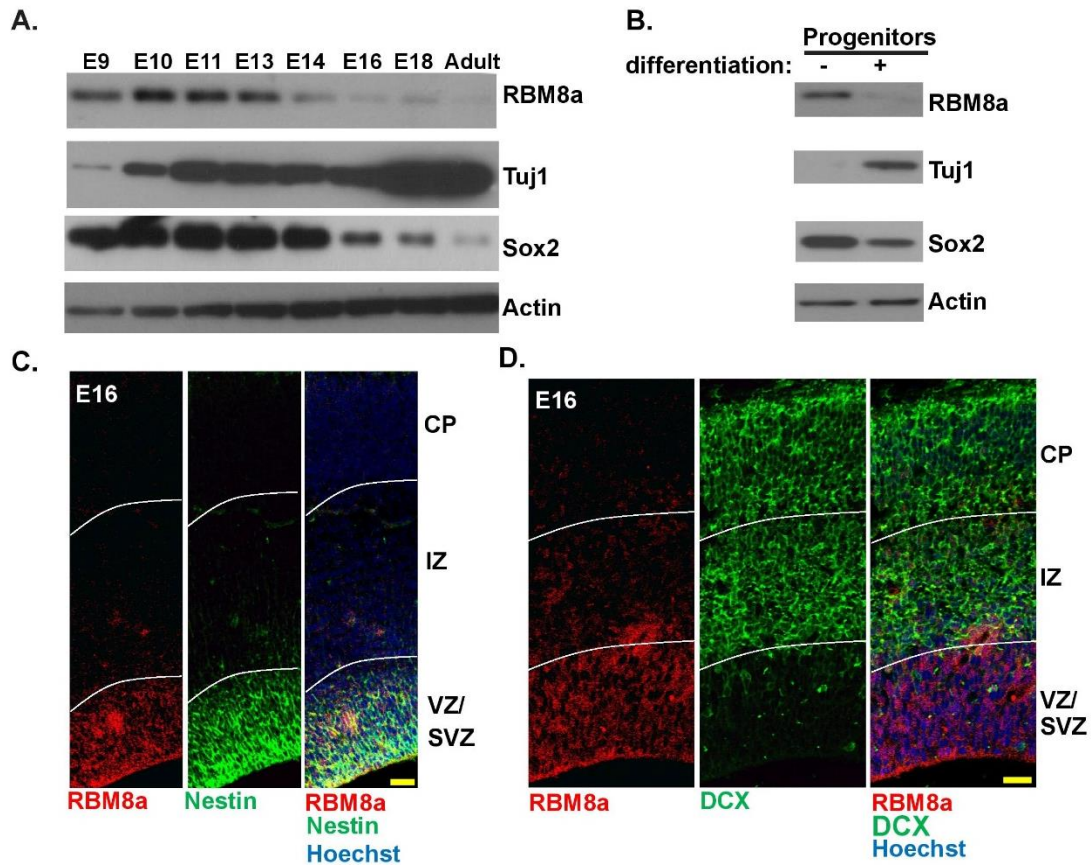


**Figure 3-1. RBM8a expression in the embryonic brain**

A) RBM8a expression in brain lysate from E9-adult illustrates RBM8a expression is highest during E10-11 and decreases during development. B) RBM8a is highly expressed in undifferentiated NPCs, and decreases in expression upon differentiation. C) Co-immunostaining of E16 brains with RBM8a (red), neural stem cell marker nestin (green), and DNA stain Hoechst (blue). D) Co-immunostaining of E16 brains with RBM8a (red), immature neuronal marker (Dcx) and DNA stain Hoechst (blue). RBM8a expression colocalizes with stem cell marker nestin, and not with immature neuron marker Dcx. Scale = 20 $\mu$ m.

### 3.3 RBM8a regulates the distribution of cells in the cortex

Next, we examined if modulating the expression level of RBM8a during development led to alterations in neurogenesis. To do this we electroporated E13 embryos with RBM8a knockdown or overexpression vectors or an empty vector as control, along with a GFP plasmid as a reporter. We then allowed the pups to develop *in utero* for three days before analyzing the

brains at E16. Sections of the developing cortices of mouse embryos were then immunostained for GFP and the number of GFP+ cell per area in the VZ/SZV, intermediate zone (IZ) or cortical plate (CP) quantified. When RBM8a was knocked down, there were significantly fewer GFP+ cells in the VZ/SVZ compared to controls, and significantly more GFP+ cells in the CP.

Conversely, when RBM8a was overexpressed, there were significantly more cells in the VZ/SVZ, and significantly fewer cells in the cortical plate (Figure 3-2). Thus, RBM8a regulates the transition from replicating NPCs in the VZ/SVZ to post mitotic neurons in the cortical plate.

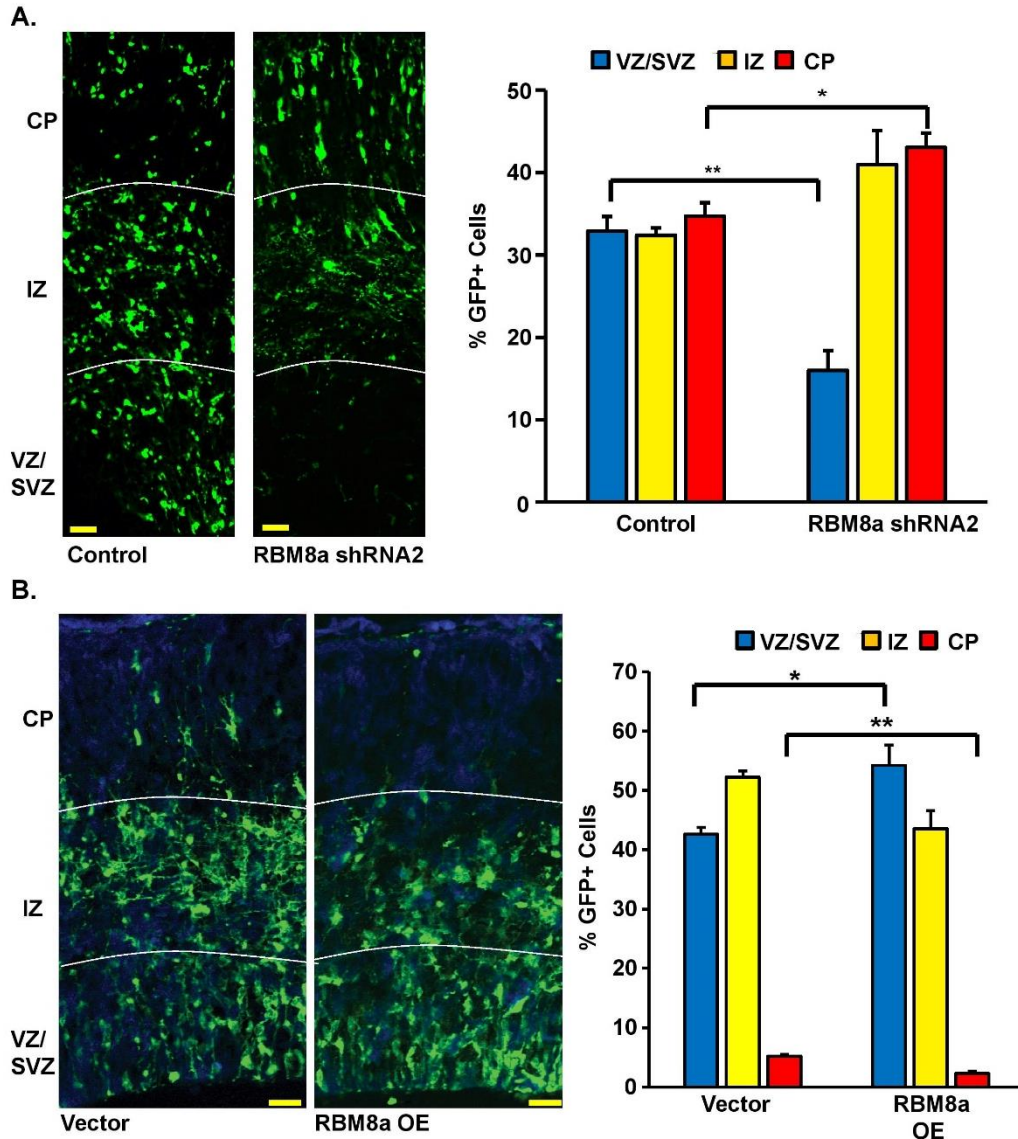


**Figure 3-2. RBM8a controls the balance between proliferation and differentiation**

A) Knockdown of RBM8a leads to decreased GFP+ cells in the VZ/SVZ and increased GFP+ cells in the CP. RBM8a shRNA or control vector were electroporated into the VZ/SVZ at E13 and allowed to develop *in utero* for three days. Coronal E16 brains were then immunostained for GFP and their position within the cortex was quantified. Scale = 20 $\mu$ m. \*  $p < 0.05$ , \*\*  $p < 0.01$ ,  $n=3$ , Student's t-test. B) Overexpression of RBM8a leads to increased GFP+ cells in the VZ/SVZ and decreased GFP+ cells in the CP. RBM8a overexpression or control vector were electroporated into the VZ/SVZ of E13 pups. Pups were then allowed to develop *in utero* for three days. E16 coronal slices were then stained for GFP and their position within the cortex was quantified. \*  $p < 0.05$ , \*\*  $p < 0.01$ ,  $n=3$ , Student's t-test. Bar graphs represent means  $\pm$  SEMs.

### **3.4 RBM8a is a positive regulatory of embryonic neural proliferation**

Since the formation of the cortex is highly dependent on neural proliferation, we examined if this change in cell positioning the cortex was due to abnormal proliferation and cell cycle exit. We co-electroporated RBM8a shRNA, overexpression plasmid, or control vector with GFP into E13 embryonic brains (VZ/SVZ), then pulse labeled replicating cells with BrdU (100mg/kg) for 2h before sacrifice at E16. BrdU will incorporate into cells during the DNA synthesis phase of the cell cycle. We then co-stained the E16 brains for BrdU, GFP, and Ki67. Cells that are BrdU/GFP double positive are cells in the S phase of the cell cycle, and cells that are Ki67/GFP double positive are cells that are in any phase of the cell cycle (G1, S, G2, M). When RBM8a is knocked down there is a significant decrease in the number of cells in the S phase of the cell cycle (BrdU/GFP double positive), as well as a significant decrease in the number of cells in any phase of the cell cycle (G1, S, G2, excludes quiescent cells in the G0 phase) (Ki67/GFP double positive) (Figure 3-3).

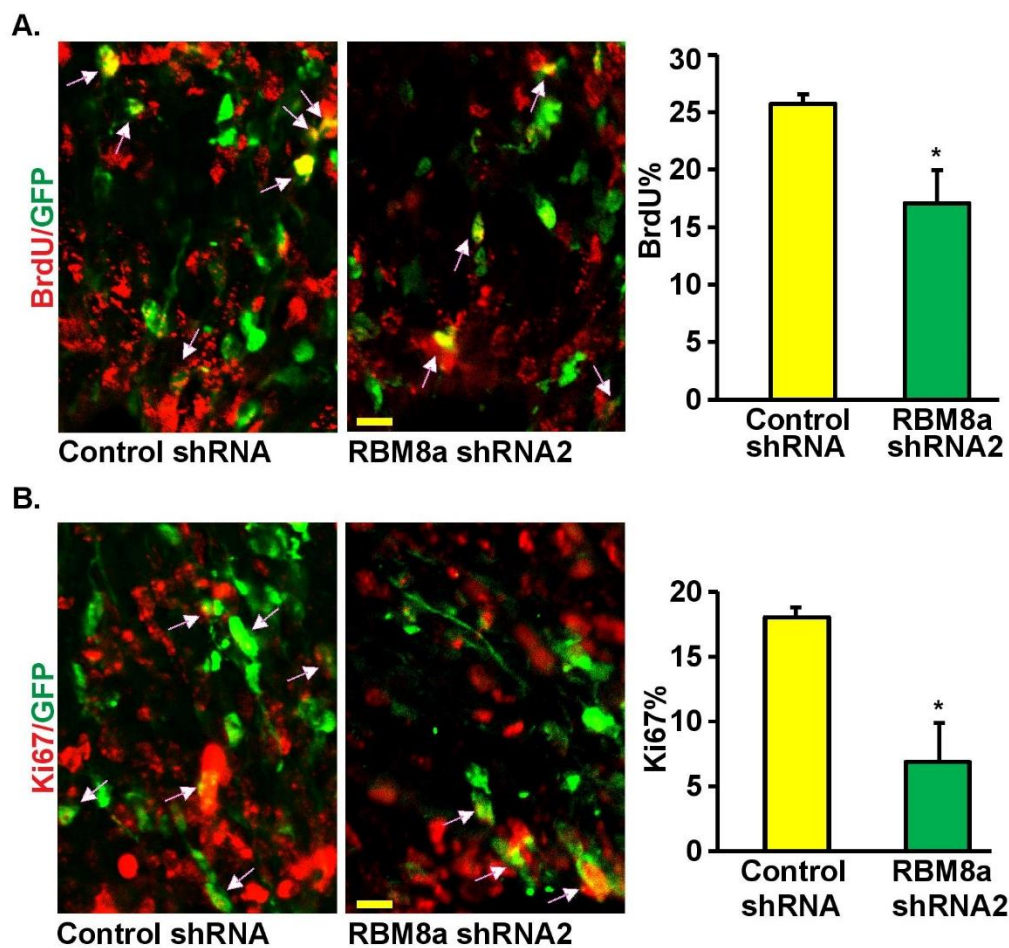


**Figure 3-3. RBM8a knockdown results in decreased proliferation**

A) RBM8a knockdown leads to a decreased percentage of cells in the S phase of the cell cycle. *In utero* electroporation was performed on E13 pups using RBM8a shRNA or control vector. Pups were then allowed to develop *in utero* for three days. Two hours before sacrifice, the pregnant dam was pulse labeled with BrdU. Coronal brain slices (E16) were then stained for GFP (green), and BrdU (red). Proliferation was indirectly assayed by quantifying the number of cells that were GFP and BrdU double positive. These cells represent cells that took up the plasmid, and were in the DNA synthesis phase of the cell cycle at the time of BrdU injection. Arrowheads indicate BrdU/GFP double positive cells, Scale = 10 $\mu$ m. \*,  $p < 0.05$ ,  $n = 3$ , Student's t-test. B) RBM8a knockdown leads to a decrease in percentage of cells active in the cell cycle (non-quiescent). The brains obtained from A) were stained for GFP (green) and Ki67 (red). GFP and Ki67 double positive cells were quantified in order to identify the percentage of cells that were active in the cell cycle at the time of sacrifice. Arrows indicate double positive cells. \*,  $p < 0.05$ ,  $n = 3$ , Student's t-test. Bar graphs represent means  $\pm$  SEMs.

Conversely, when RBM8a is overexpressed, there are significantly more cells in the S phase of the cell cycle (BrdU/GFP double positive), and significantly more cells within the cell cycle (Ki67/GFP double positive) (Figure 3-4).

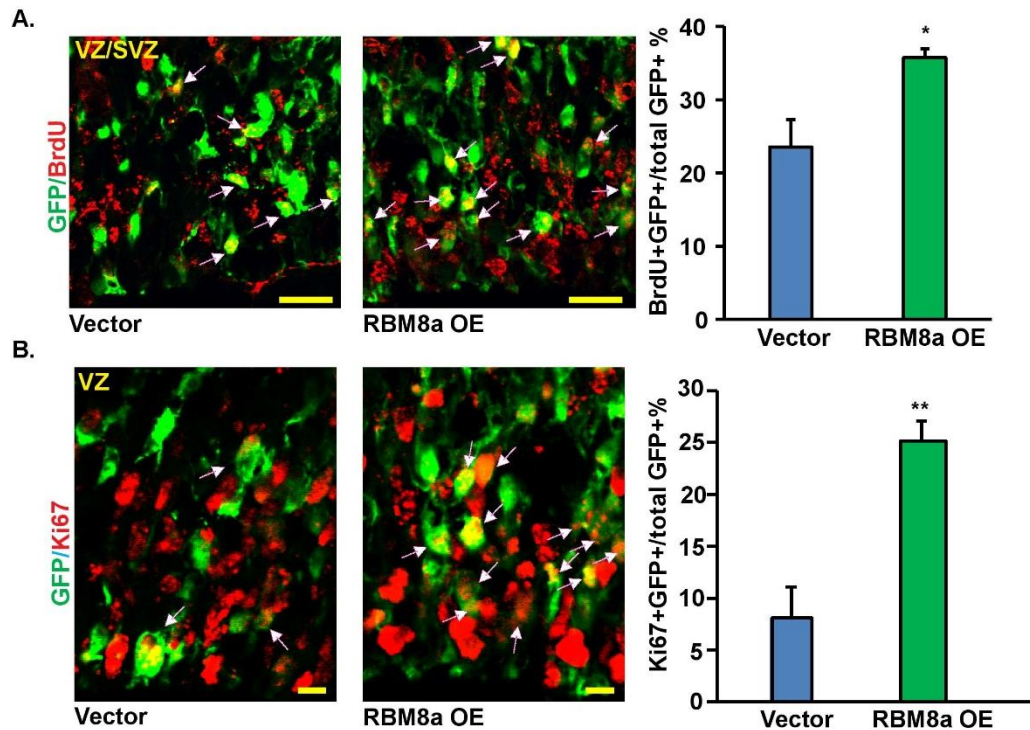


**Figure 3-4: RBM8a overexpression leads to increased proliferation**

A) RBM8a overexpression leads to an increased percentage of cells in the S-phase of the cell cycle. RBM8a OE or control vector was electroporated into E13 embryos, then pulse chased with BrdU 2hr before sacrifice on E16. Brains were stained with anti BrdU (red) and anti GFP (green) antibodies. Double positive cells were quantified to indirectly measure the percentage of proliferating cells at after BrdU injection and the two hours following. Arrowheads indicate BrdU/GFP double positive cells, Scale bar=10 $\mu$ m. \*,  $p < 0.05$ , Students t-test. B) RBM8a overexpression leads to an increased percentage of cells active in the cell cycle. Brain sections from A) were stained with anti Ki67 (red) and anti GFP (green) antibodies. GFP and Ki67 double positive cells were quantified to identify the percentage of cells that were active in the cell cycle at the time of sacrifice. Arrowheads indicate Ki67/GFP double positive cells. \*\*,  $p < 0.01$ ,  $n=3$ , Student's t-test. Bar graphs represent means  $\pm$  SEMs.

### **3.5 RBM8a regulates cell cycle exit and neural progenitor differentiation**

Since we determined RBM8a to be a positive regulator of embryonic neural progenitor proliferation, we hypothesized that it regulates proliferation through modulation of the cell cycle. To assess this, we analyzed cell cycle exit in the embryonic brains. We electroporated RBM8a or control shRNA into E13 mice, pulse chased with BrdU at E15, then sacrificed the mice at E16. The brains were then stained with anti-BrdU, anti-GFP, and anti-Ki67 antibodies. Cell cycle exit was quantified by counting the number of BrdU+/GFP+/Ki67- cells. This indicates the cells that received the knockdown or overexpression plasmid (GFP), and that they were in the DNA synthesis phase of the cell cycle at the time of BrdU injection, but exited the cell cycle (and therefore were Ki67 negative) upon sacrifice at E16. When RBM8a was knocked down there was a significant increase in cell cycle exit of progenitor cells (Figure 3-5A). We then co-stained brain slices with neuronal marker Tuj1 and GFP to determine the number of differentiated neuronal cells. Consistently, after RBM8a knockdown, we observed significantly more differentiated neuronal cells (Tuj1/GFP double positive) (Figure 3-5B).

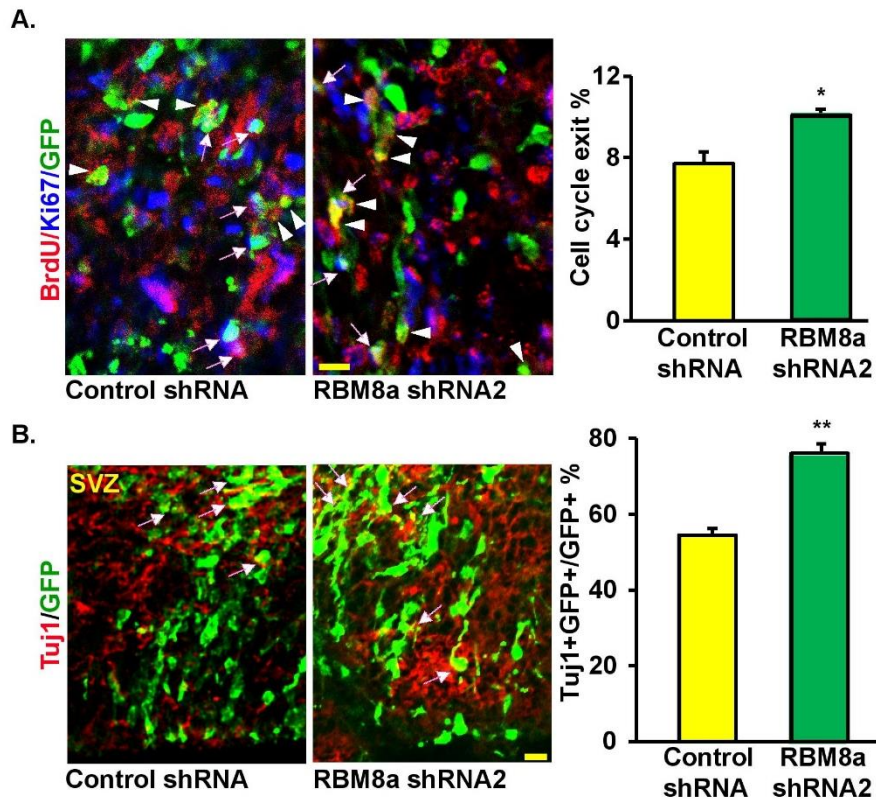


**Figure 3-5 RBM8a regulates cell cycle exit**

A) RBM8a knockdown leads to an increase in cells exiting the cell cycle. Control or RBM8a shRNA were electroporated into E13 embryonic brains. BrdU was injected at E15 and mice were sacrificed at E16. E16 coronal brain slices were stained with anti-BrdU (red), anti-Ki67 (blue) and anti-GFP (green) antibodies. BrdU +, GFP + and Ki67- cells were quantified to determine the percentage of cells that exited the cell cycle. Arrowheads indicate BrdU+/GFP+/Ki67- cells. Scale bar = 10 $\mu$ m. \*,  $p < 0.05$ ,  $n = 3$ , Students t-test. B) RBM8a knockdown leads to an increase in neuronal differentiation. Brain slices from A) were stained for TuJ1 (red) and GFP (green). TuJ1 and GFP double positive cells were quantified to determine the percentage of cells differentiating into neurons. Arrowheads indicate TuJ1/GFP double positive cells. \*\*,  $p < 0.01$ ,  $n = 3$ , Students t-test. Bar graphs represent means  $\pm$  SEMs.

We then looked at whether RBM8a overexpression affected cell cycle exit and differentiation. Similar to the knockdown protocol, E13 mice were electroporated with RBM8a overexpression or control plasmids, then pulse chased with BrdU on E15 followed by sacrifice at E16. When RBM8a is overexpressed, there is a decrease in cell cycle exit (BrdU+/GFP+/Ki67-), and a decrease in neuronal differentiation (Tuj1/GFP double positive) (Figure 3-6).

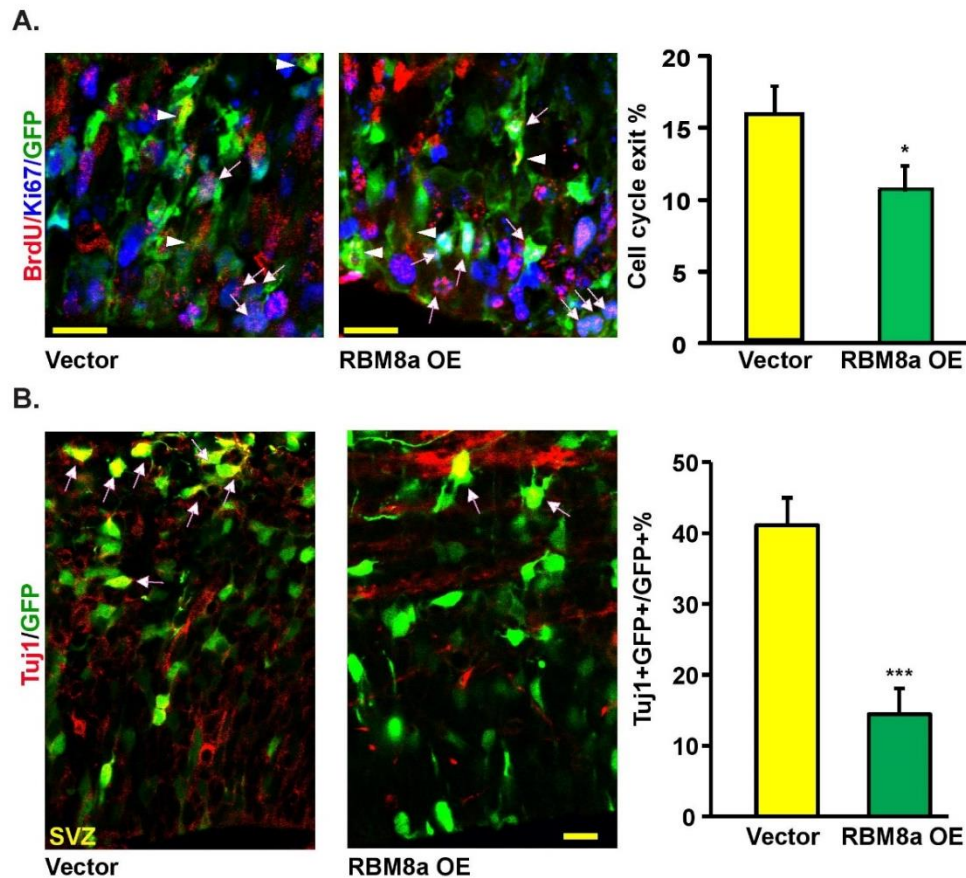


**Figure 3-6: RBM8a overexpression leads to decreased cell cycle exit**

A) RBM8a overexpression leads to decreased cell cycle exit. Control or RBM8a overexpression plasmids were electroporated into E13 embryonic brains. BrdU was injected at E15 and mice were sacrificed at E16. Brains were stained with anti-BrdU (red), anti-Ki67 (blue) and anti-GFP (green) antibodies. BrdU+, GFP+ and Ki67- cells were quantified to determine the percentage of cells exiting the cell cycle. Arrowheads indicate BrdU+/GFP+/Ki67- cells. Scale bar=10 $\mu$ m. \*,  $p < 0.05$ ,  $n = 3$ , Student's t-test. B) Brain slices from A) were stained for Tuj1 (red) and GFP (green). Tuj1 and GFP double positive cells were quantified to determine the percentage of cells differentiating into neurons. Arrowheads indicate Tuj1/GFP double positive cells. \*\*,  $p < 0.01$ , Student's t-test,  $n = 3$ . Bar graphs represent means  $\pm$  SEMs.

### **3.6 Conclusion**

These results indicate RBM8a's critical role in the proliferation and differentiation of embryonic neural progenitors. It appears that RBM8a helps regulate the balance between cells remaining in their proliferative state, and cells differentiating and migrating. When RBM8a is overexpressed, the balance is shifted toward self-renewal, so there is an expansion of the stem cells pool at the expense of differentiating NCPs. Conversely, when RBM8a is knocked down, the balance shifts toward differentiation, leading to depletion of the stem cell pool and precocious differentiation of NPCs. This change is mediated by alterations of the cell cycle in cells with abnormal RBM8a expression.

## Chapter 4

### **RBM8a haploinsufficiency leads to microcephaly and early postnatal lethality**

#### **4.1 Introduction**

Our results in Chapter 3 indicate that RBM8a is vital to neural development, and specifically is a positive regulator of NPC proliferation. However, these observed effects are limited to a small portion of the cortex, due to the limitations of *in utero* electroporation. To further probe this developmental role of RBM8a, and examine its effects on the entirety of the nervous system, we generated a conditional knockout mouse. This allowed us to examine all of the cortex, and other areas of the nervous system, and examine how cellular changes affect survival, brain structure and behavior.

#### **4.2 Generation and Verification of knockout mouse**

To further probe the developmental role of RBM8a, we generated a conditional knockout mouse (cKO). The targeting vector contains loxp sites flanking exons 2-4 of the RBM8a gene. Frt sites then flank a neomycin cassette in between exons 4 and 5 to use for selection (Figure 4-1). After selection, the neomycin cassette was removed to avoid potential detrimental effects. This was done by crossing floxed mice with actin-flpe mice, which excises the neomycin cassette. Mouse genotypes were determined using PCR to detect the presence of the loxp site, and/or cre (Figure 4-1B-C). To verify the knockout, we isolated fibroblasts from RBM8a<sup>fl/fl</sup> mice and cultured them. After infection with RFP-cre, the cultured fibroblasts infected with the virus showed no RBM8a expression. This indicates that cre expression successfully knocked out

RBM8a (Figure 4-1D). We then collected lysate from these cells and used western blot to verify that no RBM8a protein was detected (Figure 4-1E).

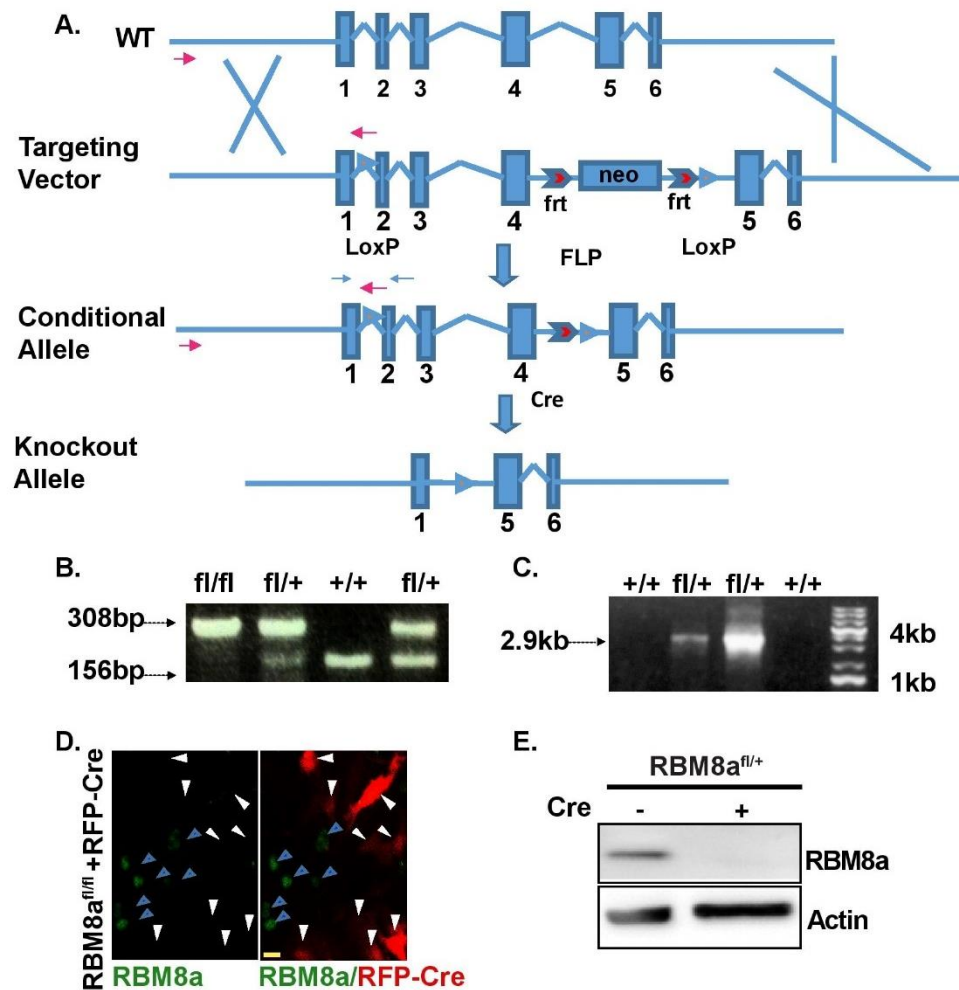


**Figure 4-1: RBM8a is successfully knocked out in cells expressing cre**

A) Strategy for conditional knockout of RBM8a. Pink arrows indicate the 5' long arm primers, blue arrows indicate the loxp primers. Blue arrows with pink insides indicate frt sites. B) LoxP using the primers indicated in blue in A indicating that the loxp site is present in the correct place in the 5' arm of the floxed mouse. C) Cre PCR indicating the loxp site present in the correct place on the 3' arm. Using the primers indicated in pink in A. Arrow indicates where a 2.9kb band should reside. D) Fibroblasts isolated and cultured from homozygous floxed mice. RBM8a is removed upon infection with RFP-cre. White arrows indicate cells expressing cre, and blue arrows indicate cre negative cells. E) Western blot detecting RBM8a expression using the lysate from isolated fibroblasts, with and without cre.

### 4.3 RBM8a haploinsufficiency causes microcephaly

Next, RBM8a<sup>fl/fl</sup> mice were crossed with Nestin-cre mice (neural stem cell specific cre). The resulting progeny consisted of 50% Nes-cre;RBM8a<sup>fl/+</sup> mice and 50% RBM8a<sup>fl/+</sup> mice. This indicates that the mice are haploinsufficient for RBM8a are born at the expected Mendelian ratio. Littermates without nestin can be used as comparative controls. Nes-cre;RBM8a<sup>fl/+</sup> deletes RBM8a in neural stem cells, which give rise to the entirety of the nervous system including most glia. The resulting RBM8a haploinsufficient mice were significantly shorter in length (cKO is 4.8cm and control is 5.8cm) and weight (cKO is 4.03g compared to the control which is 6.1g) compared to littermate controls, and have microcephaly, which is defined as a greater than 50% reduction in brain weight (0.16g in the cKO compared to 0.445 in the controls) (Figure 4-2 A-B). In particular, Nes-cre;RBM8a<sup>fl/+</sup> mice have smaller cortices, and brain hemispheres that fail to meet on the midline, leaving a large gap (Figure 4-3A). Using western blot, we verified that Nes-cre;RBM8a<sup>fl/+</sup> mice have an approximately 50% reduction in RBM8a expression (Figure 4-2C).

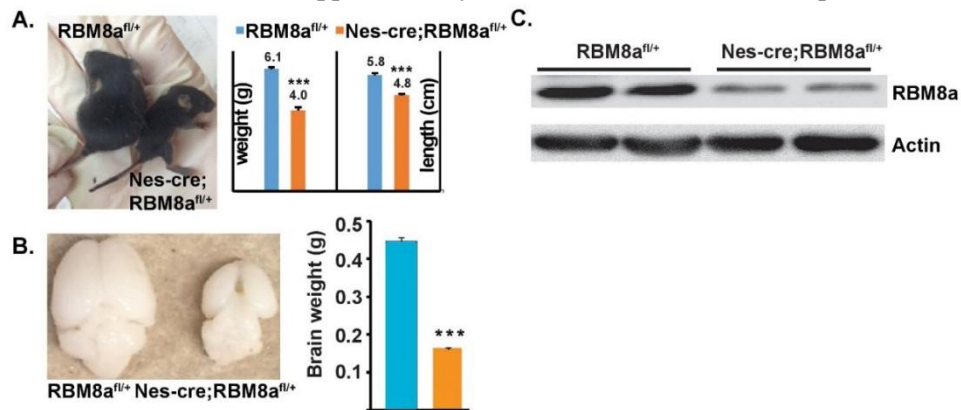


**Figure 4-2: RBM8a haploinsufficiency modulates brain size**

A) Nes-cre;RBM8a<sup>fl/+</sup> are smaller than littermate controls at P12 in both body weight and length. \*\*\*,  $p=5.4 \times 10^{-5}$  (weight),  $p=1.4 \times 10^{-4}$  (length),  $n=3$ , Student's t-test. B) Nes-cre;RBM8a<sup>fl/+</sup> mice suffer from microcephaly (small brain), even when adjusting for their smaller body size. \*\*\*,  $p=1.9 \times 10^{-5}$ ,  $n=3$ , students t-test. C) Nes-cre;RBM8a<sup>fl/+</sup> mice show an approximately 50% reduction in RBM8a protein expression, as determined by western blot. Bar graphs represent means +/- SEMs.

#### **4.4 Organ deficits in the cKO mice are specific to the nervous system**

Additionally, these mice have structural abnormalities in the hippocampus, specifically an upturned dentate gyrus, rounded CA2/3, and less cell dense CA1 (Figure 4-3B). Nes-cre;RBM8a<sup>fl/+</sup> mice also have a thinner, and less cell dense cortex (Figure 4-3C-D). We then examined the rest of the organs in the knockout mice. While there was a significant reduction in the weight of the kidney and the spleen in the cKO mice, this was rendered non-significant when normalizing the organ weight to the weight of the much smaller cKO mice (Figure 4-3E-F). Therefore, it seems the deficiencies in the cKO mice are specific to the nervous system.

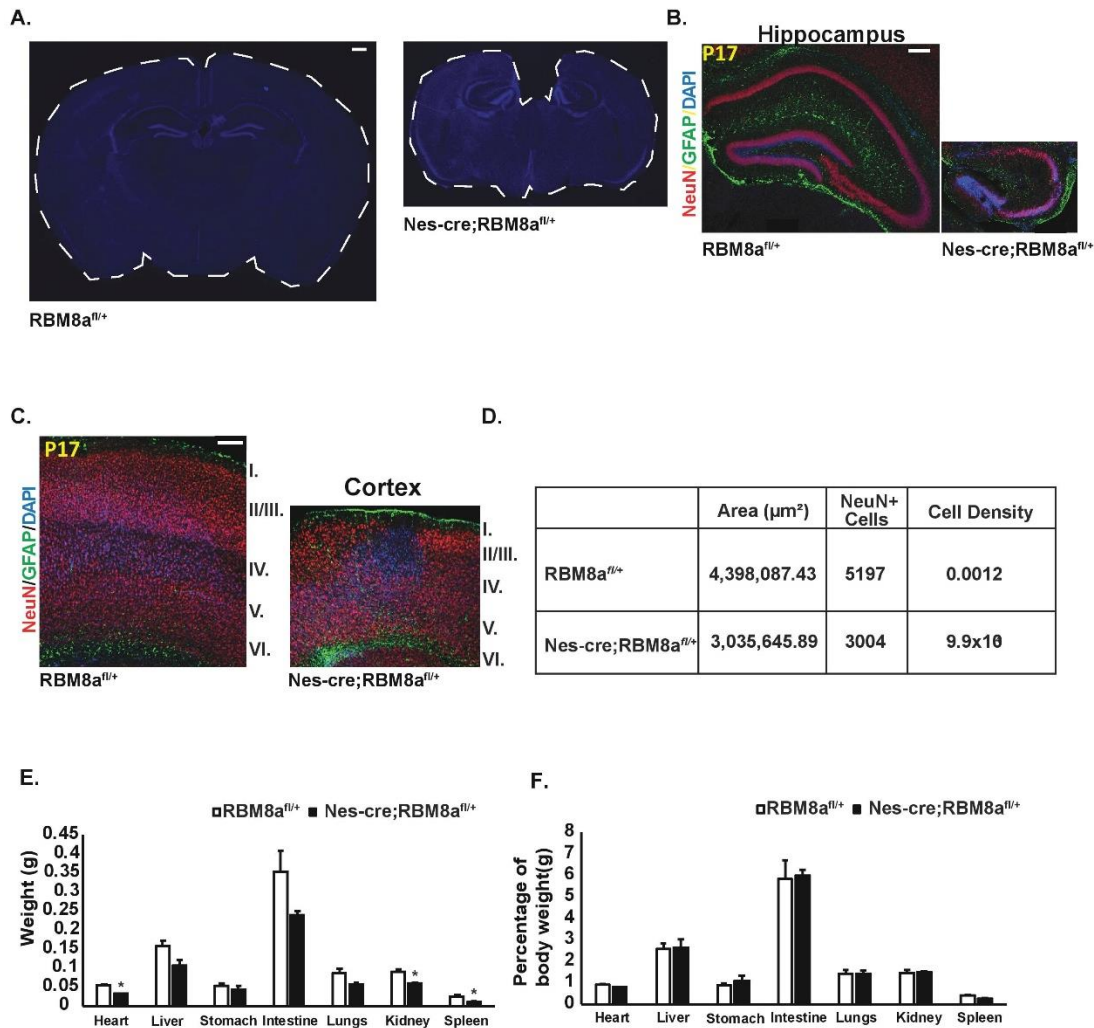


**Figure 4-3: RBM8a haploinsufficiency leads to microcephaly and profound cortical deficits**

A) Nes-cre;RBM8a<sup>fl/+</sup> mice have a smaller brain than RBM8a<sup>fl/+</sup> controls, and have cortical hemispheres that fail to meet at the midline, causing a large gap between the two cortical hemispheres. DAPI staining of coronal brain slices at P17. Scale bar = 50 $\mu\text{m}$ . B) P17 hippocampus of Nes-cre;RBM8a<sup>fl/+</sup> mice and littermate controls stained for mature neuronal neuronal marker NeuN (red), reactive astrocyte marker GFAP (green) and DNA marker DAPI (blue). C) P17 cortex stained for NeuN (red), GFAP (green) and DAPI. Nes-cre;RBM8a<sup>fl/+</sup> mice have a thinner cortex and less cell dense cortex (D). D) Quantification of the cell density of NeuN+ cells. E) Weight of organs of the Nes-cre;RBM8a<sup>fl/+</sup> mice compared to littermate controls. F) Weight of organs normalized to body weight of the Nes-cre;RBM8a<sup>fl/+</sup> mice (the percentage of the mouse's body weight of each organ) compared to littermate controls,  $p < 0.05$ ,  $n=3$ , Students t-test. When overall body weight of the mouse is taken into account, the only organ significantly changed in the Nes-cre;RBM8a<sup>fl/+</sup> mice was the brain. Bar graphs represent means  $\pm$  SEMs.

#### **4.5 RBM8a haploinsufficiency causes disorganized cortical layers**

As these mice have thin cortices, we hypothesized that they also had perturbations in the cortical layers. This could manifest in the form of thinner layers, or disorganized cortical layers (cells migrating to the wrong layer). To test this we immunostained coronal brain section of P17 Nes-cre;RBM8a<sup>fl/+</sup> mice and littermate controls with superficial layer marker Cux1 and deep cortical layer marker Foxp2. Foxp2 staining was revealed to be abnormal. Instead of staining layers 5/6 like in the control, Foxp2 labeling was found in the middle cortex, in putative layers 4/5. Cux1 staining was similarly labeling. While the lateral cortex showed the correct Cux1 distribution medially Cux1+ cells were found in the deep cortex when they should have been in the superficial cortex. This led us to accept the second hypothesis, that the thin layers were due to disorganization of the laminar structure of the cortex (Figure 4-4).

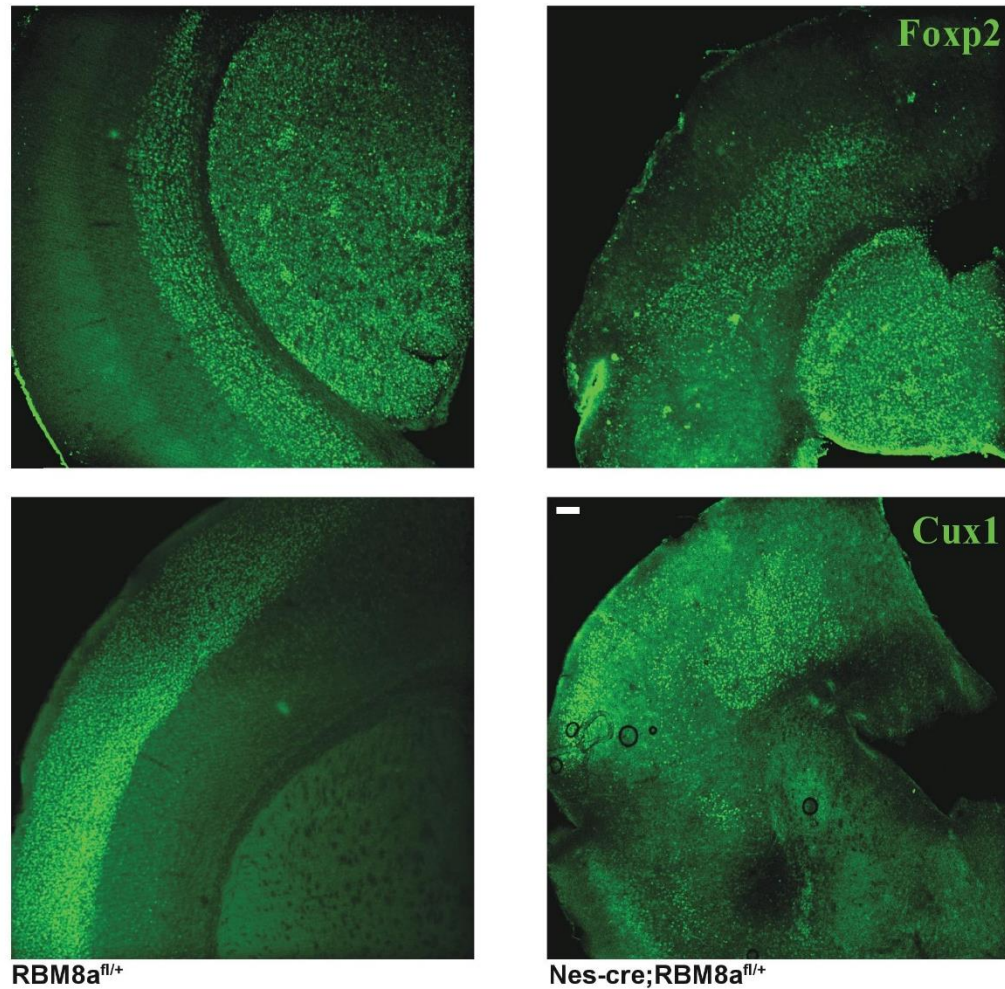


**Figure 4-4: RBM8a haploinsufficiency leads to microcephaly and profound cortical deficits**

Coronal sections of P17 Nes-cre;RBM8a<sup>fl/+</sup> and RBM8a<sup>fl/+</sup> mice brains were immunostained for the deep cortical layer marker FoxP2 (top), and the superficial layer marker Cux1 (bottom). Scale bar = 100 $\mu$ m. Nes-cre;RBM8a<sup>fl/+</sup> mice had abnormal distribution of FoxP2 (not present in putative layer 6), and Cux1 (stains deep layers in the medial cortex) staining.

#### 4.6 Conclusion

In this chapter, we concluded that RBM8a is indeed extremely important to neurodevelopment, and is in fact critical for survival. We also determined that RBM8a affects

more than just the cortex (observed in Chapter 2), and actually indicates that RBM8a affects the whole nervous system, but not other organ systems (when using a neuron specific cre). We showed that RBM8a haploinsufficiency leads to failure for the cortical hemispheres to meet on the midline, early post-natal lethality, structural abnormalities in the hippocampus and decreased cell density in the cortex.

## Chapter 5

### **RBM8a is required for normal cortical interneuron development**

#### **5.1 Introduction**

In Chapter 4 we confirmed previous results from (Mao et al., 2015), that RBM8a haploinsufficiency leads to disorganized cortical layers. We were interested in further exploring this phenotype by looking at different cell types in the cortex, and if they too form disorganized cortical layers. When observing our Nes-cre;RBM8a<sup>fl/+</sup> mice, we noticed they had spontaneous seizures around postnatal day 14-21. Since seizures are commonly caused by too little GABA signaling, we decided to focus specifically on the interneuron population in the cortex.

#### **5.2 RBM8a cKO altered number and distribution of PV+ interneurons in the cortex**

Since PV+ interneurons are the most populous cortical interneurons, we assessed the number and distribution of PV+ interneurons in our Nes-cre;RBM8a<sup>fl/+</sup> mice. P17 brain slices were stained with an antibody against PV, and the number of cells and their placement in the cortex were quantified. Nes-cre;RBM8a<sup>fl/+</sup> had significantly fewer PV+ cells in the cortex, and abnormal distribution of PV+ cells (Figure 5-1A-C). To assess the position of the cell in the cortex, the brain slices were divided into sextets, each of equal size, and the number of PV+ cells was counted in each sextet. Significantly more PV+ cells were located in sextet 1 and 2 ( $p=6.1 \times 10^{-3} \pm \text{SEM}$  and  $5.7 \times 10^{-4} \pm \text{SEM}$  respectively) of the cortex of cKO mice (superficial), but significantly fewer PV+ cells were in sextet 4 and 5 ( $p=2.6 \times 10^{-3} \pm \text{SEM}$  and  $5.5 \times 10^{-5} \pm \text{SEM}$  respectively) (deep). Sextet 3 and 6 did not have any observable difference between Nes-

cre;RBM8a<sup>fl/+</sup> and RBM8a<sup>fl/+</sup> mice (0.89 mean  $\pm$ SEM and 0.29 mean  $\pm$ SEM respectively)(Figure 5-1A-B). The abnormalities in PV+ interneurons and the small size of the cerebral cortex lead us to further investigate whether the size of PV+ interneurons was changed in the Nes-cre;RBM8a<sup>fl/+</sup> mice. We calculated the area of cells in Nes-cre;RBM8a<sup>fl/+</sup> mice and RBM8a<sup>fl/+</sup> and found that PV+ interneurons in Nes-cre;RBM8a<sup>fl/+</sup> mice were significantly larger than the control mice (Figure 5-1D-E). Since we had a very large sample size for the cell size analysis, we ran a Cohen's  $\delta$  statistical test to determine if we saw significance solely due to the large sample size. A cohens  $\delta$  of 0.562 indicates it is likely that the large sample size was not a factor in our significant result.

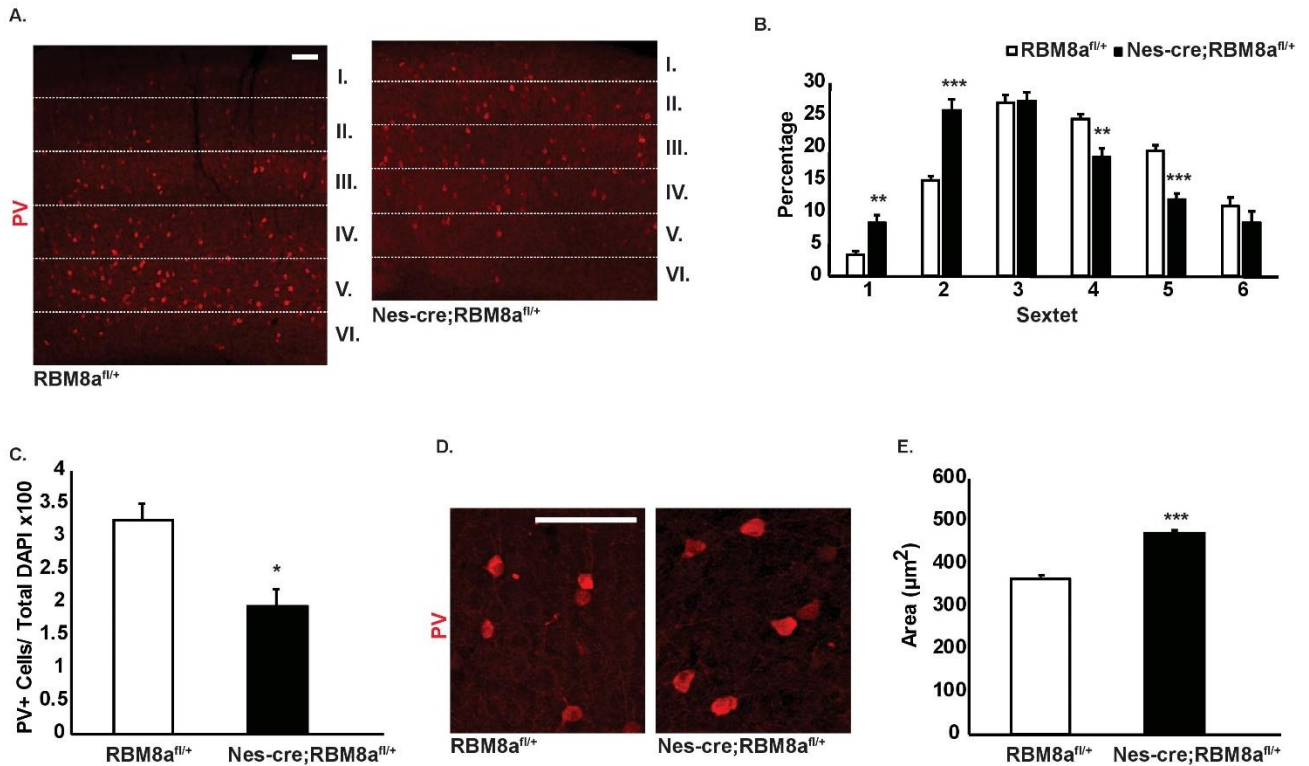


**Figure 5-1: RBM8a regulates the number, distribution and size of PV+ interneurons**

A) RBM8a haploinsufficiency leads to an altered distribution of PV+ interneurons in the cortex. PV+ interneurons are overrepresented in superficial layers, and less dense in deep cortical layers. Nes-cre;RBM8a<sup>fl/+</sup> and RBM8a<sup>fl/+</sup> mice were perfused at P17 and coronal brain slices were stained for PV. The cortex was divided into six equal bins termed “sextets”. Scale = 100µm. B) The number of PV+ cells in each sextet were quantified and divided by the total number of PV+ cells in the cortex, \*\*, p=0.01 (Sextet 1), p=0.003 (Sextet 4), \*\*\*, p=5.7 x 10<sup>-5</sup> (Sextet 2), p=5.5 x 10<sup>-5</sup> (Sextet 5), n=3, Students t-test. C) The total number of PV+ cells in the cortex was quantified, using slices obtained in A). \*, p=0.003, n=3, Students t-test. D) The PV+ cells in Nes-cre;RBM8a<sup>fl/+</sup> mice are significantly larger. E) The area of each cell was determined using ImageJ and quantified, \*\*\*, p=6.6 x 10<sup>-39</sup>, n=3, Students t-test,  $\delta=0.562$ , Cohens  $\delta$ . Bar graphs represent means +/- SEMs.

### 5.3 RBM8a cKO modulated the distribution of SST + interneuron in the cortex.

As SST+ interneurons are one of the next most abundant interneurons in the cortex, we further examined whether SST+ interneurons had an abnormal cell number and distribution. The

percentage of SST+ interneurons in the cortex was unchanged, but the distribution of SST+ cells in the cortex was abnormal compared to RBM8a<sup>fl/+</sup> mice (Figure 5-2A-C). There were significantly fewer SST+ cells in sextets 1 and a trend in sextet 2 in Nes-cre;RBM8a<sup>fl/+</sup>, (p=0.041±SEM and p=0.058±SEM respectively) and significantly more SST+ cells in sextet 3 (p=0.046±SEM). Sextets 4-6 remained unchanged (p=0.154, mean ±SEM for sextet 4 and p=0.80, mean ±SEM and p= 0.39, mean ±SEM respectively for sextets 5 and 6) (Figure 5-2C). We then examined cell size of SST+ interneurons, and found that SST+ interneurons are significantly larger in Nes-cre;RBM8a<sup>fl/+</sup> mice (Figure 5-2D-E). The Cohens  $\delta$  for this analysis was 0.359, indicating that though the change is significant, the effect is smaller than that of NPY or PV+ cell size.

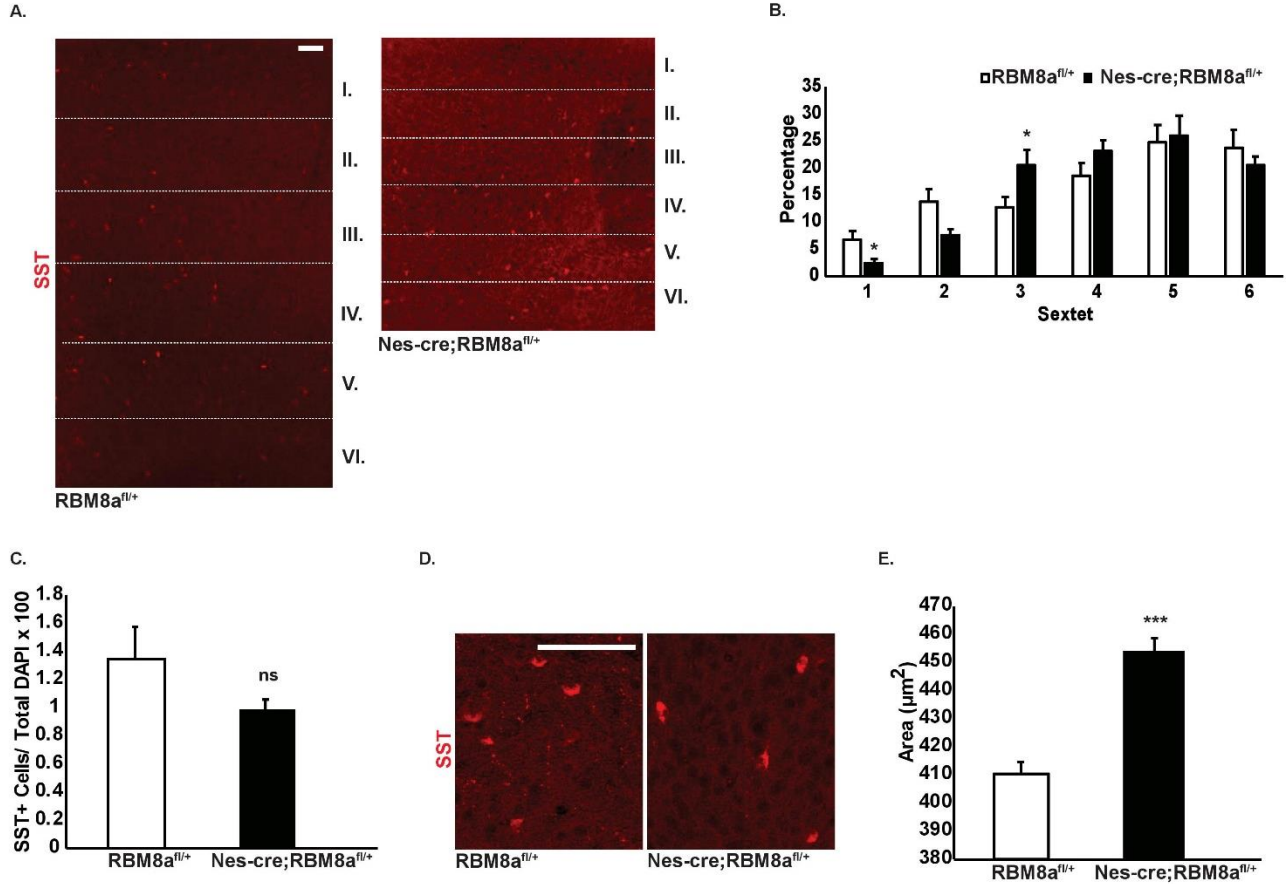


**Figure 5-2: RBM8a alters the distribution of SST+ interneurons but not the number**

A) Nes-cre;RBM8a<sup>fl/+</sup> mice have an altered distribution of SST+ interneurons in the cortex. Nes-cre;RBM8a<sup>fl/+</sup> mice had significantly fewer SST+ interneurons in sextet 1 (superficial cortex) and significantly more in sextet 3 (middle cortex). Nes-cre;RBM8a<sup>fl/+</sup> and RBM8a<sup>fl/+</sup> mice were perfused at P17 and coronal brain slices were stained for SST. The cortex was divided into six equal bins termed “sextets”, Scale = 100 μm. B) The number of SST+ cells in each sextet were quantified and divided by the total number of SST+ cells in the cortex, \*, p=0.042 (Sextet 1), p=0.046 (Sextet 3), Students t-test, n=3. C) The total number of SST+ cells in the cortex was quantified, p=0.15, mean ±SEM, n=3, students t-test. There was no observed change in the total number of cortical SST+ interneurons between Nes-cre;RBM8a<sup>fl/+</sup> and RBM8a<sup>fl/+</sup> mice. D) Nes-cre;RBM8a<sup>fl/+</sup> mice had significantly larger SST+ interneurons in the cortex. E). The area of each cell was determined using ImageJ and quantified, \*\*\*, p=1.1 x 10<sup>-17</sup>, Students t-test, n=3, δ=0.359, Cohens δ. Bar graphs represent means +/- SEMs.

#### 5.4 The effect of RBM8a cKO on NPY+ interneurons

We next examined the number and distribution of NPY+ interneurons in the cortex. Similar to PV, significantly fewer NPY+ interneurons were detected in the cortex of Nes-cre;RBM8a<sup>fl/+</sup> mice (Figure 5-3A-B). Additionally, these interneurons were significantly less abundant in sextets 1 and 2 ( $p=0.04\pm\text{SEM}$  and  $p=1.9 \times 10^{-3}\pm\text{SEM}$  respectively), and unchanged in sextets 3 and 5 ( $p=0.142\pm\text{SEM}$  and  $p=0.372\pm\text{SEM}$  respectively). Sextets 4 and 6 had trends ( $p=0.050\pm\text{SEM}$  and  $0.088\pm\text{SEM}$  respectively) (Figure 5-3C). The size of NPY+ interneurons was significantly larger in Nes-cre;RBM8a<sup>fl/+</sup> mice (Figure 5-3D-E). The Cohens  $\delta$  for this analysis was 0.793, which indicated there was a significant difference in cell size in the Nes-cre;RBM8a<sup>fl/+</sup> mice.

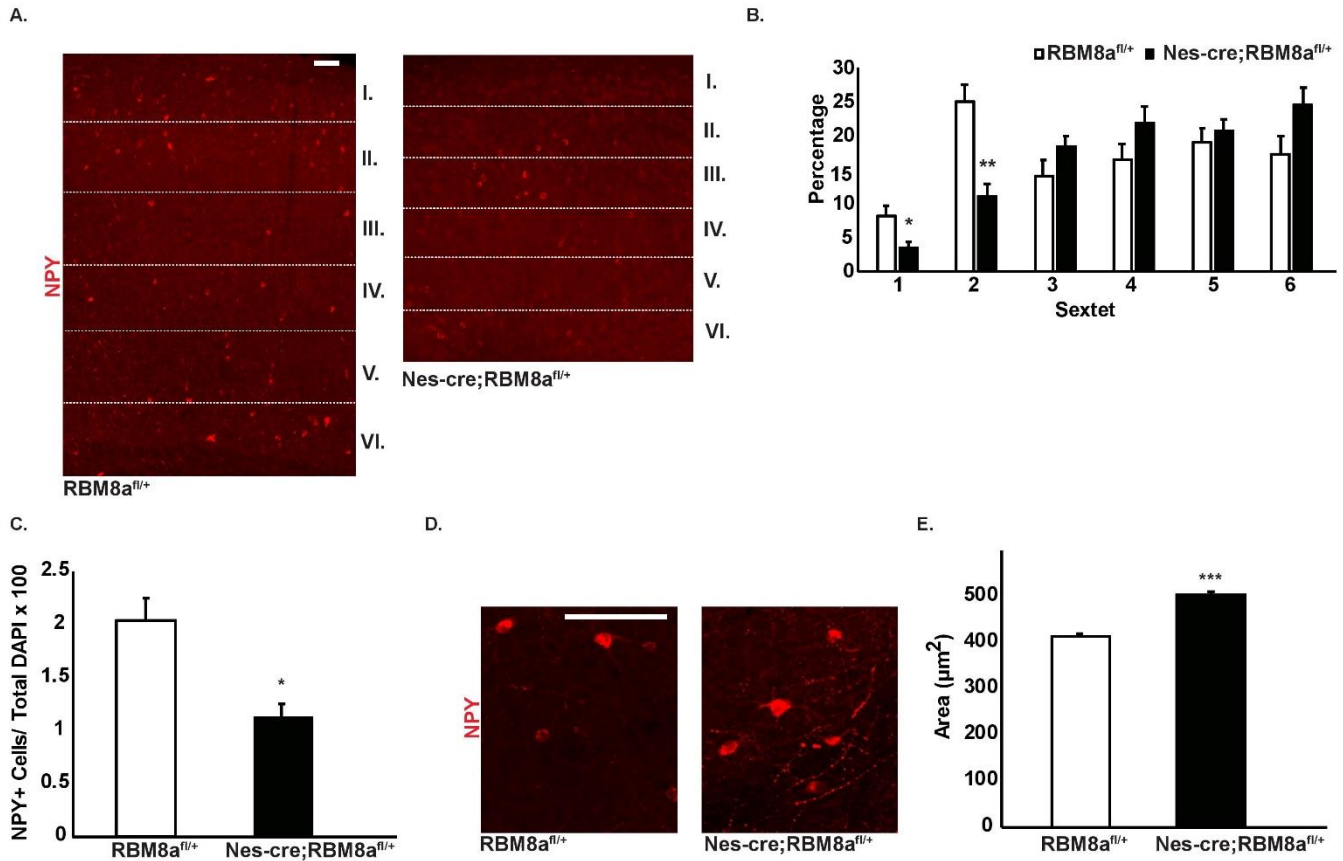


**Figure 5-3: RBM8a regulates the number, distribution and size of NPY+**

A) Nes-cre;RBM8a<sup>fl/+</sup> mice have altered distribution of NPY+ interneurons. There were significantly fewer NPY+ interneurons in sextets 1 and 2 (superficial layers). Nes-cre;RBM8a<sup>fl/+</sup> and RBM8a<sup>fl/+</sup> mice were perfused at P17 and coronal brain slices were stained for NPY Scale = 100 μm. The cortex was divided into six equal bins termed “sextets”. B) The number of NPY+ cells in each sextet were quantified and divided by the total number of NPY+ cells in the cortex. There were significantly fewer NPY+ interneurons in Nes-cre;RBM8a<sup>fl/+</sup> mice compared to RBM8a<sup>fl/+</sup> mice, \*,  $p=0.039$ , \*\*,  $p=1.9 \times 10^{-3}$ ,  $n=3$ , Students t-test. C) The total number of NPY+ cells in the cortex was quantified, \*,  $p=0.042$ ,  $n=3$ , Students t-test. D) The area of each cell was determined using ImageJ and quantified. (E) NPY+ interneurons in Nes-cre;RBM8a<sup>fl/+</sup> mice were significantly larger than RBM8a<sup>fl/+</sup> mice. Quantification, \*\*\*,  $p=1.4 \times 10^{-39}$ ,  $n=3$ , Students t-test,  $\delta=0.793$ , Cohens  $\delta$ . Bar graphs represent means +/- SEMs.

### **5.5 RBM8a haploinsufficiency does not change the number or distribution of Nkx2.1+ progenitors in the GE**

We hypothesized that the changes in the number and distribution of cortical interneurons resulted from errors in interneuron progenitor proliferation and migration. To test this hypothesis, pregnant dams at E17 were injected with EdU to label proliferating cells 1 hr before sacrifice. We determined that there were significantly fewer cells in the S phase of the cell cycle in the GE of Nes-cre;RBM8a<sup>fl/+</sup> mice (Figure 5-4A-B). The cells in S phase of the cell cycle in the Nes-cre;RBM8a<sup>fl/+</sup> mice were also less cell dense (Figure 5-4). Additionally, we stained the embryonic brains for interneuron progenitor marker Nkx2.1, in order to assess the number and distribution of these progenitors. Interestingly, there was no significant change in the percentage of Nkx2.1 + cells ((Nkx2.1+/total DAPI) x100) in the GE, or a change in cell density in Nkx2.1+ cells (Figure 5-5). We measured distance of each Nkx2.1+ cell in the GE to the lateral ventricle (LV), then divided this number by the length of the GE. This allowed us to determine approximately where in proximity to the LV each Nkx2.1 + cell resided, and from there to extrapolate the approximate distribution of these cells throughout the GE. No significant change in the distribution of Nkx2.1 + cells was observed in the GE (Figure 5-5). This result suggests that changes in interneuron distribution in the cortex may result from changes after E17. Since the decrease in cells in the S phase of the cell cycle at E15 in RBM8a haploinsufficient mice is not caused by changes in Nkx2.1 + progenitors, we hypothesize it is caused by a decrease in other progenitor types proliferating in the GE. These types could include, but are not limited to, astrocytes, oligodendrocytes, dopaminergic progenitors (will migrate to olfactory bulb), and cholinergic progenitors (will migrate to striatum) (Marin and Rubenstein, 2001). More experiments need to be conducted to conclude whether these cell types are affected.

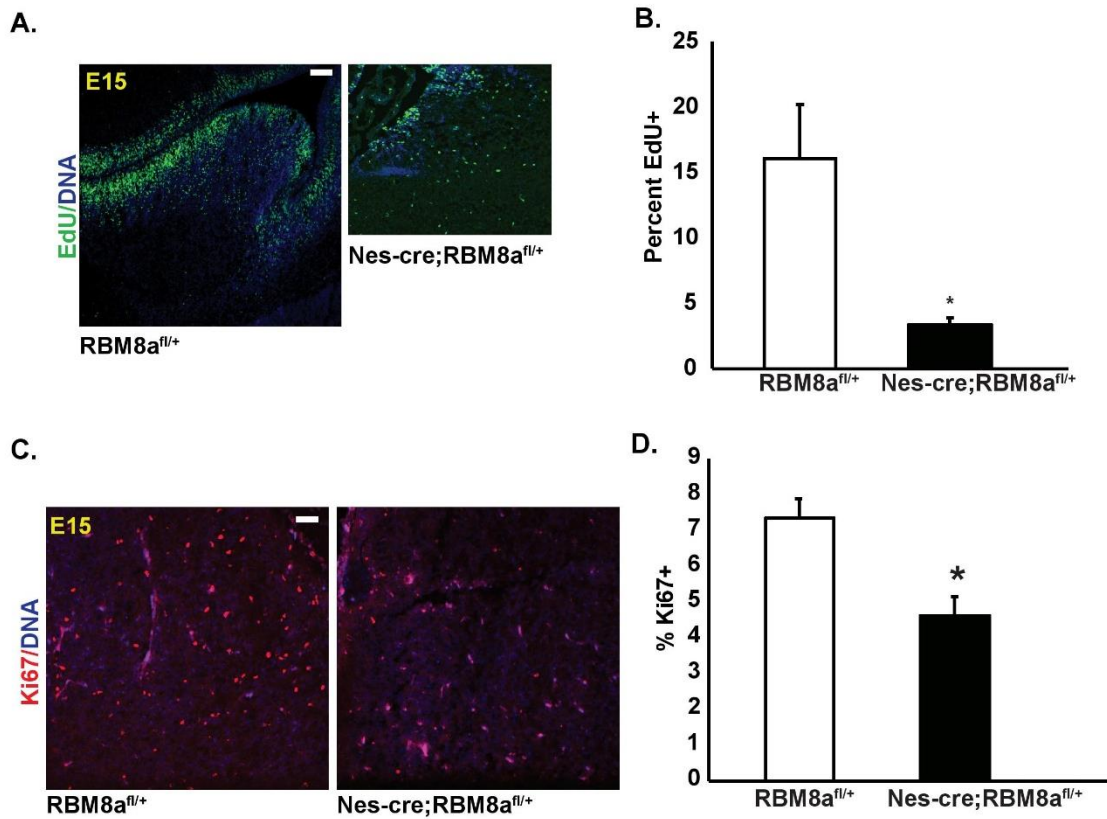


**Figure 5-4: RBM8a haploinsufficiency decreases the proliferation of cells in the ganglionic eminence (GE)**

A) Nes-cre; RBM8a<sup>fl/+</sup> mice have significantly fewer cells in the DNA synthesis phase of the cell cycle in the ganglionic eminence. Pregnant dams were injected with EdU 1hr prior to dissection of E15 embryos. Embryos were then stained for EdU using click chemistry. Scale = 100μm. B) The number of EdU + cells were quantified in the GE and divided by the total number of DAPI+ cells and multiplying by 100 to get the percentage of EdU+ cells, \*, p=0.01, n=3, Students t-test. C) Nes-cre;RBM8a<sup>fl/+</sup> mice have significantly fewer cells active in the cell cycle (non-quiescent, undifferentiated). E15 brains were stained with cell cycle marker anti-Ki67 antibody. D) The number of Ki67 + cells were quantified in the GE then divided by the total number of DAPI+ cells and multiplying by 100 to determine the percentage of Ki67 + cells, \*, p=0.02, n=3, Students t-test.

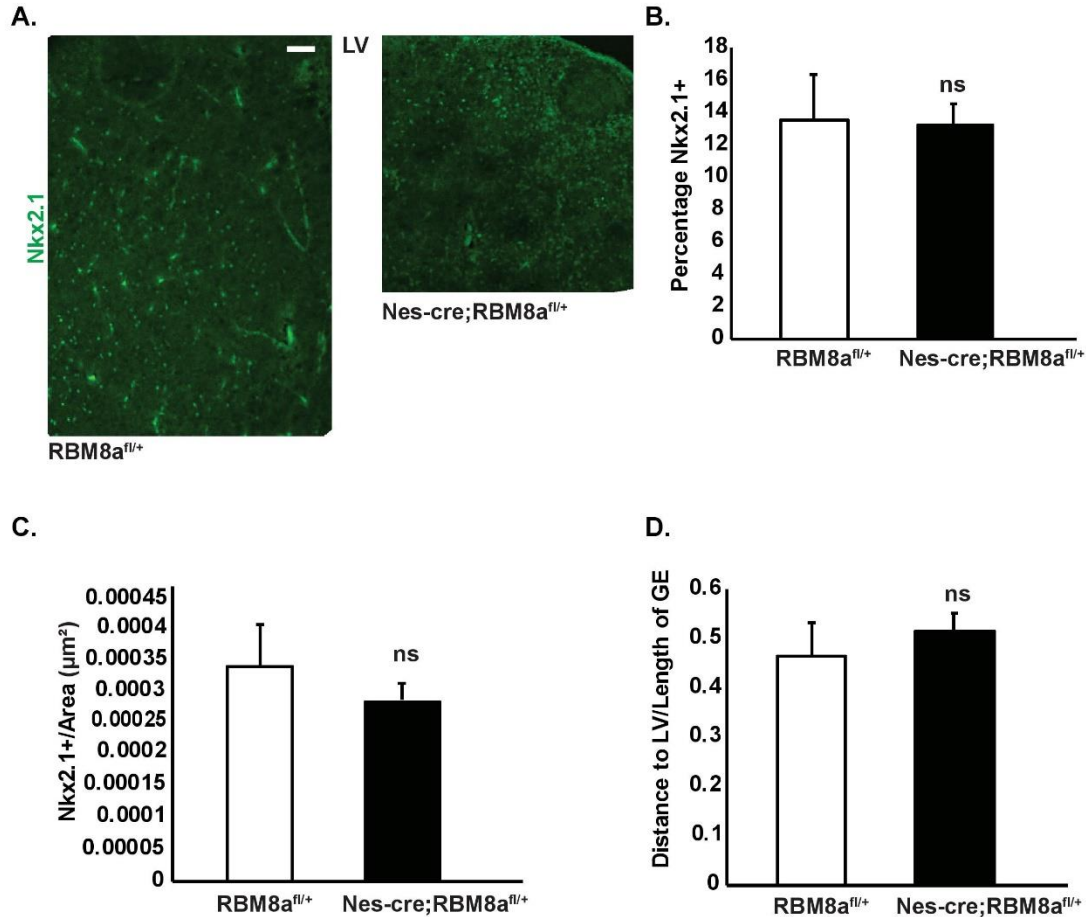


**Figure 5-5: RBM8a haploinsufficiency does not affect the number or distribution of Nkx2.1 progenitors**

A) The number of Ki67 + cells were quantified in the GE then divided by the total number of DAPI+ cells and multiplying by 100 to determine the percentage of Ki67 + cells, \*,  $p=0.02$ ,  $n=3$ , Students t-test. B) There is no change in the number (B-C) or distribution (D) of Nkx2.1+ interneuron progenitors in the GE of Nes-cre;RBM8a<sup>fl/+</sup> mice. E15 slices were stained for Nkx2.1 in the GE. B) The number of Nkx2.1+ cells in the GE was counted and divided by the number of DAPI+ cells and multiplied by 100 to determine the percentage of Nkx2.1+ cells in the GE,  $p=0.46$ ,  $n=3$ , Students t-test. C) The cell density was determined by dividing the number of Nkx2.1+ cells by the area of the GE,  $p=0.43$ ,  $n=3$ , Students t-test. D) The distribution of Nkx2.1+ cells were determined by measuring the distance of each Nkx2.1+ cell to the lateral ventricle, then dividing by the average length of the GE,  $p=0.51$ ,  $n=3$ , Students t-test. Bar graphs represent means +/- SEMs.

## 5.6 RBM8a Haploinsufficiency modulates GABAergic input onto pyramidal cells

Due to the significant perturbations in the number and distribution of interneurons in the cortex, we hypothesized that this would in turn affect the electrophysiological properties of pyramidal cells in the cortex (which form circuits with interneurons). Control and Nes-cre;RBM8a<sup>fl/+</sup> mice were sacrificed in the range of p14-p20 and spontaneous transmitter recordings were taken from putative pyramidal cells in the somatosensory cortex. We did not observe any changes the frequency or amplitude of spontaneous excitatory postsynaptic currents (sEPSCs), or the amplitude of spontaneous inhibitory postsynaptic currents (sIPSCs) (Figure 5-6A-B, E). However, there was a significant decrease in the frequency of sIPSCs released from inhibitory interneurons onto the pyramidal cells in the cKO mice (Figure 5-6D)

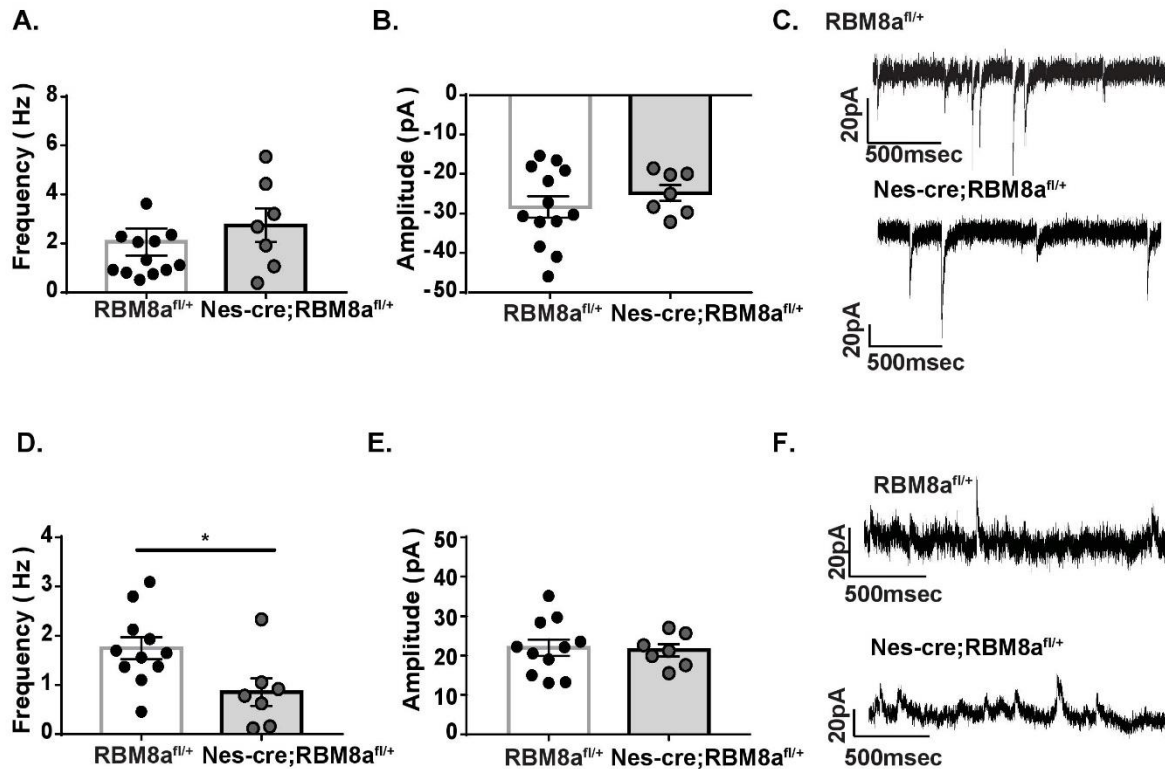


**Figure 5-6: Putative Pyramidal Cells in the somatosensory cortex have decreased GABA amplitude.**

A-B) There is no change in the frequency or amplitude of the excitatory spontaneous postsynaptic current of Nes-cre;RBM8a<sup>fl/+</sup> mice. Spontaneous excitatory postsynaptic current recordings from putative pyramidal cells in the somatosensory cortex, Student's t-test, n=4. C) Representative glutamate trace from control and cKO mice. D-E) There is a significant decrease in the frequency, but not the amplitude of the spontaneous inhibitory postsynaptic current in Nes-cre;RBM8a<sup>fl/+</sup> mice. Spontaneous inhibitory postsynaptic current recordings from putative pyramidal cells in the somatosensory cortex, \*, p<0.05, n=4, Student's t-test. F) Representative GABA trace from control and cKO mice. Bar graphs represent means +/- SEMs. This experiment was conducted by Dr. Nicole Crowley.

### 5.7 RBM8a haploinsufficiency in Nkx2.1+ progenitors leads to a muted distribution phenotype and no change in cell number

As we observed profound deficits in interneuron distribution and number, in addition to changes in Cux1+ and Foxp2+ cell distribution, we next investigated if these changes were due to intrinsic cues within the interneurons leading to altered distribution, or whether the abnormal

distribution was due to cues from the excitatory neurons, which also have altered distribution and are migrate into the cortex before the interneurons. To do this, we utilized an interneuron progenitor specific cre, Nkx2.1. By crossing our floxed mice with this cre we will selectively knockout RBM8a only in interneuron progenitors, which leaving it intact in excitatory neurons and the rest of the nervous system. If we see similar phenotypes to the Nes-cre;RBM8a<sup>fl/+</sup> mice, we can conclude the effect is cell autonomous, and the changes are due to intrinsic cues within the progenitors. If the interneuron distribution is normal, then the previous phenotype is likely due to altered cues from the excitatory neurons. At P17, we stained control and Nkx2.1-cre;RBM8a<sup>fl/+</sup> brains for PV, SST, and NPY. We did not observe any changes in overall interneuron number, unlike what we observed in the Nes-cre;RBM8a<sup>fl/+</sup> mice. While we did see some changes in distribution, it was much less severe compared to the Nes-cre;RBM8a<sup>fl/+</sup> mice (Figure 5-7). For example, for the PV stain, in the Nkx2.1;RBM8a<sup>fl/+</sup> mice, 17.78% of PV cortical interneurons were in sextet 5 compared to 18.33% in RBM8a<sup>fl/+</sup> mice. Comparatively, in the Nes-cre;RBM8a<sup>fl/+</sup> mice, 11.89% of PV cortical interneurons were in sextet 5 compared to 19.46% in RBM8a<sup>fl/+</sup> mice. As you can see, there is a change of 7.57% from control to cKO using the nestin cre (whole nervous system), while there is only a change in 0.55% using Nkx2.1 specific cre. Therefore, we concluded that RBM8a haploinsufficiency does slightly change intrinsic cues within the interneuron progenitors, but these changes are not sufficient to mimic the profound changes observed in the Nes-cre;RBM8a<sup>fl/+</sup> mice. We hypothesize that cause is likely changes in extrinsic signaling affecting the migration of the progenitors.

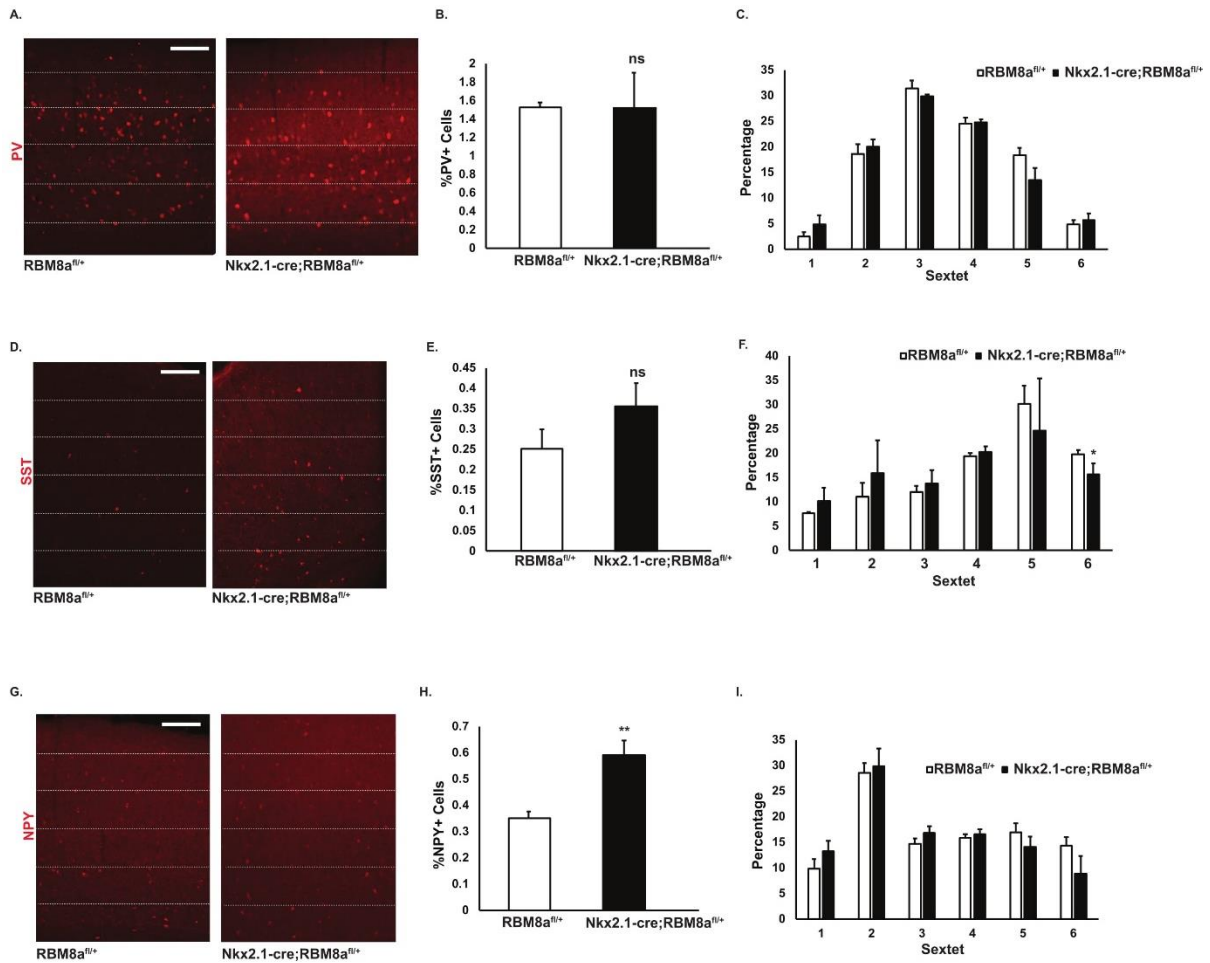


**Figure 5-7: RBM8a haploinsufficiency in Nkx2.1+ progenitors leads to a small change in the distribution of cortical interneurons**

A) There is no significant change in the distribution (B) or number (C) of PV+ interneurons in Nkx2.1-cre; RBM8a<sup>fl/+</sup> mice. Nkx2.1-cre; RBM8a<sup>fl/+</sup> and RBM8a<sup>fl/+</sup> mice were perfused at P17 and brains were stained for PV, Scale = 100 $\mu$ m. The cortex was divided into six equal bins termed “sextets” B) The number of PV+ cells in each sextet were quantified and divided by the total number of PV+ cells in the cortex, n=3, Student’s t-test. C) The total number of PV+ cells in the cortex was quantified. D) There was a slight increase in SST+ interneurons in the deepest sextet (6) of Nkx2.1-cre; RBM8a<sup>fl/+</sup> mice, but no change in the overall number of SST+ interneurons in the cortex of Nkx2.1-cre; RBM8a<sup>fl/+</sup> mice. Brain slices from A) were stained for SST, n=3, Students t-test. E) Quantification of total percentage of SST+ cells. F) Quantification of the distribution of SST+ cells in the cortex. \*, p=0.04, n=3, Student’s t-test. G) There was no change in the distribution of NPY+ cells in Nkx2.1-cre; RBM8a<sup>fl/+</sup> mice. Brain slices from A) were stained for NPY, n=3, Students t-test. H) There were significantly more NPY+ cells in the cortex of Nkx2.1-cre; RBM8a<sup>fl/+</sup> mice. Quantification for the overall percentage of NPY+ cells. I)

Quantification for the distribution of NPY+ cells. \*,  $p=0.008$ ,  $n=3$ , Students t-test. Bar graphs represent means +/- SEMs.

### **5.8 RBM8a haploinsufficiency modulates GABAergic and glutamatergic receptor expression and Notch1 signaling**

Due to our electrophysiology data, we were interested investigating the expression level of genes involved in GABAergic and glutamatergic signaling. After surveying a variety of GABAergic and glutamatergic receptor subtypes, we discovered that two were differentially expressed at the protein level, the GABA<sub>A</sub> Receptor  $\beta 3$  subunit, and the GluR1 Receptor (Figure 5-8A-D). As we saw a decrease in GABA frequency in our electrophysiology data, we also wanted to examine Gad67 levels, to determine if there were deficits in synthesizing GABA. GAD67 levels were found to be normal, indicating GABA synthesis is not causing the observed decrease in GABA transmission (Figure 5-8E-F). To fully rule out deficits in GABA synthesis, we would need to also examine other GAD levels, in addition to measuring evoked IPSCs in the cKO mice.

### **5.9 RBM8a haploinsufficiency modulates the Notch Pathway**

One pathway we considered to potentially be dysregulated in RBM8a haploinsufficient mice is the Notch pathway. This pathway is important for asymmetric division and neuronal differentiation, which makes it a logical target considering our phenotype. To answer this question, we used western blot to probe Notch pathway genes. We found about a 50% reduction in Notch1 NICD expression in the cKO mice. We then looked into additional Notch pathway genes, including Notch2 and Numb, but they were unchanged. To better understand how RBM8a affects the Notch pathway, we used the luciferase assay and a CBF1 reporter (notch reporter) to

investigate which domain of RBM8a, the RBD (RNA binding domain), C-terminus plus the RBD or the N-terminus plus the RBD, was most important for Notch regulation. Removing the C-terminus RBD was sufficient to significantly downregulate Notch expression, indicating that this is the motif in RBM8a that likely is important for Notch function. Removing the RBD or N-terminus RBD did not significantly alter Notch expression (Figure 5-9).

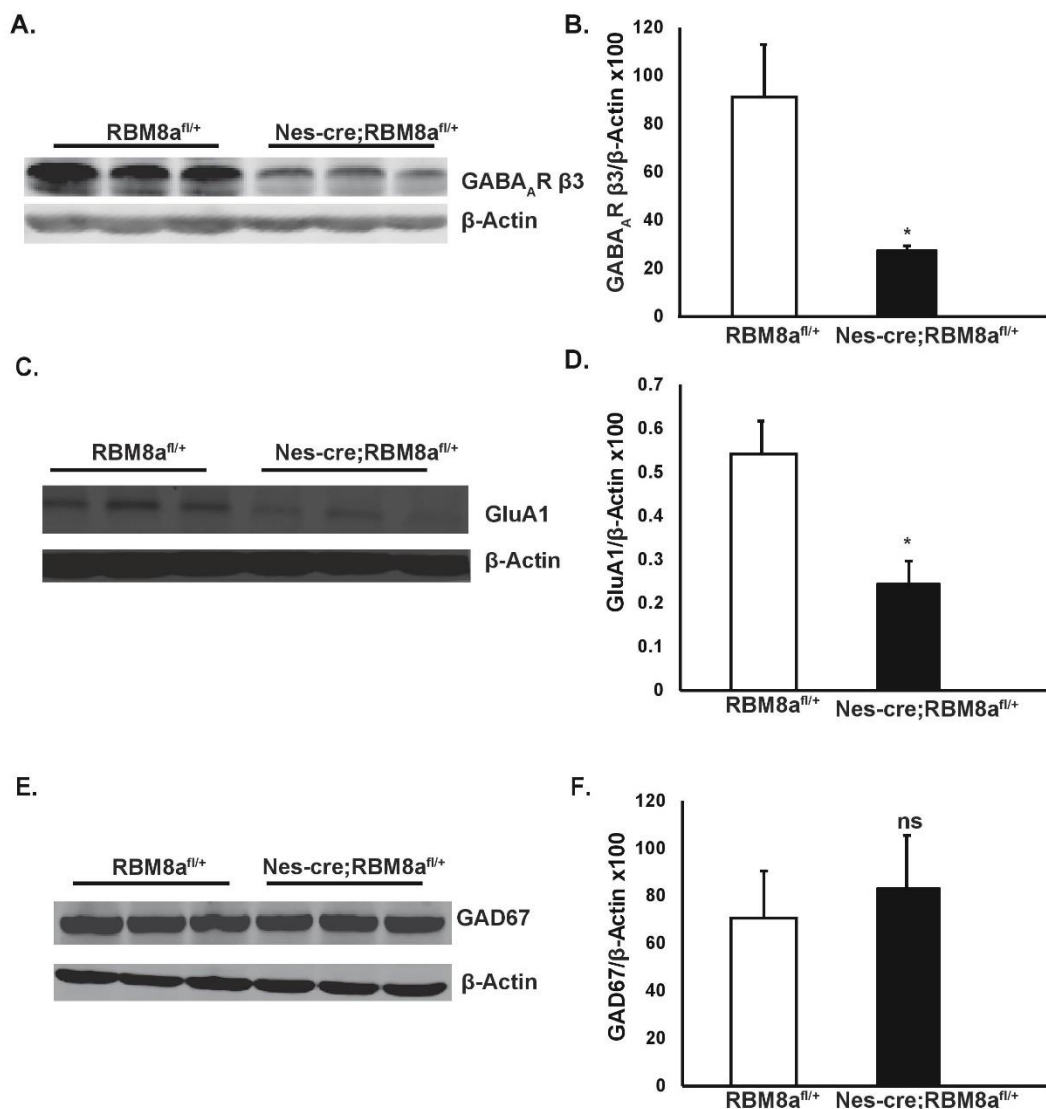


**Figure 5-8: RBM8a cKO mice have altered expression of GABRB3 and GluR1 receptors, but not GAD67**

A-C) Representative western blot and summary statistics for GABA<sub>A</sub> receptor β3 subunit, GluR1 subunit and GAD67 using whole brain lysate from P17 brains of Nes-cre;RBM8a<sup>fl/+</sup> and RBM8a<sup>fl/+</sup> mice. A) Western blot revealed a significant reduction in the total protein level of the GABA<sub>A</sub> receptor β3 subunit in Nes-cre;RBM8a<sup>fl/+</sup> mice. B) Quantification of GABA<sub>A</sub> R β3 immunofluorescence normalized to β-actin control, \*, p=0.04, n=3, Student's t-test. C) There was a significant reduction in the expression of the GluR1 subunit in Nes-cre;RBM8a<sup>fl/+</sup> mice. D) Quantification of GluA1 immunofluorescence normalized to β-actin control, \*, p=0.03, n=3, Student's t-test. E) There was no observed change in the total protein level of the enzyme GAD67. E) Quantification of GAD67 immunofluorescence normalized to β-actin control, p=0.71, n=3, Student's t-test. Bar graphs represent means ± SEMs.

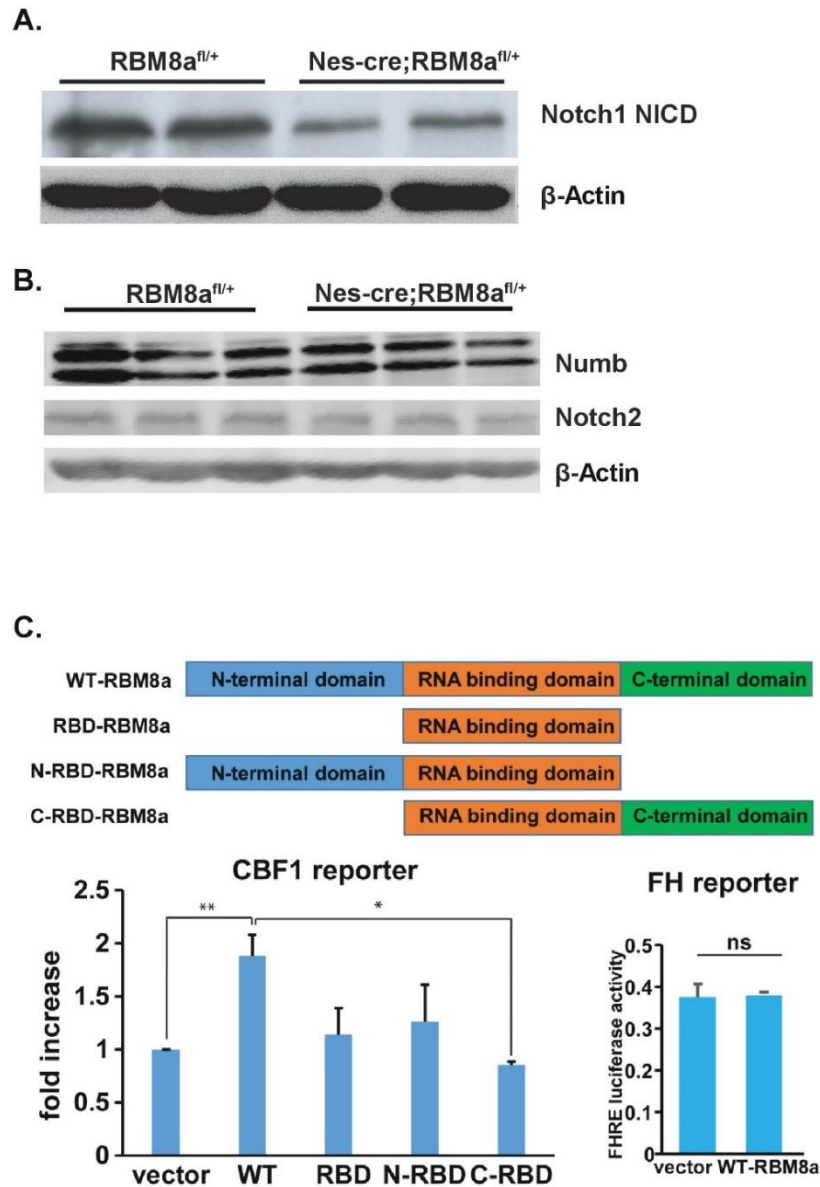


**Figure 5-9: RBM8a mediates Notch1 NICD expression**

A-B) Representative western blot using whole brain lysate from P17 brains in Nes-cre;RBM8a<sup>fl/+</sup> and RBM8a<sup>fl/+</sup> mice. A) There was a significant reduction in the expression of Notch1 intracellular domain (NICD) in the brains of Nes-cre;RBM8a<sup>fl/+</sup> mice. B) There was no observed change in the expression of notch pathway proteins Numb and Notch2. C) Luciferase assay using a Notch reporter. Each domain of RBM8a is removed and Notch expression is assessed. RBD = RNA binding domain, N-RBD= N-terminus of the RNA binding domain, C-RBD=C-terminus of the RNA binding domain. Removal of the C-terminus and RNA binding domain of RBM8a leads to a profound reduction in CBF1 expression in the luciferase assay. This indicates that the C-terminus and RNA binding domain are critical for the interaction of RBM8a and Notch pathway proteins, \*, p<0.05, n=3, Students t-test.

## 5.10 Conclusion

In this Chapter, we accepted the hypothesis that RBM8a haploinsufficiency affects the distribution and number of cortical interneurons, which could potentially explain the seizures we observed. Furthermore, the cKO mice had decreased frequency of GABAergic transmission, likely explained by the decreased number of PV+ and NPY+ interneurons. Using Nkx2.1 cre mice, we further determined that the interneuron phenotype was not due to changes in Nkx2.1 progenitors alone, as removal of RBM8a from Nkx2.1+ progenitors alone was not sufficient to fully recapitulate the phenotype. However, as some changes were observed in Nkx2.1-cre;RBM8a<sup>fl/+</sup> mice, we can conclude that RBM8a is important for interneuron differentiation, but the microcephaly and lethality phenotypes likely require additional deficits outside of interneurons. We also concluded that RBM8a haploinsufficiency leads to decreased expression of GluA1 and GABA<sub>A</sub>R  $\beta$ 3 expression, as well as Notch1 NICD expression. These changes partially explain the phenotype, but more mechanistic experiments must be conducted to fully understand the mechanism.

## Chapter 6

### **RBM8a modulates neurodevelopmental pathways and partially regulates alternative splicing and targets of NMD**

#### **6.1 Introduction**

In Chapter 5 we illustrated the profound interneuron deficits caused by RBM8a haploinsufficiency, and began to delve into the mechanisms causing it. To further explore the molecular mechanisms, we utilized RNAseq at different timepoints to understand the transcriptome changes when RBM8a expression is modulated. We used two different timepoints in the cKO mice, shortly before lethality (P17), and during embryonic development (E12). We also used SH-SY5Y cells to explore how RBM8a overexpression altered the transcriptome. Taken together these datasets should give us a better understanding of the mechanisms causing microcephaly and early post-natal lethality.

#### **6.2 RBM8a regulates genes involved in neurological and psychiatric disease**

To get a better idea of the molecular mechanisms mediating the neurogenesis and microcephaly phenotypes, we overexpressed RBM8a or a vector control in SH-SY5Y cells, and collected the RNA and ran RNAseq. We identified differentially expressed transcripts as transcripts with a  $q < 0.05$ , and a fold change (RBM8a overexpression/control) of 1.5-fold upregulation or 0.67-fold downregulation. This yielded a list of 1788 differentially expressed RNAs, which we used for all bioinformatic analyses. Of these transcripts, 95% were protein coding RNAs (Figure 6-1A). The next most populous RNA species was long noncoding RNA (lincRNA) with 1.57%, pseudogenes with 1.45% and antisense RNAs with 1.16%. Since it is

thought that RBM8a may be involved in neurological and psychiatric disease, we then cross-referenced our list of differentially expressed transcripts with databases of risk genes for ASD, SCZ, AD, ID and Crohn's disease. Interestingly, there was a significant overlap of genes mediated by RBM8a with risk genes for ASD, SCZ, AD and ID, but not Crohn's disease (control) (Figure 6-1B, Table 6-1). This illustrates that the genes RBM8a mediates are risk genes for specifically neurological and psychiatric disease. Next, we validated our RNAseq results using western blot. We tested genes thought to be involved with neurological disease. Our western blot data confirmed our RNAseq results. Additionally, we then probed the same genes using lysate from SH-SY5Y cells transfected with RBM8a shRNA, and got the opposite results as RBM8a OE and our RNAseq results (Figure 6-1C-E).

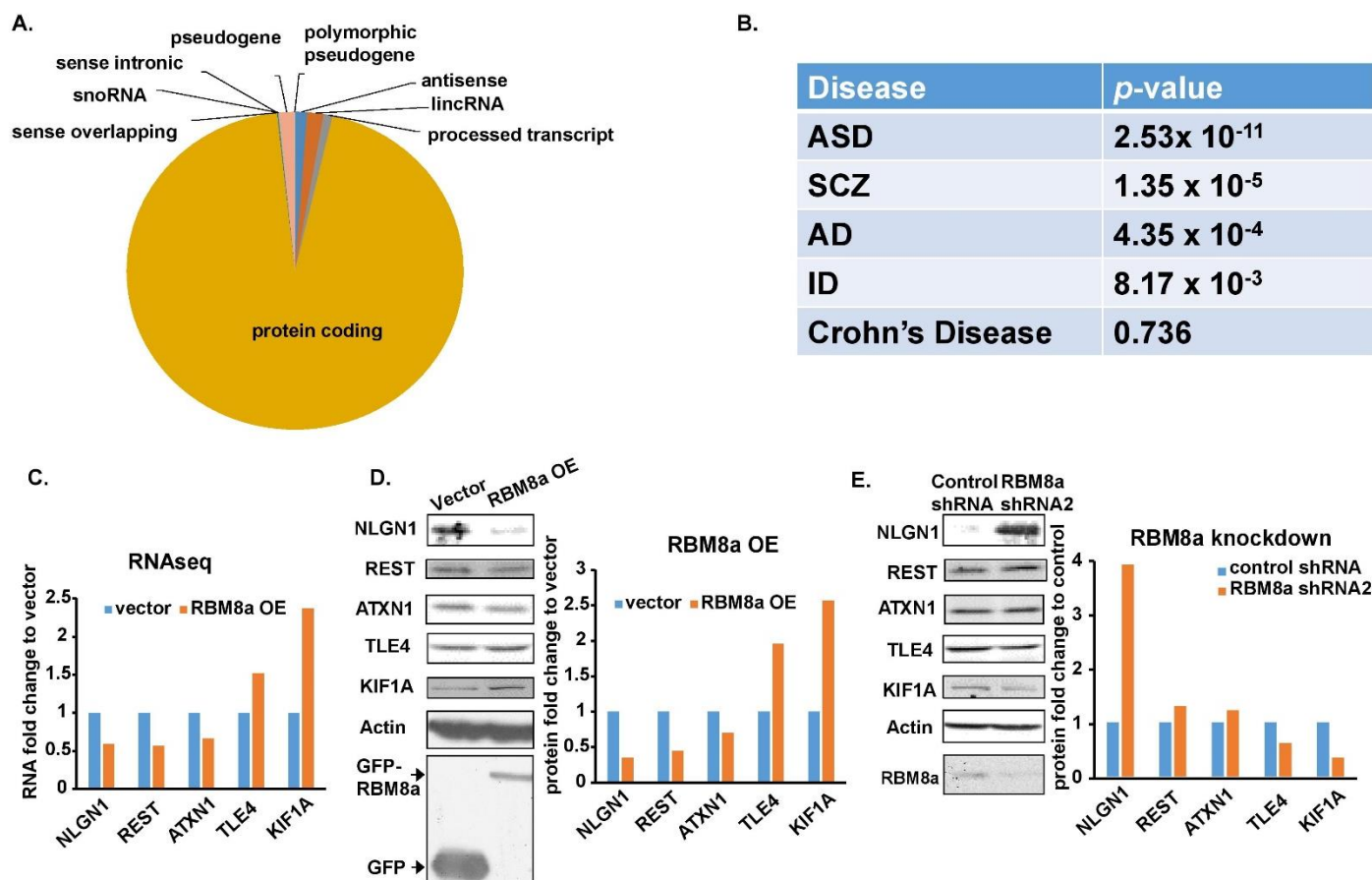


**Figure 6-1. RBM8a regulates protein coding genes that are risk genes for neurological and neuropsychiatric disease**

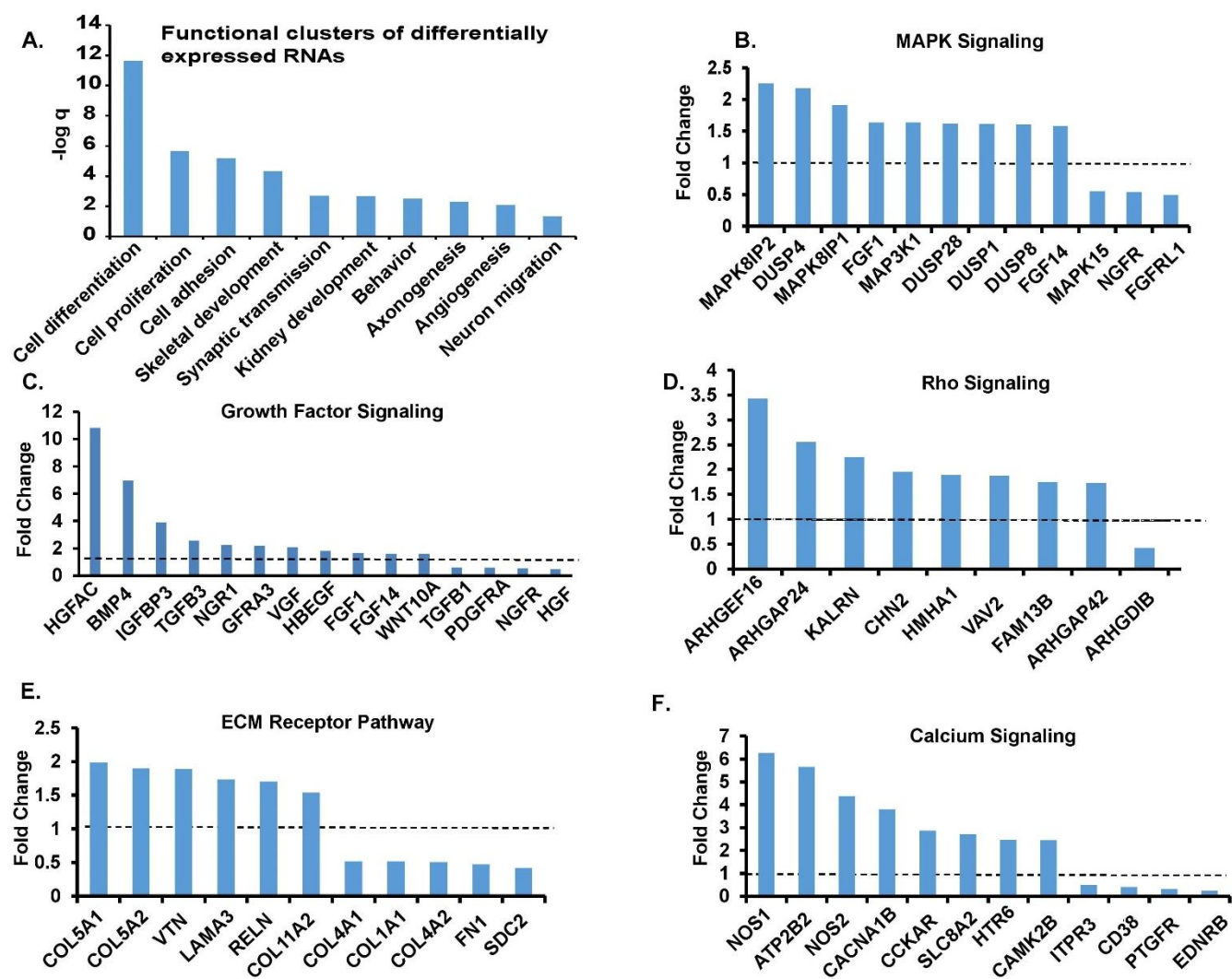
A) RNA species of the differentially expressed transcripts. Overexpression of RBM8a in SH-SY5Y cells modulates primarily protein coding mRNAs. B) RBM8a overexpression leads to differential expression of mRNAs that have been identified as risk factors for neurological and psychiatric disease. Significance of overlapping genes in differentially expressed dataset compared to risk genes for various diseases.  $p < 0.05$ , mean  $\pm$  SEM,  $n = 3$ , hypergeometric analysis. C) Validation of RNAseq data. Comparison of mRNA expression levels for differentially expressed neurological disease risk genes when RBM8a is overexpressed. D) The protein level of the mRNAs in C) were determined to be differentially expressed when RBM8a is overexpressed. Comparison of genes between vector control lysate and RBM8a overexpress in SY5Y cells. E) The protein level of the mRNAs and proteins described in D-E were also differentially expressed when RBM8a was knocked down. Comparison of genes between control shRNA and RBM8a shRNA.

Table 6-1: RBM8a regulates genes that are risk genes for neurological and psychiatric disease

ASD	AD	ID	SCZ	Crohn's
A2M, ABCA12, ABI3BP, ACTA2, ADAMTS1, ADAMTS10, ADAMTS3, AHNAK2, ALDH1L2, ALK, ANGPTL2, ANK1, AP3B2, ATP2B2, ATP2B4, ATP7B, BAIAP2, BCAR3, BCH4, BRSK2, C17orf97, CACNA2D2, CACNA2D3, CADPS, CD14, CD9, CDHR3, CERK, CGNL1, CHRND, CIT, CMPK2, CUX2, DBH, DCLK3, DDB2, DDR2, DEPDC4, DEPDC7, ECI2, EFCAB6, EPHB3, EPHX2, EPPK1, ERMP1, ERV3-1, ETHE1, EXD3, EYS, FAM65C, FBLN7, FN1, FRAS1, GABRB3, GBA, GLI2, GPC5, GPRASP1, GPX8, GRB14, GRM7, GXYLT2, HLTF, HMHA1, HSPA8, ICA1, IL20RB, IQGAP2, IQGAP3, IQSEC3, IQUB, ISLR2, JPH3, KALRN, KCNA3, KCN1, KCNS3, KIF14, KIF1A, KIRREL2, KRT80, L3MBTL1, LDLR, LGR4, LHFPL3, LINGO2, LRP4, LTBP1, MANSC1, MAP3K1, MASP2, MDM2, MGAT5B, MICALCL, MKI767, MOV10, MRC2, MSH5, MYADML2, MYH10, MYO1E, MYT1L, NFASC, NGEF, NLGN1, NOS2, NOTCH3, NR2F1, NRXN2, NSUN7, NUAKE1, OXCT1, PAPSS2, PAQR8, PAX5, PCDHB16, PDGFD, PEX5L, PHACTR1, PITPNM3, PLCD1, PLEKHA6, PLXNB2, PLXND1, PPM1D, PRKCA, PTGR1, PTPRG, PTPRK, PTPRM, PTPRN2, RAD21L1, RASSF5, RELN, REST, RIMS1, RIMS2, RPRD1A, RRP12, SCRIB, SEMA6A, SERPINB8, SFPQ, SGIP1, SH3RF3, SHANK2, SHOX2, SLC25A12, SLC8A3, SCLCO1C1, SLITRK5, SNTA1, SORBS2, SPATA13, SREBF2, STXBP3, SULF2, SYNE2, TAS2R10, TBC1D4, TBX18, TBX4, TCF7L1, TCP11L2, TECTA, TNIK, TPR, TSNARE1, TTK, UACA, UBTF, UFL1, UNC13A, UNC80, UPF1, VAV3, VPS13A, VWCE, ZC3H12B, ZMYND12,	A2M, ABCA1, ABCA12, ACE, ACHE, ACTA2, ADAM9, ADRA2A, APOE, ATXN1, BAG3, BCHE, BDNF, CAST, CCL2, CD14, CDK5R1, CDKN2A, CHRNA3, CHRNB2, CSF1, CYP39A1, DBH, DRD4, EBF3, FAS, FBP1, FDPS, FGF1, FOS, GBA, GBP2, GRB14, GRIN3A, GSTO1, GSTT1, HMMR, HSPG2, HTR6, IRF6, LIPA, MAPK8IP1, MAPT, MME, NEDD9, NGFR, NOS1, NRG1, NTRK2, PCK2, PLCE1, PPARGC1A, PTPLA, RASSF4, RELN, RXRA, S100B, SEPT3, SLIT1, SNCA, SORL1, TAP1, TCF7L2, TCN2, VLDLR	ALK, ATP7B, CUX2, DBH, ERMP1, FRAS1, GPRASP1, GRB14, KCNA3, LHFPL3, MAP3K1, MGAT5B, MYO1E, MYT1L, NGEF, PHACTR1, SREBF2, UBTF, ZMYND12, ZNF540	ATP2B4, BAIAP2, CACNA1B, CACNA2D2, CACNB4, CAMK2B, CD14, DPYD, EPHX2, ESAM, LRRC48, MAN2A1, NCAN, NGEF, SLC8A1, TLE3, TSNARE1, ZNF804A	BSN, CCL2, IKZF1, REL, TNFSF4, ZFP36L1

### **6.3 RBM8a regulates genes involved in developmental functions and signaling pathways**

Next, we examined what functions the differentially expressed transcripts mediate. To do this we uploaded our dataset into DAVID bioinformatics tool (Huang et al., 2009; Lill et al., 2012), and looked for functional clusters that were enriched for genes in our differentially expressed dataset. Significant clusters included many developmental functions, such as cell differentiation, proliferation, adhesion, migration etc. (Figure 6-2, Table 6-2). We also examined the fold change of differentially expressed genes in key developmental pathways, such as the MAPK or extracellular matrix (ECM) receptor pathway. Genes in the Mapk pathway that were overexpressed include DUSP4 (2.25x), MAPK3K1 (2x), MAPK8IP2 (2.25x), while downregulated genes included Mapk15(0.5x), Ngfr (0.5x) and FGFR1 (0.5x). Interesting ECM pathway genes that were differentially expressed include many Collagen proteins such as COL5A1 (2x), COL5A2 (1.9x), COL4A1 (0.25x) and COL4A2 (0.25x).



**Figure 6-2: RBM8a overexpression regulates transcripts involved in developmental pathways**

A) Functional clusters enriched for differentially expressed genes. RBM8a overexpression in SH-SY5Y cells leads to a significant modulation of genes that regulate developmental pathways including cell proliferation, differentiation, adhesion. B) RBM8a overexpression modulates the expression of key mRNAs in the MAPK pathway. Fold change for differentially expressed genes in the MAPK signaling pathway. C) Fold change for differentially expressed genes in the Growth Factor signaling pathway. D) Fold change for differentially expressed genes in the Rho signaling pathway. E) Fold change for differentially expressed genes in the ECM Receptor signaling pathway. F) Fold change for differentially expressed genes in the Calcium signaling pathway.

Table 6-2: Functional Clusters of RBM8a downstream genes (genes can be in multiple categories)

Function	Number of genes	<i>p</i> value	<i>q</i> value
Regulation of system processes	60	$1.9 \times 10^{-9}$	$6.9 \times 10^{-6}$
Neuron differentiation	75	$4.9 \times 10^{-9}$	$9.2 \times 10^{-6}$
Regulation of cell proliferation	114	$9.4 \times 10^{-9}$	$1.2 \times 10^{-5}$
Extracellular structure organization	38	$2.0 \times 10^{-8}$	$1.8 \times 10^{-5}$
Biological adhesion	101	$9.8 \times 10^{-8}$	$7.3 \times 10^{-5}$
Skeletal system development	56	$2.4 \times 10^{-7}$	$1.3 \times 10^{-4}$
Cell motion	74	$3.3 \times 10^{-7}$	$1.5 \times 10^{-4}$
Cell-cell signaling	88	$3.4 \times 10^{-7}$	$1.4 \times 10^{-4}$
Localization of the cell	53	$9.0 \times 10^{-7}$	$3.1 \times 10^{-4}$
Transmission of nerve impulse	57	$2.2 \times 10^{-6}$	$7.0 \times 10^{-4}$
Regulation of synaptic transmission	30	$2.6 \times 10^{-6}$	$7.0 \times 10^{-4}$
Regulation of cell development	39	$3.0 \times 10^{-6}$	$9.0 \times 10^{-4}$
Regulation of neurological system process	32	$3.7 \times 10^{-6}$	$9.1 \times 10^{-4}$
Neuron development	55	$3.9 \times 10^{-6}$	$9.0 \times 10^{-4}$
Regulation of neurogenesis	33	$7.7 \times 10^{-6}$	$1.7 \times 10^{-3}$
Synaptic transmission	49	$9.8 \times 10^{-6}$	$2.0 \times 10^{-3}$
Positive regulation of cell proliferation	62	$1.2 \times 10^{-5}$	$2.4 \times 10^{-3}$
Kidney development	23	$1.2 \times 10^{-5}$	$2.3 \times 10^{-3}$
ECM organization	24	$1.5 \times 10^{-5}$	$2.5 \times 10^{-3}$
Cell morphogenesis-differentiation	42	$1.5 \times 10^{-5}$	$2.4 \times 10^{-3}$
Response to inorganic substance	37	$1.9 \times 10^{-5}$	$2.8 \times 10^{-3}$
Response to corticosteroid stimulus	21	$2.0 \times 10^{-5}$	$2.9 \times 10^{-3}$
Enzyme linked receptor protein pathway	53	$2.2 \times 10^{-5}$	$3.1 \times 10^{-3}$
Neuron projected development	43	$2.2 \times 10^{-5}$	$3.0 \times 10^{-3}$
Forebrain development	30	$2.5 \times 10^{-5}$	$3.2 \times 10^{-3}$
Regulation of nervous system development	35	$2.7 \times 10^{-5}$	$3.3 \times 10^{-3}$
Urogenital system development	24	$3.8 \times 10^{-5}$	$4.6 \times 10^{-3}$
Vasculature development	41	$6.7 \times 10^{-5}$	$7.8 \times 10^{-3}$
Axongensis	34	$7.2 \times 10^{-5}$	$7.9 \times 10^{-3}$
Blood vessel development	40	$8.5 \times 10^{-5}$	$9.0 \times 10^{-3}$
Neuron projection morphogenesis	36	$1.0 \times 10^{-4}$	$1.0 \times 10^{-2}$
Response to oxygen levels	27	$1.2 \times 10^{-4}$	$1.2 \times 10^{-2}$
Regulation of locomotion	33	$1.5 \times 10^{-4}$	$1.4 \times 10^{-2}$
Diencephalon development	12	$1.6 \times 10^{-4}$	$1.5 \times 10^{-2}$
Sensory organ development	37	$2.0 \times 10^{-4}$	$1.8 \times 10^{-2}$
Response to glucocorticoids stimulus	18	$2.2 \times 10^{-4}$	$1.9 \times 10^{-2}$
Behavior	63	$2.6 \times 10^{-4}$	$2.1 \times 10^{-2}$
receptor tyrosine kinase pathway	36	$2.8 \times 10^{-4}$	$2.3 \times 10^{-2}$

#### **6.4 RBM8a is a moderate regulator of alternative splicing**

RBM8a is primarily known for its role in RNA regulation, namely NMD. Therefore, we decided to investigate whether RBM8a overexpression led to changes in regulatory mechanisms such as alternative splicing. To do this, our collaborator Derrick Reynolds at UC Irvine used MISO to determine if there were any alternatively spliced transcripts in our RNAseq results. Over 800 alternative splicing events were found, with the most common being skipped exon. Next, we were curious if these alternatively spliced genes had similar functions in common (Figure 6-3A-B, Table 6-3). To determine this, we input our list of alternatively spliced genes into DAVID, similar as our differentially expressed transcripts. Overall, the significant functions were relatively generic, such as anatomical structure morphogenesis.

Due to RBM8a's role in NMD, we were curious whether any differentially expressed transcripts were known targets of NMD. Independent of its regulatory role in degrading nonsense transcripts, NMD proteins also regulated a subset of RNAs that have specific characteristics, such as long 3'UTR and an intron in the 3'UTR. With the help of a script from Dr. Michael Axtell, we determined that about 50% of transcripts had characteristics predisposing them to regulation via NMD (Appendix A). Interestingly, these transcripts mediate functions important for development, such as neurogenesis and migration (Figure 6-3C-D, Table 6-4). Therefore, it is plausible that developmental functions regulated by RBM8a are done in a NMD dependent manner. We currently do not have any data to determine whether NMD is altered in RBM8a haploinsufficient mice, only that 45% of transcripts perturbed by RBM8a haploinsufficiency also contain characteristics predisposing them to degradation via NMD.

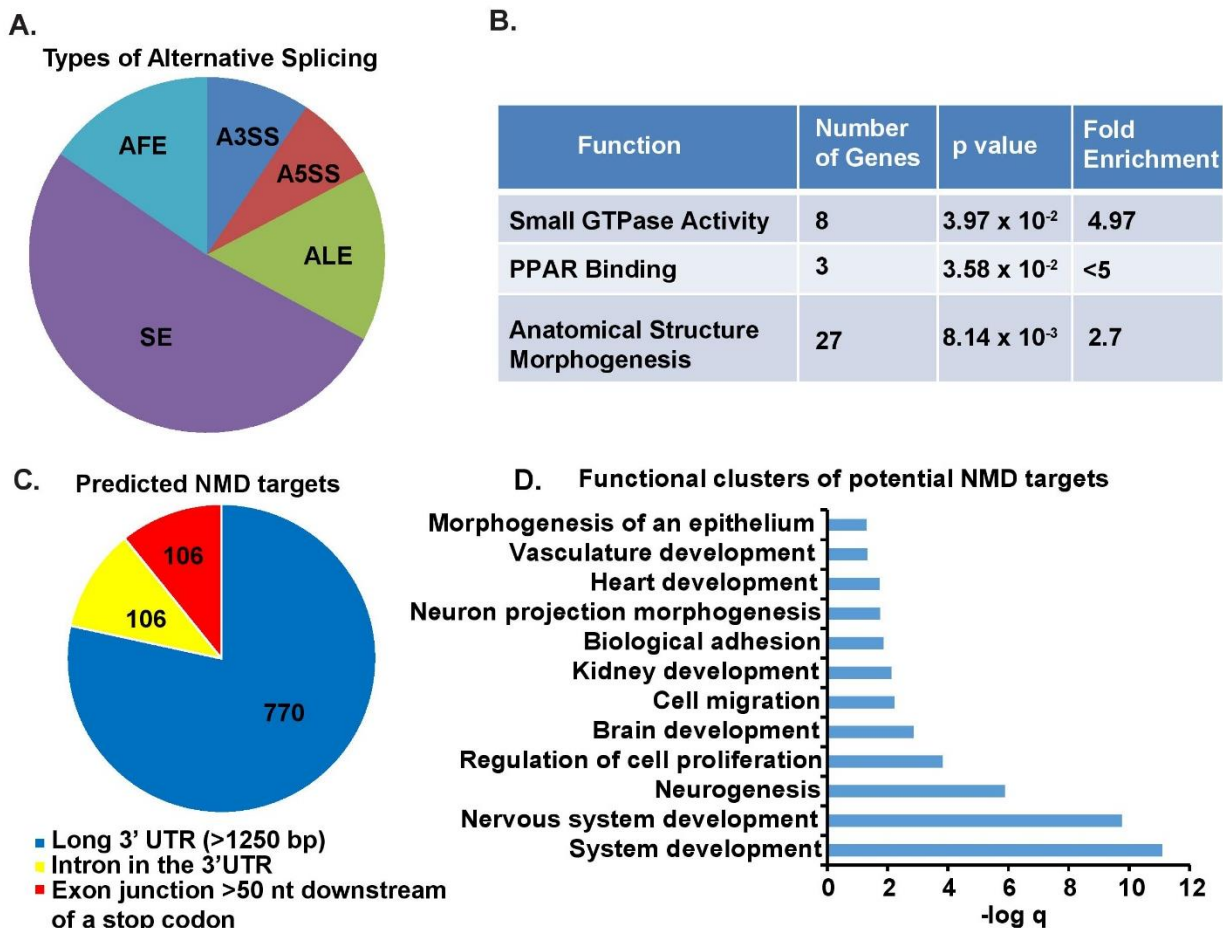


**Figure 6-3: RBM8a regulates RNAs targeted by NMD and is a moderate regulator of alternative splicing**

A) Types of alternative splicing events found in our dataset SE=skipped exon, AFE=alternative first exon, A3SS=alternative 3' splice site, A5SS=alternative 5' splice site, ALE=alternative last exon. B) Functions the alternatively spliced transcripts mediate. C) Number of predicted NMD targets in our differentially expressed dataset, and the characteristic they have. Around 50% of differentially expressed mRNAs have characteristics that predispose them to degradation via NMD. D) Functions mediated by differentially expressed genes predicted to have characteristics predisposing them to regulation via NMD. Genes can reside in multiple functional categories.

**Table 6-3: RBM8a mediated alternative splicing genes significantly overlap with ASD risk genes**

Disease	p-value
ASD	$7.57 \times 10^{-7}$
SCZ	0.326
AD	0.577
ID	0.174

Crohn's Disease	No common genes
-----------------	-----------------

Table 6-4: RBM8a mediated potential NMD targets significantly overlap with risk genes for neurological and psychiatric disease

Disease	p-value
ASD	$4.12 \times 10^{-9}$
SCZ	$6.32 \times 10^{-5}$
AD	$1.16 \times 10^{-3}$
ID	$1.30 \times 10^{-2}$
Crohn's Disease	0.232

### 6.5 RBM8a haploinsufficiency modulates primarily protein coding transcripts

Next, we sought to determine the molecular pathways that govern RBM8a's role in interneuron development. To do this, we utilized RNAseq to determine transcriptome changes in RBM8a haploinsufficient mouse brains at P17. RNA was isolated from the whole brain of P17 mice (control and cKO) and converted to cDNA and sequences using the Illumina Hiseq 2500. Differentially expressed transcripts were identified as RNAs with a  $p < 0.05$ , and a fold change of 1.5x up or down (cKO reads/control reads). This list of differentially expressed transcripts was then used for further analysis. First, we determined that the differentially expressed transcripts were primarily protein coding RNAs (94.7%), followed by lincRNAs (1.57%), antisense RNAs (1.17%) and pseudogenes (1.45%). This characterization of differentially expressed genes helps determine potential ways in which RBM8a regulation can lead to changes in neurodevelopment. That is, it RBM8a modulates mostly protein coding genes, which likely plays a large role in the observed phenotypes, but RBM8a also regulates a proportion of lincRNAs. In the future, we should investigate the location of the lincRNAs to determine what protein coding genes they could potentially modulate. It is possible that this insight might lead to clues to the overall mechanism of RBM8a's developmental role. Next, we input our gene list into DAVID, and

looked to see if the differentially expressed genes mediated any interesting functions. When we used the p value of 0.05 as the cut off, we found genes involved in functions mediated anatomical development, behavior, ossification, bone development and cell adhesion. Since functional analyses often have a lot of false positives due to multiple sampling, we further refined our differentially expressed gene list by using a q value of 0.05 (Benjamani) and fold change of 2x up or down as a cut off. Our new function list consisted of cell death, cell adhesion, cell differentiation, hindbrain and forebrain development and cell proliferation. These functions are more specific than the p value dataset, and mimic phenotypes we observed with our immunohistochemistry data (Figure 6-4). We were then interested in seeing if our differentially expressed RNAs were enriched with risk genes for psychiatric and neurological disease (as in our overexpression sequencing in SY5Y cells). Unfortunately, the gene list did not significantly overlap with any disease databases. Due to RBM8a's involvement in NMD and RNA processing, we also wanted to investigate determine changes in alternative splicing between our control and experimental samples (using MISO). It was determined that there were 371 alternative splicing events, with the majority being skipped exons. Contrary to our overexpression data, there were many more cases of retained introns in our cKO mice (Figure 6-5).

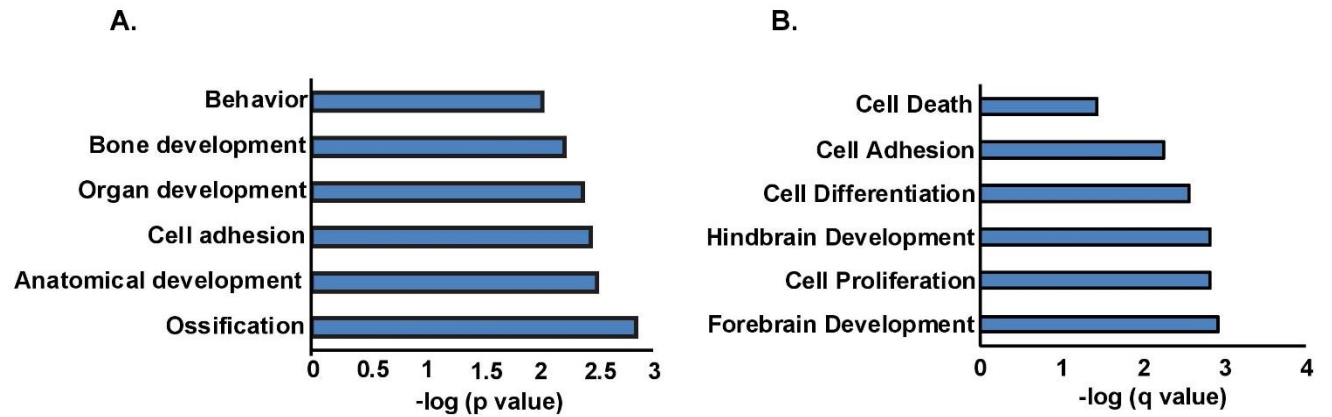


**Figure 6-4: RBM8a modulates developmental functions at P17**

A) Functions mediated by differentially expressed genes in in Nes-cre;RBM8a<sup>fl/+</sup> mice at P17 using p value of < 0.05 and fold change of 1.5x up or down as a cutoff. B) Functions mediated by differentially expressed genes in P17 in Nes-cre;RBM8a<sup>fl/+</sup> mice using q value of 0.05 and fold change of 2x up or down as a cutoff.

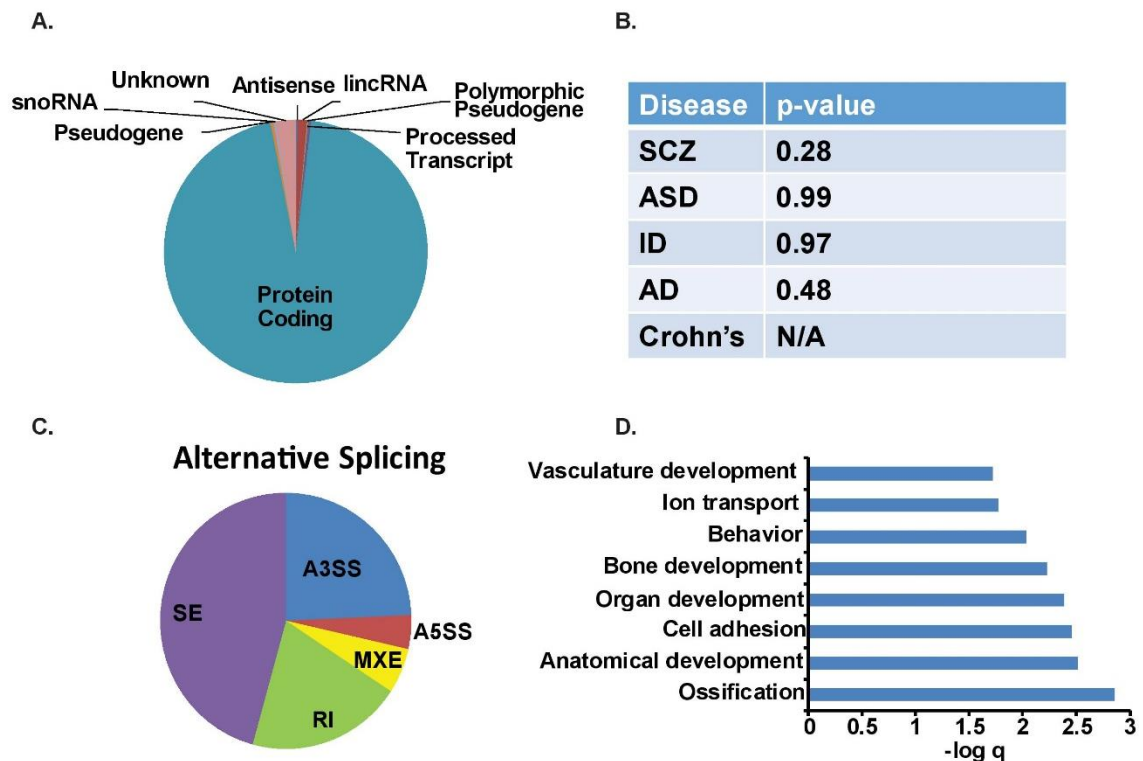


**Figure 6-5: RBM8a modulates mostly protein coding transcripts and is a moderate regulator of alternative splicing at P17**

A) The RNA species of all differentially expressed RNAs in P17 Nes-cre;RBM8a<sup>fl/+</sup> mice was determined, and the percentage of each species was calculated. The majority of differentially expressed mRNAs were protein coding mRNAs. B) The list of differentially expressed RNAs was cross referenced with different disease databases to determine if there was a significant overlap. The hypergeometric analyses were used to determine if there was any enrichment of risk genes in the dataset. There was no observed interaction with mRNAs differentially expressed at P17 in Nes-cre;RBM8a<sup>fl/+</sup> mice and risk genes for neurological and psychiatric disease. C) MISO was used to identify alternative splicing events between the cKO and control datasets. A3SS= alternative 3' splice site, A5SS=alternative 5' splice site, MXE= mutually exclusive exons, RI= retained intron, SE= skipped exon. RBM8a was found to be a moderate regulator of alternative splicing, as around 300 mRNAs were alternatively spliced in the brains of P17 in Nes-cre;RBM8a<sup>fl/+</sup> mice. D) The genes that were alternative spliced were identified and input into DAVID to determine if they mediate any biological functions. It was found that the alternatively spliced genes in P17 in Nes-cre;RBM8a<sup>fl/+</sup> mice affected functional pathways mediating vasculature, bone development and adhesion among other developmental pathways.

Table 6-5: Alternative splicing protein coding RNAs list

A3SS	A5SS	ALE	SE	AFE
ACBD3, BC038542, DDB2, GAK, GATAD2A, GLE1, MED1, MTHFD1L, NTSR1, PLK1S1, QRICH1, STK33, WNT2B	ARPC4, ARPC3- TTLL3, ATP13A1, BTAF1, C9orf24, CELSR3, FBXL20, LOC100130987, MAPK8IP3, MIR3134, NEO1, PHOSPHO2- KLHL23, PTBP3, RILPL1, SYS1, SYS1- DBNDD2		ACACA, AFF1, ARMC6, ATP13A1, CARD8, DBN1, DST, EML3, FHAD1, GAK, KCNN3, KCNQ5, KDM6B, MCOLN3, PTPRS, RAPGEF6, RECQL5, RPF2, SDK2, SLC35E2, SLC35E2B, SNAP91, ST3GAL2, TRIM16, USP36, VWA5A, WASF2, WHSCF1, ZFPM1, ZNF561	ABI1, ACOT7, ADAM2 ARFGEF1, ARHGAP10, CC2D2A, CELSR3, CHN DNHD1, ELMO2, ERC1 GCNT2, GRAMD4, GSN IFFO1, IGF2BP2, IKZF2 LMO7, MDM2, MSH5-S MVB12B, NDUFAF6, N NRG1, NRXN1, NT5DC RNF220, ROR2, SARDH SMEK2, SPATA6L, ST3 STXBP1, TCF7L1, TME VGLL4, ZNF280D, ZNF

## 6.6 RBM8a haploinsufficiency in vivo mediates developmental functions

Next, we were interested in looking at what functions these differentially expressed transcripts mediated. To do this we input our gene list into Geneontology.org and sorted by biological function and molecular pathway. Not surprisingly, many of these altered pathways were ones that govern development, such as notch signaling, growth factor signaling and RNAs

involved in the extracellular matrix (ECM) (Figure 6-6). Like in the overexpression dataset, many collagen proteins were differentially expressed, including COL8A2 (3x), COL13A1 (1.9x) and COL4A6 (1.9x). Differentially expressed Notch pathway genes include Hes7 (4.5x) and Dlk1 (2.25).

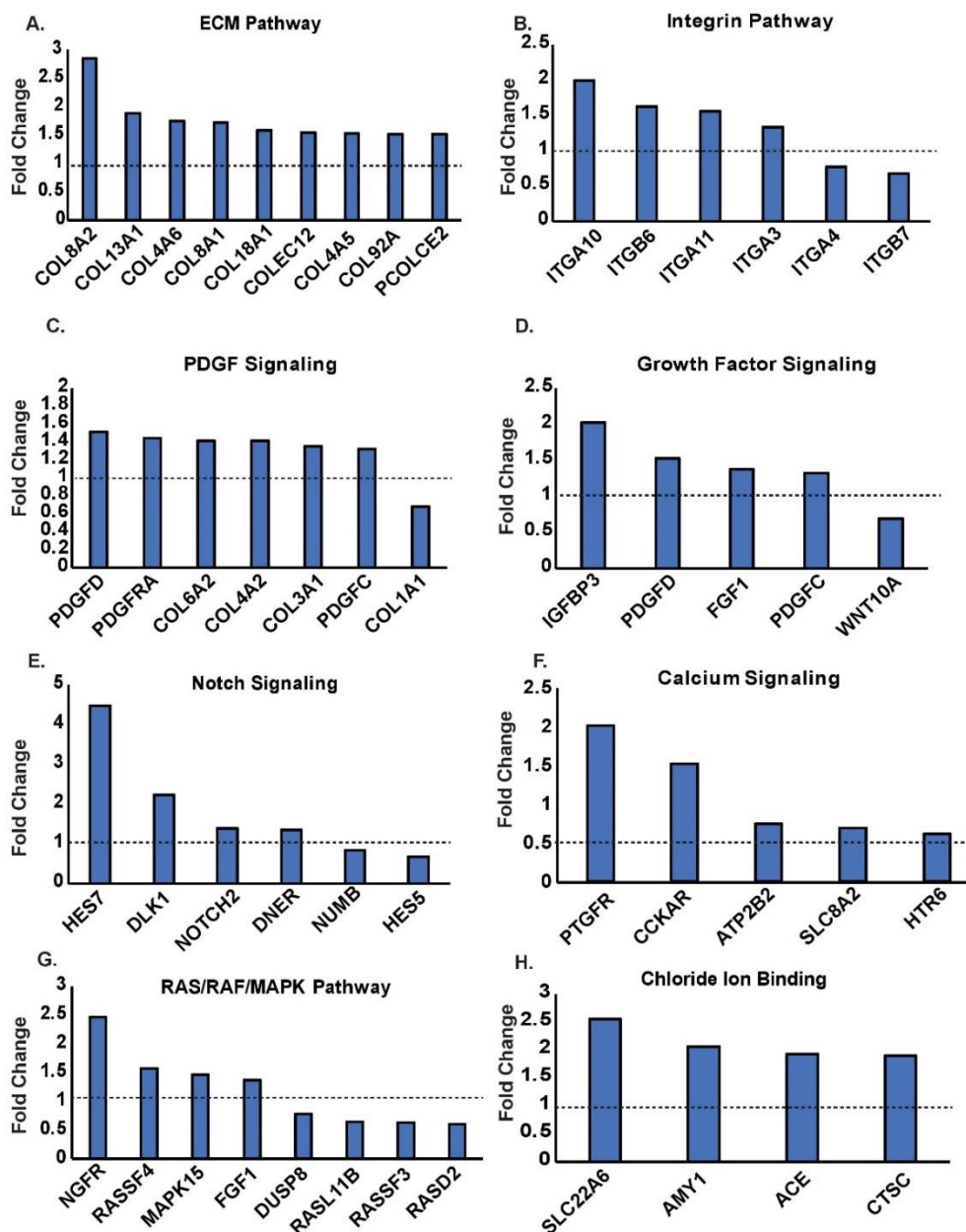


**Figure 6-6: Transcripts mediated by RBM8a at P17 regulate developmental pathways**

A) Fold change of differentially expressed RNAs in the Extracellular Matrix (ECM) pathway in RBM8a haploinsufficient mice. B) Fold change of differentially expressed RNAs in the Integrin pathway. C) Fold change of differentially expressed RNAs in the PDGF pathway. D) Fold change of differentially expressed RNAs in the Growth Factor pathway. E) Fold change of differentially expressed RNAs in the Notch pathway. F) Fold change of differentially expressed RNAs in the Calcium pathway. G) Fold change of differentially expressed RNAs in the Ras/Raf/MapK pathway. H) Fold change of differentially expressed RNAs in the Chloride Ion Binding pathway.

## 6.7 Transcriptome of RBM8a cKO mice during embryonic development

Since the tissue sequencing was done using postnatal brains, the results give us a snapshot of the transcriptome at the time when the mice usually die. In order to understand how the transcriptome leads to these developmental deficits, we repeated our sequencing experiment using E12 brains, separated into the cortex and midbrain/hindbrain. By separating the cortex and hindbrain, we can get a better idea on how different transcripts regulate the development of different structures within the brain. Similar to sequencing at P17, the differentially expressed RNAs in the E12 datasets were primarily comprised of protein coding RNAs. The next highest RNA species in the E12 datasets were processed pseudogenes, lincRNAs, and antisense RNAs (Figure 6-7A-D). To better understand how transcriptomic changes could potentially lead to our phenotype, we divided our datasets into upregulated and downregulated RNAs, then input the lists into gene ontology. The functions mediated by transcripts in the cortical dataset resembled the P17 data, regulating functions in cell proliferation (upregulated) and the cell cycle (downregulated). Interestingly, the upregulated transcripts include functions regarding the immune system, such as immune response and TNF production. In the hindbrain datasets, we saw similar functions to the P17 dataset, such as cell death, cell proliferation and skeletal system development (upregulated). In the downregulated dataset, we saw some interesting new functions that aligned well with our interneuron data. Specifically, these differentially expressed RNAs mediated GABAergic neuron differentiation and forebrain development. To get a better of the molecular mechanisms behind our phenotype, we also determined pathways that were enriched in our differentially expressed transcripts. To do this we input our list of differentially expressed transcripts (upregulated and downregulated combined) into DAVID Functional Annotation Bioinformatics Microarray Analysis web application (Huang et al., 2009; Huang da et al., 2009) and used their pathway analysis tool.

We had quite a few pathways differentially expressed in the cortex dataset, but relatively few in the hindbrain dataset (none that were significant using pathway analysis). Affected pathways included the phagosome pathway, lysosome pathway, osteoclast differentiation pathway, nicotine addiction pathway, and p53 pathway (Figure 6-7).

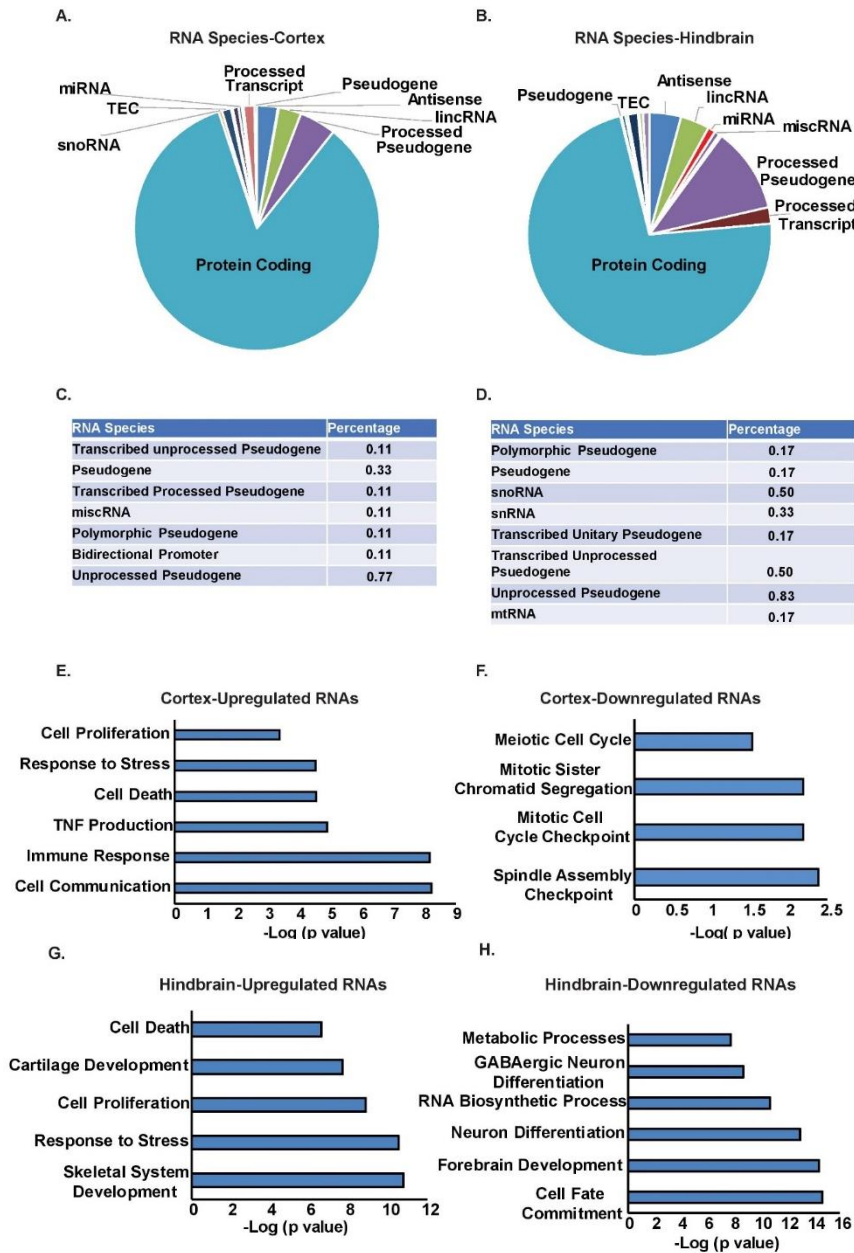


**Figure 6-7: RBM8a modulates different functions in different brain areas at E12, but consistently regulates cell proliferation**

A) The RNA species for differentially expressed transcripts in the cortex dataset (E12) of *Nes-cre;RBM8a<sup>fl/+</sup>* mice were identified. Primarily protein coding mRNAs were differentially expressed. B) The RNA species for differentially expressed transcripts in the hindbrain dataset (E12) were identified. Similar to the cortex, primarily protein coding mRNAs were affected. C-D) RNA species that represented less than 1% of differentially expressed transcripts in the cortex (E12) and hindbrain dataset respectively. E/F) Functions mediated by differentially expressed transcripts in the cortex dataset at E12, E (upregulated transcripts), F (downregulated transcripts). G/H) Functions mediated by differentially expressed transcripts in the hindbrain dataset at E12, G (upregulated transcripts), H (downregulated transcripts).

## **6.8 Cortical RNAs regulated by RBM8a at E12 mediate degradation pathways**

Like the overexpression and P17 datasets, we input our differentially expressed gene list into DAVID to identify pathways modulated by our gene list. At the E12 datapoint, we had significantly different hits compared to our P17 timepoints. We found significant representation of genes involved in the lysosome and phagosome signaling. Some hits were still reminiscent of other datapoint such as osteoclast differentiation (bone development) nicotine addition (psychiatric behaviors), and the p53 pathway (Figure 6-8), which was previously reported in (Mao et al., 2016). The only function to remain once we used more strict parameters (q value of 0.05 and fold change of 2x up or down), was p53 signaling.

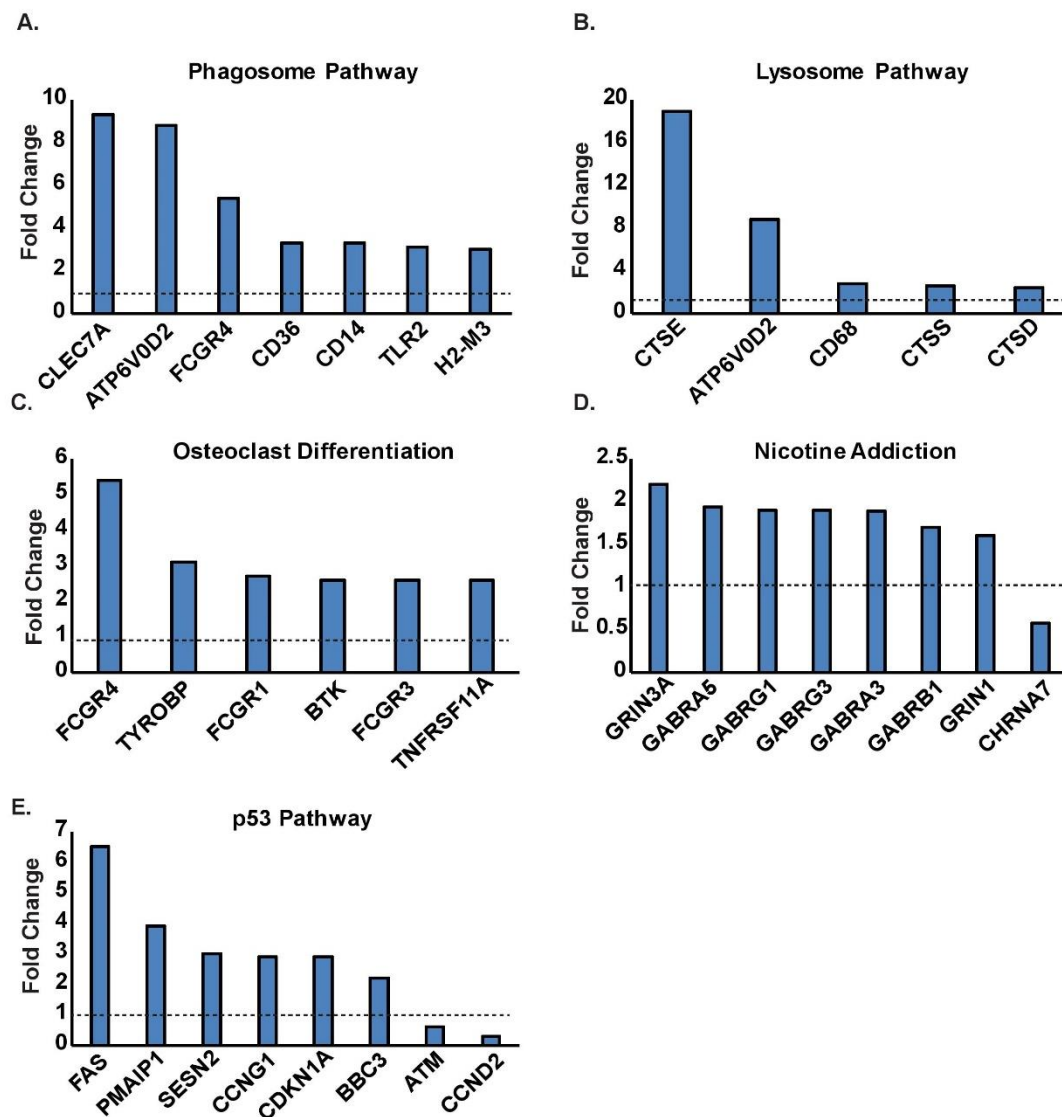


**Figure 6-8: Cortical RNAs mediated by RBM8a at E12 regulate a variety of pathways involved in immune response, addiction and cell death.**

A) Fold change of differentially expressed RNAs in the cortex of E12 Nes-cre;RBM8a<sup>fl/+</sup> mice in the Phagosome pathway. B) Fold change of differentially expressed RNAs in the Lysosome pathway. C) Fold change of differentially expressed RNAs in the Osteoclast differentiation pathway. D) Fold change of differentially expressed RNAs in the Nicotine Addiction pathway. E) Fold change of differentially expressed RNAs in the p53 pathway.

## 6.9 Conclusion

The results of this Chapter indicate the profound role of RBM8a in mediating developmental pathways and functions, such as the Notch pathway, cell proliferation, GABAergic interneuron differentiation etc. Specifically, RBM8a is required for cell proliferation and differentiation (as illustrated with our *in vivo* studies, and when perturbed results in aberrant cortical development.

We also illustrated that RBM8a is a moderate regulator of alternative splicing, and also regulates transcripts predisposed to degradation via NMD. We hypothesize that RBM8a exerts control on cortical development through its role in RNA stability. When RBM8a expression is altered, we suggest that RNAs become unstable and degrade via NMD regulated gene expression. Taken together these results indicate that different roles of RBM8a, namely in RNA stability and development, might actually be involved as opposed to being independent functions, as previously thought. More experiments need to be conducted to support this hypothesis.

## Chapter 7

### **RBM8a modulates anxiety and other neuropsychiatric behaviors**

#### **7.1 Introduction**

As RBM8a clearly plays an important role in the nervous system, we were interested if it had any effect on behavior. Especially seeing as there are tentative links between RBM8a and psychiatric disease. Since the cKO mouse is lethal, we utilized an RFP tagged lentivirus to either overexpress or knockdown RBM8a for behavioral experiments. A vector only virus (missing the insert) was used as a control. RBM8a expression is highest in development, and drops off during adulthood. However, it is highly expressed in adulthood in a few key regions, the hippocampus, olfactory bulb, hypothalamus, and cerebellum (Figure 7-1). As the hippocampus also plays a role in learning and memory, we chose this region as our target. We injected the virus bilaterally into the dentate gyrus of two-month-old male mice. After at least two weeks of recovery, we ran them through battery of behavioral tests.

#### **7.2 RBM8a expression does not affect locomotion**

Most behavioral tests rely on intact motor function, we wanted to first assess if modulating RBM8a expression in the hippocampus affected locomotion, as it could be a potential confound. This was done testing the total distance moved in a 10-min period in an open field. There was no significant different between RBM8a knockdown or vector controls in the total distance travelled (Figure 7-2).

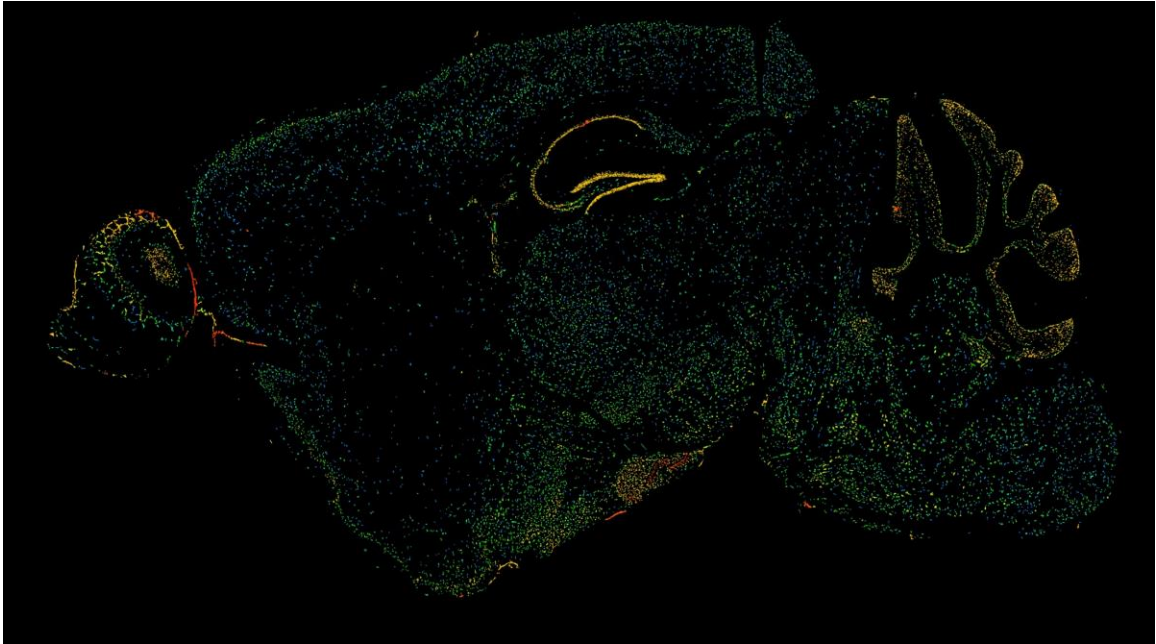


**Figure 7-1: Expression pattern of RBM8a in the adult mouse. Taken from the Allen Brain Atlas Expression Database.**

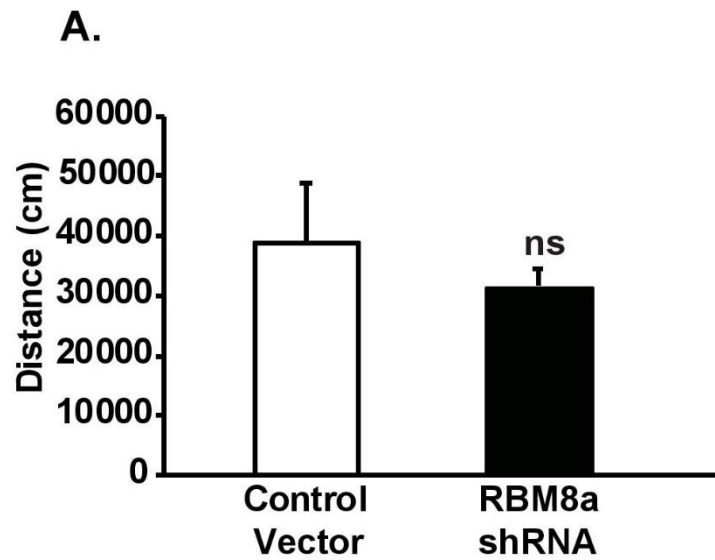


**Figure 7-2: RBM8a expression does not affect locomotion**

A) RBM8a shRNA vs control vector mice in distance travelled in an open field during 10 minutes,  $p=0.49$ ,  $n=9-11$ , Students t-test. Bar graphs represent means  $\pm$  SEMs.

### 7.3 RBM8a mediates anxiety behaviors

Next, we sought to investigate anxiety behaviors in the mice, as anxiety is often comorbid with many psychiatric diseases. To do this we placed the mice in a novel open field, and measured the amount of time they spent in the center vs the extremities of the field. A more anxious mouse will spend significantly less time in the center of a novel environment, as they are more vulnerable. Interestingly, RBM8a knockdown mice showed anxious behaviors, and spent significantly less time in the center of the novel open field (Figure 7-3), which is the same phenotype observed when RBM8a is overexpressed (reported previously by the lab) (Alachkar et al., 2013).

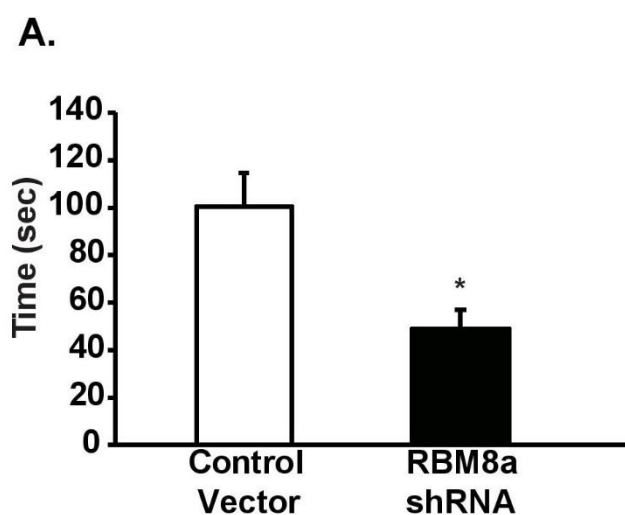


**Figure 7-3: RBM8a modulates anxiety behaviors**

A) RBM8a shRNA vs vector control, time spent in the center of a novel open field, \*,  $p=0.01$ ,  $n=9-11$ , Student's t-test. Bar graphs represent means  $\pm$  SEMs.

### 7.4 RBM8a knockdown but not overexpression affects learning and memory

As the hippocampus is important for learning and memory, we next evaluated whether RBM8a expression affects learning and memory. To do this we used contextual fear conditioning,

where a mouse is trained to associate a given environment (fear conditioning apparatus) with a shock. If the mouse correctly associates the environment with the shock, and remembers the environment (which relies on intact learning and memory), they will exhibit fear behaviors (freezing), which can be quantified. RBM8a knockdown mice froze significantly less than controls, indicating impaired learning and memory. RBM8a overexpression mice however did not differ significantly from controls, and maintained a freezing level around 80% (Figure 7-4).

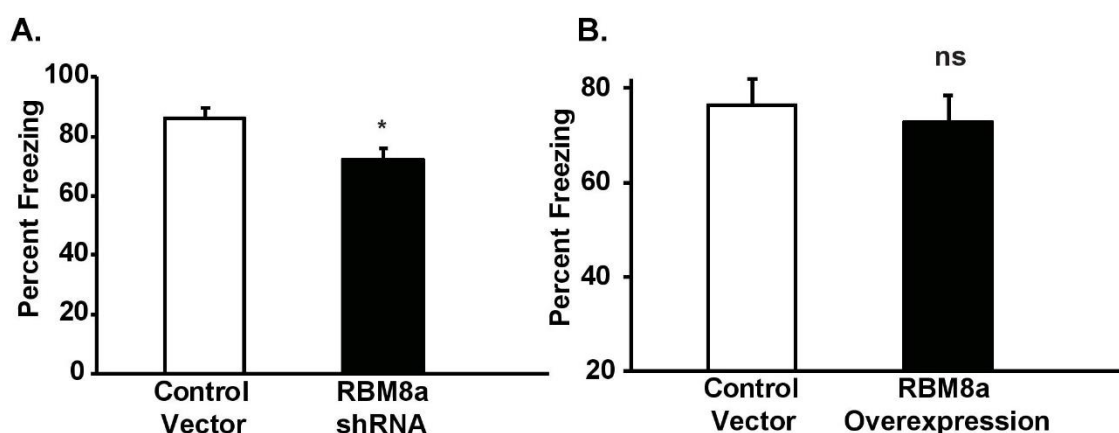


**Figure 7-4: RBM8a knockdown affects learning and memory**

A) Contextual fear conditioning RBM8a knockdown mice vs vector control, \*,  $p=0.01$ ,  $n=9-11$ , Students t-test. B) Contextual fear conditioning RBM8a overexpression mice vs vector control,  $p=0.53$ ,  $n=9-11$ , students t-test. Bar graphs represent means  $\pm$  SEMs.

### 7.5 RBM8a knockdown does not affect anti-depressive behaviors

Finally, we assessed anti-depressive behaviors in the mice, as depression is often common in psychiatric disease. Anti-depressive behaviors are assessed by putting a mouse in a novel bucket of water, and measuring the time floating vs swimming. Floating is considered behavioral despair, or giving up. Behavioral despair in this paradigm has been rescued with

administration of anti-depressants, validating this method as a measure of the anti-depressive phenotype. RBM8a knockdown mice did not differ from controls in this experiment. (Figure 7-5).

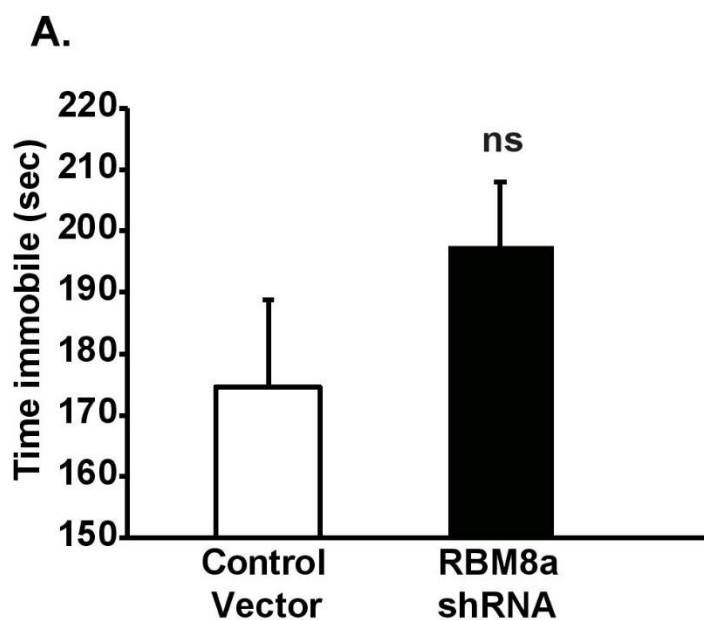


**Figure 7-5: RBM8a knockdown does not affect the anti-depressive phenotype**

A) Forced Swim Test in RBM8a knockdown vs vector control (6 min total time),  $p=0.21$ ,  $n=9-11$ , Students t-test. Latency to immobility was not measured. Bar graphs represent means  $\pm$  SEMs.

### **7.6 RFP expression in the dentate gyrus indicates successful injection of the virus**

Since the surgeries to inject the virus into the brain were done using a stereotactic apparatus, we could not verify that the virus was injected into the correct region until after the mice were euthanized. To do this we sliced the brains and stained them for RFP, as the virus was tagged with RFP. If the cells in the dentate gyrus are RFP positive, we know the virus was

successfully injected into the correct region, and we could accurately interpret the behavioral results. Figure 7-6 illustrates a successful injection into the dentate gyrus.

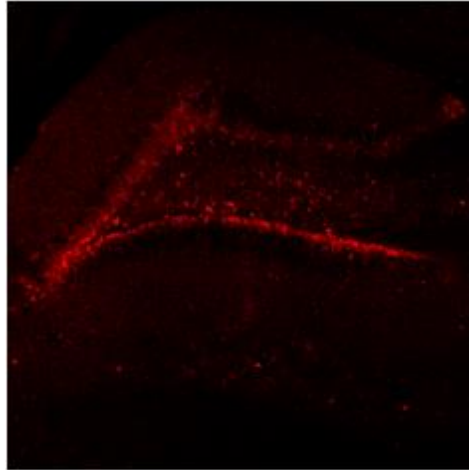


**Figure 7-6: The RFP tagged virus was successfully incorporated into the Dentate Gyrus**

A) RFP staining of behavior mice indicates the virus was injected into the correct brain area.

## 7.7 Conclusion

In this final chapter, we illustrated that RBM8a expression can modulate animal behaviors, specifically in paradigms used to assess behaviors found in psychiatric disease. RBM8a has previously been linked to rare cases of ASD, and TAR syndrome (which results in ID in 7% of cases). These behavioral experiments illustrate that RBM8a can affect psychiatric behaviors, and further shed light on the potential role of RBM8a in clinical neuropsychiatric disease.

## Chapter 8

### Discussion

#### 8.1 RBM8a is a positive regulator of neural progenitor cell proliferation

During early cortical development, NPCs in the SVZ/VZ undergo symmetric and asymmetric division and either self-renew or differentiate into neurons. This division is tightly regulated and ensures that the proper number of NPCs self-renew to maintain the stem cell pool, while enough cells differentiate and migrate in an inside out fashion to form the cortex.

Previously, RBM8a was mainly known for its role in NMD as a part of the EJC. However, research on other EJC factors has revealed alternative roles for these proteins independent of NMD. Specifically, the protein Magoh, with which RBM8a forms a heterodimer, has been implicated in the regulation of intermediate neural progenitors (INPs) (Silver et al., 2010). Additionally, Upf2 has been linked to the development of hematopoietic stem cells (Weischenfeldt et al., 2008). Upf1, another NMD protein has also been shown to promote neural differentiation and inhibit NPC proliferation *in vitro* (Lou et al., 2014). During NMD, the EJC proteins (RBM8a, Magoh, eIF4A3, Btz) reside on the exon-exon junctions and help the cell identify mRNAs with PTCs. Once the mRNAs identified to have a PTC, Upf1 and SMG1 (as part of the SURF complex) are recruited to join the EJC with the help of Upf2 and interact with eRF1. Then Upf1 is phosphorylated by SMG1 which tags the mRNA for decay.

Due to the developmental role of Magoh, and the fact that RBM8a and NMD proteins are associated with neurodevelopmental disorders, we were interested in investigating the potential role of RBM8a in neural development. First, we established that RBM8a has highest expression in the brain during embryonic development (specifically E10-13), and is present primarily in

Nestin + NSCs/NPCs (Zou et al., 2015). Next, we tested how knockdown or overexpression of RBM8a in the VZ/SVZ during embryonic development would affect the proliferation and differentiation of neural progenitors. Using *in utero* electroporation, we showed that RBM8a knockdown lead to significantly more differentiated neurons in the CP and significantly fewer NPCs in the VZ/SVZ while RBM8a overexpression produced significantly fewer neurons in the CP and significantly more NPCs in the VZ/SVZ. During development, after an initial phase of symmetric division of neuroepithelial cells, RGs undergo asymmetric division, in which one daughter cells continues to remain a NPC and self-renew in the VZ/SVZ. The other daughter cell produced in asymmetric division differentiates into a neuron and migrates to the CP. This balance between self-renewal and differentiation is tightly regulated, and critical for the successful development of the brain. It seems that RBM8a is essential for that balance. Decrease RBM8a expression and the balance tips towards differentiation, resulting in precocious differentiation and depletion of the NPC pools. Overexpression of RBM8a, and the balance tips towards proliferation, leading to over maintenance of the NPC pool at the expense of differentiated cells.

To further understand the mechanism by which RBM8a regulates the balance between self-renewal and differentiation of NPCs, we assessed how RBM8a regulates proliferation and cell cycle exit. Not surprisingly, RBM8a knockdown lead to decreased proliferation and decreased number of cells in the cell cycle, while RBM8a overexpression led to increased proliferation and number of cells in the cell cycle. The observation that RBM8a knockdown led to cell cycle exit (represented by GFP+/BrdU+/Ki67- cells) is consistent with our previous *in utero* electroporation data, which showed that RBM8a knockdown results in precocious differentiation. RBM8a overexpression was found to lead to decreased cell cycle exit, which is expected due to the large number of NPCs remaining in the stem cell fate.

Our knockdown data is consistent with a recently published paper that illustrated that RBM8a haploinsufficiency causes ectopic neuronal differentiation, and disrupts the balance between proliferation and differentiation (Mao et al., 2015). However, our data suggests that RBM8a overexpression tips the balance between proliferation and differentiation in the opposite direction as RBM8a knockdown, which they did not detect. This difference may most likely be attributed to the promoter used to drive RBM8a expression. Different promoters can lead to a different level of RBM8a expression, which might explain the variation of phenotype. We used an EF1 $\alpha$  promoter while (Mao et al., 2016) used a CAG promoter. (Zou et al., 2015). Both the EF1 $\alpha$  and CAG promoters are strong eukaryotic mRNA promoters, but nonetheless, any differences in plasmid construct could induce variation into results.

## **8.2 Using RNAseq to identify RBM8a's role in developmental functions, NMD regulation and alternative splicing**

In order to better understand the function of RBM8a, we examined which RNAs are regulated by RBM8a by performing RNAseq on SH-SY5Y cells transfected with RBM8a overexpression or control vectors. We then ran differential expression analyses to determine any change in RNA expression between the experimental (RBM8a overexpression) and control samples. We finally utilized DAVID to assess functions and pathways mediated by these RNAs.

Functional analyses of our RNAseq data indicates that overexpression of RBM8a impairs neuronal migration. ECM proteins including integrin and collagens are crucial for neurogenesis (Matsunaga et al., 2017; Myers et al., 2011). ECMs are differentially expressed when RBM8a is overexpressed, suggesting that RBM8a potentially regulates neuronal migration through ECM proteins. This sequencing data further demonstrates that RBM8a regulates multiple processes during brain development. Functionally, we were also able to determine what biological functions

are significantly mediated by the RNAs regulated by RBM8a. These functional categories include neuronal differentiation, cell proliferation, biological adhesion, and cell migration, which is consistent with our *in vivo* data. Also of note is that there is a significant number of RNAs in our dataset that regulate skeletal development and vascular development. This is particularly interesting, since TAR syndrome, which is caused by a compound mutation in RBM8a, is characterized by missing radii bones (skeletal development) and low blood platelet counts (vasculature). However, we only sampled brain tissue, so bone tissue needs to be sampled to fully understand the role of RBM8a in bone development.

Due to RBM8a associations with psychiatric disease, we were interested in assessing whether our list of differentially expressed transcripts was enriched for risk genes for psychiatric and neurological disease. Using the hypergeometric analysis, we determined that ASD, SCZ, ID and AD risk genes were significantly overrepresented in our differentially expressed dataset. We speculate that perhaps RBM8a plays a role in regulating genes that increase the risk for these neurological/neuropsychiatric phenotypes.

As previously mentioned, RBM8a assists in NMD as a member of the EJC to help identify mRNAs with PTCs. However, NMD proteins also regulate a subset of transcripts containing certain characteristics, such as an intron in the 3' UTR, long 3' UTR, and exon junction > 50nt downstream of a stop codon. To determine if RBM8e regulates transcripts targeted by NMD, we examined our list of differentially expressed transcripts and identified how many expressed characteristics that would make them prone to degradation via NMD. We found that 45.5% of RNAs regulated by RBM8a possessed features predisposing them to degradation by NMD. Therefore, we think that perhaps the role of RBM8a in NMD and neurogenesis are not so independent after all. It is possible that the neurogenic phenotypes are due to alternative expression and regulation of transcripts regulated by both RBM8a and NMD. In support of this

idea, the NMD targeted transcripts also mediate similar functions to the whole dataset, namely those prominent in development such as neurogenesis, cell motility and communication. Renal development was also a function these RNAs mediate, which is interesting in light of kidney pathology commonly found in TAR syndrome patients. Further experiments are needed to confirm that mRNAs targeted by NMD are responsible for the alteration in neurogenesis seen with RBM8a overexpression.

EJC factors have also been implicated in alternative splicing (Glisovic et al., 2008; Green et al., 2003; Lejeune and Maquat, 2005; McGlincy and Smith, 2008; Michelle et al., 2012; Ni et al., 2007; Nott et al., 2004; Tange et al., 2005). Therefore, we were curious as to whether RBM8a overexpression in SH-SY5Y cells would lead to changes in alternative splicing. There were 314 alternative splicing events found in our dataset, spanning a variety of types of alternative splicing. The most prominent type of alternative splicing was skipped exon (61.4 %), followed by alternative last exon (18.5 %). 9.24% of alternative splicing events were alternative 5' splicing site, while 11.15 % were alternative 3' splicing site. This data indicates that RBM8a overexpression does seem to have an effect on alternative splicing even though the effect is small. The genes that were determined to be alternatively spliced were also enriched for ASD risk genes, but not SCZ, AD, ID, or Crohn's disease risk genes. This data supports the hypothesis that RBM8a may be involved in the pathogenesis of ASD through an increase in alternative splicing of ASD risk genes.

Throughout all of our analyses of our RNAseq data, alterations in developmental processes, specifically neurogenesis, have remained consistent among all of our datasets (differentially expressed RNAs, cross-reference with ASD, NMD targets, alternatively spliced genes etc.). These processes were those also found to be abnormal in our overexpression and

knockdown experiments, indicating an important role for RBM8a in neural development, and the risk for neurological and psychiatric disease.

Studies of RBM8a and other NMD factors in embryonic brain development may help understand the pathophysiology of several neurodevelopmental disorders such as ID, ASD and SCZ. The NMD gene *Upf3b* gene has already been implicated in ID, ASD and SCZ. Chromosomal abnormalities such as copy number variations (CNVs) including both duplications and deletions are enriched in many patients with ID, ASD and SCZ (Mefford et al., 2008). Some of these CNVs, including 1q21 (Brunetti-Pierri et al., 2008), are significantly associated with all three disorders. As RBM8a is localized in the 1q21 region, examination of the function of this gene may provide insight on the causes of mental illnesses and could facilitate the development of new targets for neurodevelopmental illnesses.

### **8.3 RBM8a haploinsufficiency leads to microcephaly and altered distribution and number of cortical interneurons**

Here we illustrate RBM8a's pivotal role in the differentiation and migration of inhibitory neuronal progenitors. First, we established that RBM8a haploinsufficiency leads to lethality in early postnatal development (prior to weaning) and results in microcephaly, decreased cortical thickness, and disorganized cortical layers. This phenotype has been previously reported (Mao et al., 2015), and is consistent with our observations. Interestingly, similar phenotype is observed in the *Magoh* cKO mouse (*Magoh* forms a heterodimer with RBM8a) (Silver et al., 2010, 2013).

While observing the *Nes-cre;RBM8a<sup>fl/+</sup>* mice, we noticed they exhibited spontaneous seizures around P14-P21. Therefore, we thought that perhaps there were interneuron deficits in addition to the previously reported excitatory neuron defects.

We established that RBM8a cKO in NPCs resulted decreased PV + and NPY+ cortical interneurons, and abnormal distribution of PV+, SST+ and NPY+ interneurons in the cortex. Our data showed a significant decrease in the number of PV+ interneurons in the cortex of Nes-cre;RBM8a<sup>fl/+</sup> mice. As PV+ interneurons are the most populous interneuron subtype in the cortex, this deficit has the ability to significantly alter the E/I balance. Additionally, the distribution of PV+ interneurons in the cortex was altered, with more cells residing in the superficial layers, at the expense of the deeper layers. It is well known that each cortical layer receives input from specific areas in the brain, and sends their axons to specific areas of the brain. A disruption in the cell numbers in each cortical layer, especially inhibitory cells, can seriously disrupt the neuronal networks of the brain, which can negatively affect behaviors, such as cognition, and even autonomic function (Amilhon et al., 2015; Verret et al., 2012). The decrease in cell number was not observed with SST+ cells, but was with NPY+ cells. The abnormal laminar distribution was observed for all interneuron cell types. Taken together, this illustrated a profound deficit in inhibitory circuitry in the Nes-cre;RBM8a<sup>fl/+</sup> mice. Our study demonstrated that RBM8a was involved in the differentiation of interneuron subtypes. During the process of interneuron development, the absence of RBM8a leads to changes in cell number, migration, and size of interneuron subtypes. The novel role of RBM8a in the interneuron fate specification and migration could arise as a result of abnormal tangential migration of interneuron progenitors, combined with paracrine and juxtacrine signaling of excitatory neurons.

#### **8.4 *In utero* mechanisms behind the abnormal interneuron distribution and number**

To examine whether changes in interneuron progenitors are responsible for this the changes in interneuron number and distribution, we first sought to determine if there were

changes in proliferation in the GE, where interneuron progenitors reside. We examined this by injecting pregnant dams with EdU 1hr before perfusion, to label cells in the S phase of the cell cycle. We did find a significant decrease in the number of EdU+ cells in the ganglionic eminence, illustrating that deficits in proliferation are partially responsible for the observed phenotype. To further explore this, we stained E17 brain slices for interneuron progenitor marker Nkx2.1. Interestingly, we did not see changes in the number of Nkx2.1+ progenitors in the GE. A possible explanation for why we saw decreased proliferation in the GE, but no change in Nkx2.1+ progenitors, is that the proliferation deficit is due to other cell types present in the GE, such as glial cells and dopaminergic neurons.

Since we determined that the interneuron progenitor population is normal at E15, we hypothesized that the change in number and distribution of cortical interneurons was due to abnormal tangential migration of the progenitors. That is, the incorrect distribution of interneurons was arising as the progenitors were migrating from the GE to the cortex. To investigate this, we crossed our RBM8a<sup>fl/fl</sup> mice with and Nkx2.1 cre. Nkx2.1;RBM8a<sup>fl/+</sup> mice will only have RBM8a heterozygously knocked out of interneuron progenitors. This will allow us to assess whether our interneuron phenotype is due to intrinsic changes in the interneuron progenitors (cell autonomous) or due to extrinsic cues from the already perturbed excitatory interneurons (cell non-autonomous). By looking at the postnatal distribution of the interneurons in these mice, we will also be able to indirectly tell if the migration of these progenitors is causing these deficits. In addition, more direct experiments will need to be conducted to conclusively investigate these migration defects (by labeling the progenitors and tracking them through their migration to the cortex). We found that there was no change in the cell number of PV+, SST+, or NPY+ cells, and there was a small change in the distribution of SST+ cells, and a trend towards a change in distribution phenotype of PV+ and NPY+ cells. This indicates that while there are

some changes in the intrinsic properties of the interneuron progenitors, it is not sufficient to cause the significant decrease in interneurons in the cortex and the altered distribution, as observed in the Nes-cre;RBM8a<sup>fl/+</sup> mice. These abnormalities are likely due to cues from excitatory cells and other cell types already present in the cortex as the interneurons are migrating.

### **8.5 Molecular mechanisms regulating interneuron development**

In order to better understand the molecular mechanisms in the cKO mouse, we used RNA sequencing to look at the brain transcriptome at P17 and E12. Initially, we used a p value of 0.05 and fold change of 1.5x up or down as a cutoff, so we had more genes in our list which enabled us to do more functional analyses. However, these functional analyses use multiple sampling, and thus have a high rate of false positives. Q values (using false discovery rate or Benjamani) are typically used to circumvent this phenomenon. We initially used the less conservative p value, which indicates our results likely have false positives. We then repeated the functional analyses using a cutoff of a q value of 0.05 and a fold change of 2x up or down. While the resulting functions were slightly different than the p value results, the q value results mirrored both our *in vivo* data, and RBM8a overexpression (in SY5Y cells) dataset. Our p value dataset still contains useful information, but needs to be validated in order to be conclusive (as is such with any RNAseq data).

Functions that emerged from the P17 dataset (using p value as a cutoff) include vascular development, bone development, ossification, and cell adhesion. These are interesting, as TAR syndrome (caused by compound mutations in RBM8a) results in phenotypes surrounding bone and vascular development (namely thrombocytopenia and missing radii bones). Therefore, it was very intriguing to see that RNAs regulated by RBM8a mediate these functions. Again, bone tissue

needs to be examined to further explore this observation. After repeating this experiment using stricter cutoffs, our dataset was found to mediate functions including cell proliferation, cell adhesion, hindbrain and forebrain development, cell death, and cell differentiation. These results are consistent with both our RBM8a overexpression dataset, and *in vivo* data.

We wanted to examine the transcriptome at E12, since that is during peak neurogenesis, and likely when RBM8a has its most pivotal function. We did RNAseq on the cortex and hindbrain separately (using a p value of 0.05 and fold change of 1.5 up or down as a cutoff). RNAs differentially expressed in the cortex included expected functions such as cell cycle, cell death, proliferation. RBM8a has been implicated in neurogenesis, so these results were not surprising. Interestingly, we observed changes in quite a few immune system related RNAs including TNF signaling and immune response. There have been recent papers linking the immune system and neurodevelopment to psychiatric disease, it's possible that the immune system is dysfunctional leading to the observed phenotypes. However, we cannot determine whether these immune deficits are causative for the observed phenotype, or if they simply result from other RBM8a-mediated changes in RNA expression during development. Some particularly interesting functional hits were sister chromatid segregation, cell cycle checkpoint and mitotic spindle assembly. These are all functions that regulate asymmetric division, which we illustrated to be perturbed when RBM8a expression is altered. This result indicates to me that the sequencing worked correctly, and also leads me to believe that asymmetric division and the molecules that govern it likely play a large role in the phenotype. Finally, in the hindbrain dataset, we had hits in forebrain development and GABAergic differentiation. This further cements the important role of RBM8a in neural development, in particular that of the interneurons. We repeated this analysis using more strict parameters (q value of 0.05 and fold change of 2x up or down) and only found

one significant function, p53 signaling. The connection between p53 and the EJC complex has been previously reported, which supports our RNAseq results (Mao et al., 2016).

In terms of altered pathways, our RNAseq results point to some expected signaling pathways, such as ECM, GF, Notch, and Calcium. These are all pathways that are very important during development, so it is not surprising that they are affected in our knockout mouse. At the embryonic time point, we had some more unexpected results, namely phagosome and lysosome signaling. These results suggest that these mice could potentially have issues with breaking down cellular debris. This would definitely be an interesting avenue to explore in the future, but at this time we have no additional data to support this hypothesis.

Based on the observed spontaneous seizures the Nes-cre;RBM8a<sup>fl/+</sup> mice experience, in addition to the decreased number of PV+ and NPY+ cells, we hypothesized that the electrophysiological properties of the pyramidal cells in the cortex were likely altered. To assess this we conducted spontaneous transmitter recordings in the somatosensory cortex, and discovered a significant decrease in the frequency of GABA transmission, but no change in the frequency of glutamate transmission or the amplitude of GABA or glutamate transmission. Paired with our data indicated decreased interneuron number, we speculate this decrease in the frequency of GABA transmission is due to the decreased number of interneurons, and not due the neurotransmitter volume in the synaptic vesicles. This hypothesis is further supported that there is no change in GAD67 expression, which indicates there is no deficiency in synthesizing GABA. To conclusively assess this hypothesis, we would need to conduct mini IPSC electrophysiological recordings.

Finally, the biggest question we want to eventually answer is can we rescue this phenotype. To start, we wanted to isolate one signaling pathway that we think has the strongest effect on the phenotype. Due to RNAseq data we obtained, the fact that Notch regulates

asymmetric division (mimicking phenotypes we observed in our *in utero* electroporation experiments), and is absolutely vital for neurogenesis, we thought the notch pathway would be a good target. First, we used western blot to see if any proteins in the pathway were altered. We found that the cKO mice had about a 50% reduction in Notch1 NICD (notch intracellular domain). When notch ligands bind to the receptor, NICD is cleaved and travels into the nucleus to modulate gene expression. If this protein is downregulated it will likely lead to dysregulation of the notch pathway and downstream targets, which could definitely have effects on neurogenesis and explain our phenotype. This is an excellent starting point, but more experiments need to be done to conclusively link this pathway to the phenotype and determine whether restoration of Notch signaling is sufficient to rescue the deficits seen with RBM8a cKO.

### **Future Directions**

Two big questions remain at the end of this project:

1. Where during interneuron development does the interneuron number and distribution phenotype emerge?
2. Does the Notch pathway regulate the changes seen in the cKO mice?

Here I will illustrate the experiments that should answer these questions. To answer question 1, the Nkx2.1;RBM8a<sup>fl/+</sup> mice can be crossed to a RFP cre reporter, so that any cell with RBM8a knocked out is also RFP (or GFP) positive. Then, we can track these interneuron progenitors during development (E12-E18, 0.5-day increments) to determine if they are migrating to the wrong area (not the cortex), is migration delayed leading to them migrating to the wrong layer, or are they undergoing apoptosis (or a mixture of all 3). This will help shed light on when exactly the deficits are emerging. Based on my analysis of P17 brains in the Nkx2.1;RBM8a<sup>fl/+</sup> mice, I speculate that there are definite intrinsic deficits in the interneuron progenitors, but they are likely also responding to cues from other impacted cells, leading to their altered distribution. This was

evident as removing RBM8a from interneurons alone did not recapitulate all of the cell number/distribution phenotypes, but only a few.

To answer the second question, two experiments are key. First, we can cross the cKO mice to Notch reporter (GFP) and observe GFP expression in the GE embryonically as a proxy for evaluating notch expression. The most important experiment however, is to rescue the phenotype. Since Notch1 NICD is downregulated, we can cross the cKO mice with a Notch overexpression mouse (cre dependent), or electroporate a Notch overexpression plasmid into the VZ during development. If this rescues the phenotype, then we can conclusively say that Notch signaling is causing the observed phenotypes.

## Appendix

### Differentially expressed RNAs that are potential NMD targets

Long 3' UTR (> 1250 bp)	Intron in the 3' UTR	Exon Junction > 50 nt downstream of a stop codon
-------------------------	----------------------	--

<p>ABAT, ABCA1, ABTB2, ACPP, ACSL6, ADAM9, ADAMTS1, ADAMTS3, ADAMTS9, ADRA2A, AEN, AFAP1, AHRR, AIF1L, AK4, AKAP12, ALDH1A3, ALDH1L2, ALDH4A1, ALPK1, ALPK3, AMOTL2, ANGPTL2, ANK1, ANKRD33B, ANO3, ANP32E, AP5Z1, APC2, APCDD1L, APOL4, APOLD1, ARC, ARHGAP24, ARHGAP29, ARHGAP42, ARHGEF6, ARID5B, ARRDC4, ARSJ, ASCC3, ASIC1, ASTN1, ATCAY, ATF3, ATP1B2, ATP2B2, ATP7B, ATP81A, ATXN1, B3GALT6, B3GALT7, B3GALT8, BAALC, BAHCC1, BAIAP2, BDNF, BEND6, BHLHE40, BLOC1S2, BNC2, BRSK2, BSN, BTG2, BTN3A2, C10orf32, C11orf70, C12orf5, C17orf51, C18orf54, C3orf14, C3orf52, C3orf62, C4orf25, C7, C8orf37, CABP7, CACNA1B, CACNA2D2, CALB1, CALCRL, CAMK2B, CAMK2N1, CAMKV, CAPN6, CAST, CBLN1, CCDC25, CCDC3, CCDC64, CCDC68, CCDC88C, CCND1, CCPG1, CCR6, CDC42EP4, CDHR1, CDHR3, CDK18, CDK5R1, CDKN1A, CECR6, CELF3, CELF4, CELF5, CELF6, CEP170B, CEP44, CERK, CERKL, CGNL1, CHCHD7, CHL1, CHN2, CHRNA3, CHRNB2, CHRND, CHST1, CHST15, CIT, CLIC2, CLMN, CLSTN2, CMPK2, CNR1, CNTN1, CNTN2, CNTNAP2, COBL, COBLL1, COL1A1, COL4A1, COL5A1, COLQ, CO17, CORIN, CPLX1, CPLX2, CPNE4, CSF1, CTBS, CUX2, CXorf38, CYB561, CYFIP2, CYS1, DAAM2, DAPK2, DCLK3, DCX, DDIT4L, DDN, DDX51, DDX60L, DGKI, DGKK, DIAPH2, DIEXF, DKK2, DLG3, DNAJC30, DNAJC5, DOCK3, DOCK5, DOK4, DOK6, DPP10, DRAM1, DSEL, DUSP4, DUSP8, EBF3, EDA2R, EDARADD, EDNRA, EDNRB, EFCAB1, EFN1, EFN2,</p>	<p>ADAM8, ADAMTS9, AKAP12, ALDH4A1, ANK1, ANP32E, ARC, ARBCF, ASB9, B2M, B3GAT1, BAIAP2, BCL2L12, BEND6, BRSK2, BSN, BST2, BTN3A2, C10orf32, C16orf95, C1orf54, C21orf58, C8orf31, CAMK2B, CAST, CDKN2A, CELF3, CELF4, CELF5, CELF6, CHCHD7, CLYBL, COX17, CSF1, CXorf38, DDC, DUSP28, EDA2R, EFCAB1, ENC1, FHIT, FLT3LG, FOXO1, FRMD4A, GCAT, GLB1L2, GLRX, GRIA4, GRM7, GRM8, HBEGF, HLA-E, HRAS, HRK, ID2, ID3, ID4, IGFBP3, INSIG1, JPH1, KCNC3, KRBOX4, LDB2, LHFPL5, LDB2, LHFPL5, LRRC23, MEIS1, MICAL2, MMP28, MND1, MORN5, NRG1, PBX1, PHLDA3, PLCE1, PLCH1, PLEKHA5, PLEKHA6, PZLC3, PROM1, PTPRO, PWWP2B, RAP1GAP, RBM3, RBPMS2, RGS7, SCN3B, SKAP2, SLC29A3, SPECC1, STMN4, SYP, TAC3, TCFL2, TMEM63A, TOM1L1, TPI1P2, ULBP1, UPF1, VMO1, YBX2, ZDHHC11, ZDHHC15, ZFP36L1, ZNF217, ZNF418</p>	<p>ADAM8, ADAMTS9, AKAP12, ALDH4A1, ANK1, ANP32E, ARC, ARBCF, ASB9, B2M, B3GAT1, BAIAP2, BCL2L12, BEND6, BRSK2, BSN, BST2, BTN3A2, C10orf32, C16orf95, C1orf54, C21orf58, C8orf31, CAMK2B, CAST, CDKN2A, CELF3, CELF4, CELF5, CELF6, CHCHD7, CLYBL, COX17, CSF1, CXorf38, DDC, DUSP28, EDA2R, EFCAB1, ENC1, FHIT, FLT3LG, FOXO1, FRMD4A, GCAT, GLB1L2, GLRX, GRIA4, GRM7, GRM8, HBEGF, HLA-E, HRAS, HRK, ID2, ID3, ID4, IGFBP3, INSIG1, JPH1, KCNC3, KRBOX4, LDB2, LHFPL5, LDB2, LHFPL5, LRRC23, MEIS1, MICAL2, MMP28, MND1, MORN5, NRG1, PBX1, PHLDA3, PLCE1, PLCH1, PLEKHA5, PLEKHA6, PZLC3, PROM1, PTPRO, PWWP2B, RAP1GAP, RBM3, RBPMS2, RGS7, SCN3B, SKAP2, SLC29A3, SPECC1, STMN4, SYP, TAC3, TCFL2, TMEM63A, TOM1L1, TPI1P2, ULBP1, UPF1, VMO1, YBX2, ZDHHC11, ZDHHC15, ZFP36L1, ZNF217, ZNF418</p>
---	---	---

<p>ELAVL3, ELMOD1, ELOVL5, EMP2, ENC1, ENDOD1, ENPP6, EPB41L4B, EPHA10, EPHA8, EPN3, ERMP1, ERO1L, ESRRG, ETV1, EYA4, EYS, F2RL1, FAM114A1, FAM124A, FAM129A, FAM132B, FAM134B, FAM135A, FAM13B, FAM13C, FAM155B, FAM212B, FAM46A, FAM71F2, FAM83H, FAS, FAXC, FBXO32, FBXO39, FERMT1, FGF1, FGF14, FGFR1, FKBP5, FLCN, FLJ45513, FMN1, FNDC5, FOXC1, FOXO1, FOXR2, FRAS1, FREM1, FREM2, FRMD3, FRMD4A, FRMD4B, FRZB, FSTL1, FSTL3, FSTL5, FUT10, FUT8, FZD4, FZD7, GABRB3, GABRP, GAREM, GATA2, GBP2, GDAP1L1, GINS4, GJA1, GLI2, GOLGA7B, GPC4, GPD1, GPM6A, GPR124, GPR155, GPR176, GPR56, GPRC5B, GPX8, GRAMD4, GRHL1, GRIA4, GRIN3A, GRIP1, GYG2, H1F0, HBEGF, HEG1, HES2, HIF3A, HLA-E, HLTF, HMGXB4, HMHA1, HMP19, HNF4G, HPCAL4, HR, HS6ST3, HSPB7, HTR6, HYOU1, ID4, IFIT1, IGDCC3, IGF2BP2, IGFBP3, IGFBP5, IGLON5, IKZF1, IMPACT, INA, INADL, INSC, INSIG1, INTS6, IPO5P1, IQSEC3, IRF6, IRGQ, IRS2, ISLR2, ITGAV, ITIH5, ITPKB, ITPR2, JAG1, JAG2, JAM2, JAZF1, JDP2, JPH1, JPH3, JRKL, KALRN, KAT2B, KCNC1, KCNG3, KCNJ2, KCNJ9, KCNK3, KCNMB2, KIAA0825, KIAA1024, KIAA1217, KIAA1377, KIAA1549L, KIAA1958, KIF14, KIF1A, KIF21B, KIRREL, KLF10, KLF11, KLF9, KLHL14, KRBOX4, KRT80, L3MBTL3, LAMC1, LANCL2, LBH, LDB2, LDB3, LDLR, LDLRAD4, LEPR, LGR4, LHFPL3, LHFPL4, LIF, LIMCH1, LIPA, LMO3, LM04, LOC100130705, LOC653602, LRP1B, LRP4, LSAMP, LURAP1L, LYNX1, LZTS1, MAK, MAN2A1, MANEAL, MAP2, MAP3K1,</p>		
--	--	--

<p>MAP3K14, MAP6, MAP7, MAPT, MB21D2, MBOAT1, MDM2, MEIS1, MEX3B, MFSD4, MFSD8, MGLL, MICAL2, MITF, MKI67, MLF1, MLLT3, MLLT4, MMAA, MME, MMP24, MPPED2, MPV17L, MRAP2, MST4, MTL5, MTUS1, MVB12B, MYCL, MYH10, MYLIP, MYO10, MYO1E, MYT1, MYT1L, NANOS1, NAT8L, NAV1, NCAN, NCAPG, NCOA5, NDST3, NEDD4, NEDD9, NEGR1, NEURL1, NFASC, NFATC4, NGFR, NHS, NKD1, NLGN1, NMNAT2, NOS1, NOTCH2, NPTXR, NPY2R, NRBP2, NRCAM, NRG1, NSG1, NT5E, NTRK2, NUAK1, NUDT10, NYAP2, OLFM3, OPN3, OXCT1, PAM, PAPSS2, PAQR5, PAQR8, PARP11, PATZ1, PAX5, PBX1, PCDH18, PCDHB16, PCTP, PDCD4, PDE11A, PDE8B, PDGFC, PDGFD, PDGFRA, PDGFRB, PDK1, PDK4, PEAR1, PER2, PER3, PEX5L, PFKFB2, PGBD5, PHEX, PHF21B, PHKA1, PHKB, PHYHIPL, PI4K2B, PID1, PIFO, PIGN, PITPNC1, PITPNM3, PKP2, PLCH1, PLD1, PLD6, PLEKHA2, PLEKHA6, PLEKHA7, PLEKHG4B, PLEKHH2, PLS3, PLXNA2, PLXNA2, PLXNA4, PMEPA1, PNMA3, PNMAL2, POC1B, POLD3, POU3F2, POU4F1, PPAP2B, PPARGC1A, PPFIA4, PPFIBP1, PPM1D, PP1R16B, PPP2R2C, PRDM11, PRICKLE1, PRKCA, PROX1, PRPS2, PRR11, PRR18, PRRT2, PRSS23, PRTFDC1, PTCHD4, PTER, PTGFR, PTGFRN, PTGR2, PTP4A3, PTPN14, PTPRB, PTPRE, PTPRG, PTPRK, PTPRN2, PTPRO, PVRL4, QKI, RAB11FIP4, RAB27A, RAB31, RABGAP1L, RALGPS2, RASSF4, RASSF5, RASSF8, RAX, RBM24, RBM3, RCN1, RD3, REL, RERG, REST, RET, RGL1, RGMB, RHOB, RIMKLA, RIMS1, RIMS2, RIMS4, RIN2, RNASEH2C,</p>		
---	--	--

<p>RPRD1A, RPS6KL1, RREB1, RUNX1T1, RXRA, SARM1, SCAMP5, SCG3, SCML1, SCN3A, SCN3B, SCN4B, SCN9A, SCRT1, SDC2, SDC3, SEMA3A, SEMA5A, SEMA6A, SERPINB8, SERPINB9, SERTAD2, SEZ6L, SFRP1, SGIP1, SH3BP5, SH3RF3, SHANK2, SHOX2, SIX1, SIX3, SIX4, SKAP2, SLC12A7, SLC16A12, SLC1A2, SLC25A12, SLC25A34, SLC29A3, SLCA12, SLCA4, SLC35F3, SLC43A2, SLC47A1, SLC6A2, SLC7A11, SLC7A14, SLCA5P1, SLC8A1, SLC8A2, SLC8A3, SLCO4C1, SLIT1, SLITRK5, SMG7, SMIM17, SMOC1, SMPD3, SNCA, SORBS2, SORL1, SOX4, SOX7, SOX9, SPARC, SPATA13, SPATA18, SPATAS2L, SPECC1, SPOCK1, SPOCK3, SPON1, SPRYD4, SPSB1, SRC, SREBF2, SRGAP2, SRRM3, SRRM4, ST8SIA3, ST8SIA4, STC2, STMN2, STMN3, STMN4, STON1, STS, STX1A, SULT4A1, SUSD5, SVOP, SYP, SYT13, SYT14, SYT2, SYT4, SYT7, SYTL5, TBC1D30, TBC1D4, TBX18, TCF7L2, TCTA, TEC, TFAP2B, TFPI, THRB, THSD4, TIMP3, TIPARP, TLE3, TLE4, TMCC3, TMEM104, TMEM105, TMEM108, TMEM123, TMEM151B, TMEM179, TMEM2, TMEME255A, TMEM35, TMEM56, TMEM63A, TMTC1, TNFRSF10B, TNFRSF19, TNFSF3, TNIK, TOR4A, TP53INP1, TPI1P2, TPPP, TPR, TRAF5, TRHDE, TRIM59, TRIM67, TRMT61A, TRPS1, TRPV1, TSHR, TSLP, TSNARE1, TSPAN18, TSPEAR, TTBK1, UACA, UAP1L1, UBASH3B, UBTF, UFL1, ULBP1, UNC13A, UNC5CL, UNC80, UPF1, USP25, VAV2, VAV3, VEGFA, VIPR2, VPS13A, VSIG10, WDFY2, WDR52, WDR77, WIPF1, WSB1, WWC2, WWTR1, XKR5, XYLB, YAP1, ZC3H12B, ZC3H14, ZDHHC15, ZDHHC22, ZFP3,</p>		
---	--	--

ZFP35L1, ZFP3, ZFP36L1, ZFR2, ZMAT3, ZMAT4, ZNF117, ZNF124, ZNF135, ZNF208, ZNF217, ZNF319, ZNF334, ZNF418, ZNF488, ZNF528, ZNF578, ZNF662, ZNF667, ZNF677, ZNF764, ZSCAN31		
--	--	--

## References

- Aaku-Saraste, E., Hellwig, A., and Huttner, W.B. (1996). Loss of occludin and functional tight junctions, but not ZO-1, during neural tube closure--remodeling of the neuroepithelium prior to neurogenesis. *Dev. Biol.* *180*, 664–679.
- Alachkar, A., Jiang, D., Harrison, M., Zhou, Y., Chen, G., and Mao, Y. (2013). An EJC factor RBM8a Regulates Anxiety Behaviors. *Curr Mol Med* *13*, 887–899.
- Albers, C.A., Paul, D.S., Schulze, H., Freson, K., Stephens, J.C., Smethurst, P.A., Jolley, J.D., Cvejic, A., Kostadima, M., Bertone, P., et al. (2012). Compound inheritance of a low-frequency regulatory SNP and a rare null mutation in exon-junction complex subunit RBM8A causes TAR syndrome. *Nat. Genet.* *44*, 435–439, S1-2.
- Alderton, G.K., Galbiati, L., Griffith, E., Surinya, K.H., Neitzel, H., Jackson, A.P., Jeggo, P.A., and O’Driscoll, M. (2006). Regulation of mitotic entry by microcephalin and its overlap with ATR signalling. *Nat. Cell Biol.* *8*, 725–733.
- Anderson, S.A., Marin, O., Horn, C., Jennings, K., and Rubenstein, J.L. (2001). Distinct cortical migrations from the medial and lateral ganglionic eminences. *Dev. Camb. Engl.* *128*, 353–363.
- Barry, G., Briggs, J.A., Vanichkina, D.P., Poth, E.M., Beveridge, N.J., Ratnu, V.S., Nayler, S.P., Nones, K., Hu, J., Bredy, T.W., et al. (2014). The long non-coding RNA Gomafu is acutely regulated in response to neuronal activation and involved in schizophrenia-associated alternative splicing. *Mol. Psychiatry* *19*, 486–494.
- Behm-Ansmant, I., and Izaurralde, E. (2006). Quality control of gene expression: a stepwise assembly pathway for the surveillance complex that triggers nonsense-mediated mRNA decay. *Genes Dev* *20*, 391–398.
- Bernier, R., Steinman, K.J., Reilly, B., Wallace, A.S., Sherr, E.H., Pojman, N., Mefford, H.C., Gerdts, J., Earl, R., Hanson, E., et al. (2015). Clinical phenotype of the recurrent 1q21.1 copy-number variant. *Genet Med*.
- Bhuvanagiri, M., Schlitter, A.M., Hentze, M.W., and Kulozik, A.E. (Aug 27). NMD: RNA biology meets human genetic medicine. *Biochem J* *430*, 365–377.
- Brinkley, B.R. (2001). Managing the centrosome numbers game: from chaos to stability in cancer cell division. *Trends Cell Biol.* *11*, 18–21.
- Brogna, S., and Wen, J. (2009). Nonsense-mediated mRNA decay (NMD) mechanisms. *Nat Struct Mol Biol* *16*, 107–113.
- Brunetti-Pierri, N., Berg, J.S., Scaglia, F., Belmont, J., Bacino, C.A., Sahoo, T., Lalani, S.R., Graham, B., Lee, B., Shinawi, M., et al. (2008). Recurrent reciprocal 1q21.1 deletions and duplications associated with microcephaly or macrocephaly and developmental and behavioral abnormalities. *Nat Genet* *40*, 1466–1471.

Butt, S.J., Sousa, V.H., Fuccillo, M.V., Hjerling-Leffler, J., Miyoshi, G., Kimura, S., and Fishell, G. (2008). The requirement of Nkx2-1 in the temporal specification of cortical interneuron subtypes. *Neuron* 59, 722–732.

Campbell, K., and Gotz, M. (2002). Radial glia: multi-purpose cells for vertebrate brain development. *Trends Neurosci.* 25, 235–238.

Carroll, P.E., Okuda, M., Horn, H.F., Biddinger, P., Stambrook, P.J., Gleich, L.L., Li, Y.Q., Tarapore, P., and Fukasawa, K. (1999). Centrosome hyperamplification in human cancer: chromosome instability induced by p53 mutation and/or Mdm2 overexpression. *Oncogene* 18, 1935–1944.

Chang, Y.F., Imam, J.S., and Wilkinson, M.F. (2007). The nonsense-mediated decay RNA surveillance pathway. *Annu Rev Biochem* 76, 51–74.

Chenn, A., Zhang, Y.A., Chang, B.T., and McConnell, S.K. (1998). Intrinsic polarity of mammalian neuroepithelial cells. *Mol. Cell. Neurosci.* 11, 183–193.

Chih, B., Gollan, L., and Scheiffele, P. (2006). Alternative splicing controls selective trans-synaptic interactions of the neuroligin-neurexin complex. *Neuron* 51, 171–178.

Crowley, N.A., Bloodgood, D.W., Hardaway, J.A., Kendra, A.M., McCall, J.G., Al-Hasani, R., McCall, N.M., Yu, W., Schools, Z.L., Krashes, M.J., et al. (2016). Dynorphin Controls the Gain of an Amygdalar Anxiety Circuit. *Cell Rep.* 14, 2774–2783.

D’Arcangelo, G. (2005). The reeler mouse: anatomy of a mutant. *Int. Rev. Neurobiol.* 71, 383–417.

Darvish, H., Esmaeeli-Nieh, S., Monajemi, G.B., Mohseni, M., Ghasemi-Firouzabadi, S., Abedini, S.S., Bahman, I., Jamali, P., Azimi, S., Mojahedi, F., et al. (2010). A clinical and molecular genetic study of 112 Iranian families with primary microcephaly. *J. Med. Genet.* 47, 823–828.

DeDiego, I., Smith-Fernandez, A., and Fairen, A. (1994). Cortical cells that migrate beyond area boundaries: characterization of an early neuronal population in the lower intermediate zone of prenatal rats. *Eur. J. Neurosci.* 6, 983–997.

DeFelipe, J., Lopez-Cruz, P.L., Benavides-Piccione, R., Bielza, C., Larranaga, P., Anderson, S., Burkhalter, A., Cauli, B., Fairen, A., Feldmeyer, D., et al. (2013). New insights into the classification and nomenclature of cortical GABAergic interneurons. *Nat Rev Neurosci* 14, 202–216.

Dolcetti, A., Silversides, C.K., Marshall, C.R., Lionel, A.C., Stavropoulos, D.J., Scherer, S.W., and Bassett, A.S. (2013). 1q21.1 Microduplication expression in adults. *Genet Med* 15, 282–289.

Euteneuer, U., and McIntosh, J.R. (1981). Structural polarity of kinetochore microtubules in PtK1 cells. *J. Cell Biol.* 89, 338–345.

- Evans, T., Rosenthal, E.T., Youngblom, J., Distel, D., and Hunt, T. (1983). Cyclin: a protein specified by maternal mRNA in sea urchin eggs that is destroyed at each cleavage division. *Cell* 33, 389–396.
- Fatemi, S.H., Emamian, E.S., Kist, D., Sidwell, R.W., Nakajima, K., Akhter, P., Shier, A., Sheikh, S., and Bailey, K. (1999). Defective corticogenesis and reduction in Reelin immunoreactivity in cortex and hippocampus of prenatally infected neonatal mice. *Mol. Psychiatry* 4, 145–154.
- Garshasbi, M., Motazacker, M.M., Kahrizi, K., Behjati, F., Abedini, S.S., Nieh, S.E., Firouzabadi, S.G., Becker, C., Ruschendorf, F., Nurnberg, P., et al. (2006). SNP array-based homozygosity mapping reveals MCPH1 deletion in family with autosomal recessive mental retardation and mild microcephaly. *Hum. Genet.* 118, 708–715.
- Gehring, N.H., Neu-Yilik, G., Schell, T., Hentze, M.W., and Kulozik, A.E. (2003). Y14 and hUpf3b form an NMD-activating complex. *Mol Cell* 11, 939–949.
- Giansanti, M.G., Gatti, M., and Bonaccorsi, S. (2001). The role of centrosomes and astral microtubules during asymmetric division of *Drosophila* neuroblasts. *Dev. Camb. Engl.* 128, 1137–1145.
- Glisovic, T., Bachorik, J.L., Yong, J., and Dreyfuss, G. (2008). RNA-binding proteins and post-transcriptional gene regulation. *FEBS Lett.* 582, 1977–1986.
- Gonchar, Y., and Burkhalter, A. (1997). Three distinct families of GABAergic neurons in rat visual cortex. *Cereb. Cortex N. Y. N* 1991 7, 347–358.
- Gotz, M. (2003). Glial cells generate neurons--master control within CNS regions: developmental perspectives on neural stem cells. *Neurosci. Rev. J. Bringing Neurobiol. Neurol. Psychiatry* 9, 379–397.
- Gotz, M., and Huttner, W.B. (2005). The cell biology of neurogenesis. *Nat. Rev. Mol. Cell Biol.* 6, 777–788.
- Gray, G.E., Glover, J.C., Majors, J., and Sanes, J.R. (1988). Radial arrangement of clonally related cells in the chicken optic tectum: lineage analysis with a recombinant retrovirus. *Proc. Natl. Acad. Sci. U. S. A.* 85, 7356–7360.
- Green, R.E., Lewis, B.P., Hillman, R.T., Blanchette, M., Lareau, L.F., Garnett, A.T., Rio, D.C., and Brenner, S.E. (2003). Widespread predicted nonsense-mediated mRNA decay of alternatively-spliced transcripts of human normal and disease genes. *Bioinforma. Oxf. Engl.* 19 *Suppl 1*, i118-121.
- Greenhalgh, K.L., Howell, R.T., Bottani, A., Ancliff, P.J., Brunner, H.G., Verschuuren-Bemelmans, C.C., Vernon, E., Brown, K.W., and Newbury-Ecob, R.A. (2002). Thrombocytopenia-absent radius syndrome: a clinical genetic study. *J Med Genet* 39, 876–881.

- Groszer, M., Erickson, R., Scripture-Adams, D.D., Lesche, R., Trumpp, A., Zack, J.A., Kornblum, H.I., Liu, X., and Wu, H. (2001). Negative regulation of neural stem/progenitor cell proliferation by the Pten tumor suppressor gene in vivo. *Science* 294, 2186–2189.
- Grove, E.A., and Fukuchi-Shimogori, T. (2003). Generating the cerebral cortical area map. *Annu Rev Neurosci* 26, 355–380.
- Gruber, R., Zhou, Z., Sukchev, M., Joerss, T., Frappart, P.-O., and Wang, Z.-Q. (2011). MCPH1 regulates the neuroprogenitor division mode by coupling the centrosomal cycle with mitotic entry through the Chk1-Cdc25 pathway. *Nat. Cell Biol.* 13, 1325–1334.
- Hartfuss, E., Galli, R., Heins, N., and Gotz, M. (2001). Characterization of CNS precursor subtypes and radial glia. *Dev. Biol.* 229, 15–30.
- Haubensak, W., Attardo, A., Denk, W., and Huttner, W.B. (2004). Neurons arise in the basal neuroepithelium of the early mammalian telencephalon: a major site of neurogenesis. *Proc. Natl. Acad. Sci. U. S. A.* 101, 3196–3201.
- Hinchcliffe, E.H., and Sluder, G. (2001). “It takes two to tango”: understanding how centrosome duplication is regulated throughout the cell cycle. *Genes Dev.* 15, 1167–1181.
- Homans, A.C., Cohen, J.L., and Mazur, E.M. (1988). Defective megakaryocytopoiesis in the syndrome of thrombocytopenia with absent radii. *Br. J. Haematol.* 70, 205–210.
- Hornick, J.E., Mader, C.C., Tribble, E.K., Bagne, C.C., Vaughan, K.T., Shaw, S.L., and Hinchcliffe, E.H. (2011). Amphiatral mitotic spindle assembly in vertebrate cells lacking centrosomes. *Curr. Biol. CB* 21, 598–605.
- Hosoda, N. (2006). [Features of NMD (nonsense-mediated mRNA decay) in mammalian cells]. *Tanpakushitsu Kakusan Koso* 51, 2544–2548.
- Huang, D.W., Sherman, B.T., and Lempicki, R.A. (2009). Bioinformatics enrichment tools: paths toward the comprehensive functional analysis of large gene lists. *Nucleic Acids Res.* 37, 1–13.
- Huang da, W., Sherman, B.T., and Lempicki, R.A. (2009). Systematic and integrative analysis of large gene lists using DAVID bioinformatics resources. *Nat Protoc* 4, 44–57.
- Huttner, W.B., and Brand, M. (1997). Asymmetric division and polarity of neuroepithelial cells. *Curr. Opin. Neurobiol.* 7, 29–39.
- Inan, M., and Anderson, S.A. (2014). The chandelier cell, form and function. *Curr. Opin. Neurobiol.* 26, 142–148.
- Iossifov, I., Ronemus, M., Levy, D., Wang, Z., Hakker, I., Rosenbaum, J., Yamrom, B., Lee, Y.H., Narzisi, G., Leotta, A., et al. (2012). De novo gene disruptions in children on the autistic spectrum. *Neuron* 74, 285–299.

Isken, O., and Maquat, L.E. (2007). Quality control of eukaryotic mRNA: safeguarding cells from abnormal mRNA function. *Genes Dev* 21, 1833–1856.

Isken, O., and Maquat, L.E. (2008). The multiple lives of NMD factors: balancing roles in gene and genome regulation. *Nat Rev Genet* 9, 699–712.

Isken, O., Kim, Y.K., Hosoda, N., Mayeur, G.L., Hershey, J.W., and Maquat, L.E. (2008). Upf1 phosphorylation triggers translational repression during nonsense-mediated mRNA decay. *Cell* 133, 314–327.

Jackson, A.P., Eastwood, H., Bell, S.M., Adu, J., Toomes, C., Carr, I.M., Roberts, E., Hampshire, D.J., Crow, Y.J., Mighell, A.J., et al. (2002). Identification of microcephalin, a protein implicated in determining the size of the human brain. *Am. J. Hum. Genet.* 71, 136–142.

Kaltschmidt, J.A., Davidson, C.M., Brown, N.H., and Brand, A.H. (2000). Rotation and asymmetry of the mitotic spindle direct asymmetric cell division in the developing central nervous system. *Nat. Cell Biol.* 2, 7–12.

Kashima, I., Yamashita, A., Izumi, N., Kataoka, N., Morishita, R., Hoshino, S., Ohno, M., Dreyfuss, G., and Ohno, S. (2006). Binding of a novel SMG-1-Upf1-eRF1-eRF3 complex (SURF) to the exon junction complex triggers Upf1 phosphorylation and nonsense-mediated mRNA decay. *Genes Dev* 20, 355–367.

Kawaguchi, Y., and Kubota, Y. (1997). GABAergic cell subtypes and their synaptic connections in rat frontal cortex. *Cereb. Cortex N. Y. N* 1991 7, 476–486.

Kervestin, S., and Jacobson, A. (2012). NMD: a multifaceted response to premature translational termination. *Nat. Rev. Mol. Cell Biol.* 13, 700–712.

Konno, D., Shioi, G., Shitamukai, A., Mori, A., Kiyonari, H., Miyata, T., and Matsuzaki, F. (2008). Neuroepithelial progenitors undergo LGN-dependent planar divisions to maintain self-renewability during mammalian neurogenesis. *Nat. Cell Biol.* 10, 93–101.

Kornack, D.R., and Rakic, P. (1995). Radial and horizontal deployment of clonally related cells in the primate neocortex: relationship to distinct mitotic lineages. *Neuron* 15, 311–321.

Kriegstein, A.R., and Gotz, M. (2003). Radial glia diversity: a matter of cell fate. *Glia* 43, 37–43.

Lee, G.H., and D’Arcangelo, G. (2016). New Insights into Reelin-Mediated Signaling Pathways. *Front. Cell. Neurosci.* 10, 122.

Lejeune, F., and Maquat, L.E. (2005). Mechanistic links between nonsense-mediated mRNA decay and pre-mRNA splicing in mammalian cells. *Curr Opin Cell Biol* 17, 309–315.

Li, H., Handsaker, B., Wysoker, A., Fennell, T., Ruan, J., Homer, N., Marth, G., Abecasis, G., and Durbin, R. (2009). The Sequence Alignment/Map format and SAMtools. *Bioinformatics* 25, 2078–2079.

- Lingle, W.L., Lutz, W.H., Ingle, J.N., Maible, N.J., and Salisbury, J.L. (1998). Centrosome hypertrophy in human breast tumors: implications for genomic stability and cell polarity. *Proc. Natl. Acad. Sci. U. S. A.* *95*, 2950–2955.
- Lizarraga, S.B., Margossian, S.P., Harris, M.H., Campagna, D.R., Han, A.-P., Blevins, S., Mudbhary, R., Barker, J.E., Walsh, C.A., and Fleming, M.D. (2010). Cdk5rap2 regulates centrosome function and chromosome segregation in neuronal progenitors. *Dev. Camb. Engl.* *137*, 1907–1917.
- Longo, P.A., Kavran, J.M., Kim, M.S., and Leahy, D.J. (2013). Transient mammalian cell transfection with polyethylenimine (PEI). *Methods Enzym.* *529*, 227–240.
- Lou, C.H., Shao, A., Shum, E.Y., Espinoza, J.L., Huang, L., Karam, R., and Wilkinson, M.F. (2014). Posttranscriptional control of the stem cell and neurogenic programs by the nonsense-mediated RNA decay pathway. *Cell Rep* *6*, 748–764.
- Luskin, M.B., Pearlman, A.L., and Sanes, J.R. (1988). Cell lineage in the cerebral cortex of the mouse studied in vivo and in vitro with a recombinant retrovirus. *Neuron* *1*, 635–647.
- Maiato, H., and Logarinho, E. (2014). Mitotic spindle multipolarity without centrosome amplification. *Nat. Cell Biol.* *16*, 386–394.
- Mao, Y., and Lee, A.W. (2005). A novel role for Gab2 in bFGF-mediated cell survival during retinoic acid-induced neuronal differentiation. *J Cell Biol* *170*, 305–316.
- Mao, H., Pilaz, L.J., McMahon, J.J., Golzio, C., Wu, D., Shi, L., Katsanis, N., and Silver, D.L. (2015). Rbm8a haploinsufficiency disrupts embryonic cortical development resulting in microcephaly. *J Neurosci* *35*, 7003–7018.
- Mao, H., McMahon, J.J., Tsai, Y.-H., Wang, Z., and Silver, D.L. (2016). Haploinsufficiency for Core Exon Junction Complex Components Disrupts Embryonic Neurogenesis and Causes p53-Mediated Microcephaly. *PLoS Genet.* *12*, e1006282.
- Mao, H., Brown, H.E., and Silver, D.L. (2017). Mouse models of Casc3 reveal developmental functions distinct from other components of the exon junction complex. *RNA N. Y.* *N 23*, 23–31.
- Mao, Y., Ge, X., Frank, C.L., Madison, J.M., Koehler, A.N., Doud, M.K., Tassa, C., Berry, E.M., Soda, T., Singh, K.K., et al. (2009). Disrupted in schizophrenia 1 regulates neuronal progenitor proliferation via modulation of GSK3beta/beta-catenin signaling. *Cell* *136*, 1017–1031.
- Marin, O., and Rubenstein, J.L. (2001). A long, remarkable journey: tangential migration in the telencephalon. *Nat. Rev. Neurosci.* *2*, 780–790.
- Matsunaga, Y., Noda, M., Murakawa, H., Hayashi, K., Nagasaka, A., Inoue, S., Miyata, T., Miura, T., Kubo, K.-I., and Nakajima, K. (2017). Reelin transiently promotes N-cadherin-dependent neuronal adhesion during mouse cortical development. *Proc. Natl. Acad. Sci. U. S. A.* *114*, 2048–2053.

- Mazia, D. (1987). The chromosome cycle and the centrosome cycle in the mitotic cycle. *Int. Rev. Cytol.* 100, 49–92.
- McConnell, S.K. (1995). Constructing the cerebral cortex: neurogenesis and fate determination. *Neuron* 15, 761–768.
- McGlinchy, N.J., and Smith, C.W. (2008). Alternative splicing resulting in nonsense-mediated mRNA decay: what is the meaning of nonsense? *Trends Biochem Sci* 33, 385–393.
- McMahon, J.J., Shi, L., and Silver, D.L. (2014). Generation of a Magoh conditional allele in mice. *Genesis* 52, 752–758.
- McSweeney, C., and Mao, Y. (2015). Applying stereotactic injection technique to study genetic effects on animal behaviors. *J Vis Exp*.
- Mefford, H.C., Sharp, A.J., Baker, C., Itsara, A., Jiang, Z., Buysse, K., Huang, S., Maloney, V.K., Crolla, J.A., Baralle, D., et al. (2008). Recurrent rearrangements of chromosome 1q21.1 and variable pediatric phenotypes. *N Engl J Med* 359, 1685–1699.
- Menghsol, S.C., Harris, R.D., and Ornvold, K. (2003). Thrombocytopenia and absent radii, TAR syndrome: report of cerebellar dysgenesis and newly identified cardiac and renal anomalies. *Am J Med Genet A* 123A, 193–196.
- Meyer, A.H., Katona, I., Blatow, M., Rozov, A., and Monyer, H. (2002). In vivo labeling of parvalbumin-positive interneurons and analysis of electrical coupling in identified neurons. *J. Neurosci. Off. J. Soc. Neurosci.* 22, 7055–7064.
- Michelle, L., Cloutier, A., Toutant, J., Shkreta, L., Thibault, P., Durand, M., Garneau, D., Gendron, D., Lapointe, E., Couture, S., et al. (2012). Proteins associated with the exon junction complex also control the alternative splicing of apoptotic regulators. *Mol Cell Biol* 32, 954–967.
- Mione, M.C., Cavanagh, J.F., Harris, B., and Parnavelas, J.G. (1997). Cell fate specification and symmetrical/asymmetrical divisions in the developing cerebral cortex. *J. Neurosci. Off. J. Soc. Neurosci.* 17, 2018–2029.
- Miyata, T., Kawaguchi, A., Okano, H., and Ogawa, M. (2001). Asymmetric inheritance of radial glial fibers by cortical neurons. *Neuron* 31, 727–741.
- Miyata, T., Kawaguchi, A., Saito, K., Kawano, M., Muto, T., and Ogawa, M. (2004). Asymmetric production of surface-dividing and non-surface-dividing cortical progenitor cells. *Dev. Camb. Engl.* 131, 3133–3145.
- Monyer, H., and Markram, H. (2004). Interneuron Diversity series: Molecular and genetic tools to study GABAergic interneuron diversity and function. *Trends Neurosci.* 27, 90–97.
- Morgan, D.O. (1995). Principles of CDK regulation. *Nature* 374, 131–134.

- Morin, X., and Bellaïche, Y. (2011). Mitotic spindle orientation in asymmetric and symmetric cell divisions during animal development. *Dev. Cell* *21*, 102–119.
- Morrison, S.J., and Kimble, J. (2006). Asymmetric and symmetric stem-cell divisions in development and cancer. *Nature* *441*, 1068–1074.
- Myers, J.P., Santiago-Medina, M., and Gomez, T.M. (2011). Regulation of axonal outgrowth and pathfinding by integrin-ECM interactions. *Dev Neurobiol* *71*, 901–923.
- Nadarajah, B., and Parnavelas, J.G. (2002). Modes of neuronal migration in the developing cerebral cortex. *Nat. Rev. Neurosci.* *3*, 423–432.
- Nagy, E., and Maquat, L.E. (1998). A rule for termination-codon position within intron-containing genes: when nonsense affects RNA abundance. *Trends Biochem. Sci.* *23*, 198–199.
- Nakata, K., Lipska, B.K., Hyde, T.M., Ye, T., Newburn, E.N., Morita, Y., Vakkalanka, R., Barenboim, M., Sei, Y., Weinberger, D.R., et al. DISC1 splice variants are upregulated in schizophrenia and associated with risk polymorphisms. *Proc Natl Acad Sci U A* *106*, 15873–15878.
- Neitzel, H., Neumann, L.M., Schindler, D., Wirges, A., Tonnies, H., Trimborn, M., Krebsova, A., Richter, R., and Sperling, K. (2002). Premature chromosome condensation in humans associated with microcephaly and mental retardation: a novel autosomal recessive condition. *Am. J. Hum. Genet.* *70*, 1015–1022.
- Nery, S., Fishell, G., and Corbin, J.G. (2002). The caudal ganglionic eminence is a source of distinct cortical and subcortical cell populations. *Nat. Neurosci.* *5*, 1279–1287.
- Nery, S., Corbin, J.G., and Fishell, G. (2003). Dlx2 progenitor migration in wild type and Nkx2.1 mutant telencephalon. *Cereb. Cortex N. Y. N* *13*, 895–903.
- Ni, J.Z., Grate, L., Donohue, J.P., Preston, C., Nobida, N., O'Brien, G., Shiue, L., Clark, T.A., Blume, J.E., and Ares, M. (2007). Ultraconserved elements are associated with homeostatic control of splicing regulators by alternative splicing and nonsense-mediated decay. *Genes Dev* *21*, 708–718.
- Noctor, S.C., Martinez-Cerdeno, V., and Kriegstein, A.R. (2008). Distinct behaviors of neural stem and progenitor cells underlie cortical neurogenesis. *J Comp Neurol* *508*, 28–44.
- Norbury, C., and Nurse, P. (1992). Animal cell cycles and their control. *Annu. Rev. Biochem.* *61*, 441–470.
- Nott, A., Le Hir, H., and Moore, M.J. (2004). Splicing enhances translation in mammalian cells: an additional function of the exon junction complex. *Genes Dev* *18*, 210–222.
- Ohnishi, T., Yamashita, A., Kashima, I., Schell, T., Anders, K.R., Grimson, A., Hachiya, T., Hentze, M.W., Anderson, P., and Ohno, S. (2003). Phosphorylation of hUPF1 induces formation of mRNA surveillance complexes containing hSMG-5 and hSMG-7. *Mol Cell* *12*, 1187–1200.

- Orr-Weaver, T.L., and Weinberg, R.A. (1998). A checkpoint on the road to cancer. *Nature* 392, 223–224.
- Paridaen, J.T.M.L., and Huttner, W.B. (2014). Neurogenesis during development of the vertebrate central nervous system. *EMBO Rep.* 15, 351–364.
- Peccarelli, M., and Kebaara, B.W. (2014). Regulation of natural mRNAs by the nonsense-mediated mRNA decay pathway. *Eukaryot. Cell* 13, 1126–1135.
- Pihan, G.A., Purohit, A., Wallace, J., Knecht, H., Woda, B., Quesenberry, P., and Doxsey, S.J. (1998). Centrosome defects and genetic instability in malignant tumors. *Cancer Res.* 58, 3974–3985.
- Pilaz, L.-J., McMahon, J.J., Miller, E.E., Lennox, A.L., Suzuki, A., Salmon, E., and Silver, D.L. (2016). Prolonged Mitosis of Neural Progenitors Alters Cell Fate in the Developing Brain. *Neuron* 89, 83–99.
- Pines, J. (1991). Cyclins: wheels within wheels. *Cell Growth Differ. Mol. Biol. J. Am. Assoc. Cancer Res.* 2, 305–310.
- Pines, J. (1995). Cyclins, CDKs and cancer. *Semin. Cancer Biol.* 6, 63–72.
- Pleil, K.E., Lowery-Gionta, E.G., Crowley, N.A., Li, C., Marcinkiewicz, C.A., Rose, J.H., McCall, N.M., Maldonado-Devincci, A.M., Morrow, A.L., Jones, S.R., et al. (2015). Effects of chronic ethanol exposure on neuronal function in the prefrontal cortex and extended amygdala. *Neuropharmacology* 99, 735–749.
- Price, J., and Thurlow, L. (1988). Cell lineage in the rat cerebral cortex: a study using retroviral-mediated gene transfer. *Dev. Camb. Engl.* 104, 473–482.
- Quinlan, A.R., and Hall, I.M. (2010). BEDTools: a flexible suite of utilities for comparing genomic features. *Bioinformatics* 26, 841–842.
- Rakic, P. (2007). The radial edifice of cortical architecture: from neuronal silhouettes to genetic engineering. *Brain Res Rev* 55, 204–219.
- Reid, C.B., Tavazoie, S.F., and Walsh, C.A. (1997). Clonal dispersion and evidence for asymmetric cell division in ferret cortex. *Dev. Camb. Engl.* 124, 2441–2450.
- Rodriguez, C.I., Buchholz, F., Galloway, J., Sequerra, R., Kasper, J., Ayala, R., Stewart, A.F., and Dymecki, S.M. (2000). High-efficiency deleter mice show that FLP<sub>e</sub> is an alternative to Cre-loxP. *Nat. Genet.* 25, 139–140.
- Rudy, B., Fishell, G., Lee, S., and Hjerling-Leffler, J. (2011). Three groups of interneurons account for nearly 100% of neocortical GABAergic neurons. *Dev. Neurobiol.* 71, 45–61.

- Shen, M., Yoshida, E., Yan, W., Kawamoto, T., Suardita, K., Koyano, Y., Fujimoto, K., Noshiro, M., and Kato, Y. (2002). Basic helix-loop-helix protein DEC1 promotes chondrocyte differentiation at the early and terminal stages. *J Biol Chem* *277*, 50112–50120.
- Shoji, H., Takao, K., Hattori, S., and Miyakawa, T. (2014). Contextual and cued fear conditioning test using a video analyzing system in mice. *J Vis Exp*.
- Silver, D.L., Watkins-Chow, D.E., Schreck, K.C., Pierfelice, T.J., Larson, D.M., Burnett, A.J., Liaw, H.J., Myung, K., Walsh, C.A., Gaiano, N., et al. (2010). The exon junction complex component Magoh controls brain size by regulating neural stem cell division. *Nat Neurosci* *13*, 551–558.
- Skorka, A., Bielicka-Cymermann, J., Gieruszczak-Bialek, D., and Korniszewski, L. (2005). Thrombocytopenia-absent radius (tar) syndrome: a case with agenesis of corpus callosum, hypoplasia of cerebellar vermis and horseshoe kidney. *Genet Couns* *16*, 377–382.
- Soriano, P. (1997). The PDGF alpha receptor is required for neural crest cell development and for normal patterning of the somites. *Development* *124*, 2691–2700.
- Sun, T., and Hevner, R.F. (2014). Growth and folding of the mammalian cerebral cortex: from molecules to malformations. *Nat. Rev. Neurosci.* *15*, 217–232.
- Sun, C., Cheng, M.C., Qin, R., Liao, D.L., Chen, T.T., Koong, F.J., Chen, G., and Chen, C.H. (2011). Identification and functional characterization of rare mutations of the neuroligin-2 gene (NLGN2) associated with schizophrenia. *Hum Mol Genet* *20*, 3042–3051.
- Tange, T.O., Shibuya, T., Jurica, M.S., and Moore, M.J. (2005). Biochemical analysis of the EJC reveals two new factors and a stable tetrameric protein core. *RNA* *11*, 1869–1883.
- Tassano, E., Gimelli, S., Divizia, M.T., Lerone, M., Vaccari, C., Puliti, A., and Gimelli, G. (2015). Thrombocytopenia-absent radius (TAR) syndrome due to compound inheritance for a 1q21.1 microdeletion and a low-frequency noncoding RBM8A SNP: a new familial case. *Mol. Cytogenet.* *8*, 87.
- Taverna, E., Gotz, M., and Huttner, W.B. (2014). The cell biology of neurogenesis: toward an understanding of the development and evolution of the neocortex. *Annu. Rev. Cell Dev. Biol.* *30*, 465–502.
- Trapnell, C., Pachter, L., and Salzberg, S.L. (2009). TopHat: discovering splice junctions with RNA-Seq. *Bioinformatics* *25*, 1105–1111.
- Trapnell, C., Roberts, A., Goff, L., Pertea, G., Kim, D., Kelley, D.R., Pimentel, H., Salzberg, S.L., Rinn, J.L., and Pachter, L. (2012). Differential gene and transcript expression analysis of RNA-seq experiments with TopHat and Cufflinks. *Nat Protoc* *7*, 562–578.
- Tremblay, R., Lee, S., and Rudy, B. (2016). GABAergic Interneurons in the Neocortex: From Cellular Properties to Circuits. *Neuron* *91*, 260–292.

Valcanis, H., and Tan, S.-S. (2003). Layer specification of transplanted interneurons in developing mouse neocortex. *J. Neurosci. Off. J. Soc. Neurosci.* 23, 5113–5122.

Vermeulen, K., Van Bockstaele, D.R., and Berneman, Z.N. (2003). The cell cycle: a review of regulation, deregulation and therapeutic targets in cancer. *Cell Prolif.* 36, 131–149.

Weischenfeldt, J., Damgaard, I., Bryder, D., Theilgaard-Monch, K., Thoren, L.A., Nielsen, F.C., Jacobsen, S.E., Nerlov, C., and Porse, B.T. (2008). NMD is essential for hematopoietic stem and progenitor cells and for eliminating by-products of programmed DNA rearrangements. *Genes Dev* 22, 1381–1396.

Wichterle, H., Turnbull, D.H., Nery, S., Fishell, G., and Alvarez-Buylla, A. (2001). In utero fate mapping reveals distinct migratory pathways and fates of neurons born in the mammalian basal forebrain. *Dev. Camb. Engl.* 128, 3759–3771.

Wittmann, J., Hol, E.M., and Jack, H.M. (2006). hUPF2 silencing identifies physiologic substrates of mammalian nonsense-mediated mRNA decay. *Mol Cell Biol* 26, 1272–1287.

Wodarz, A., and Huttner, W.B. (2003). Asymmetric cell division during neurogenesis in *Drosophila* and vertebrates. *Mech. Dev.* 120, 1297–1309.

Wonders, C.P., and Anderson, S.A. (2006). The origin and specification of cortical interneurons. *Nat Rev Neurosci* 7, 687–696.

Yamashita, Y.M., Mahowald, A.P., Perlin, J.R., and Fuller, M.T. (2007). Asymmetric inheritance of mother versus daughter centrosome in stem cell division. *Science* 315, 518–521.

Zou, D., McSweeney, C., Sebastian, A., Reynolds, D.J., Dong, F., Zhou, Y., Deng, D., Wang, Y., Liu, L., Zhu, J., et al. (2015). A critical role of RBM8a in proliferation and differentiation of embryonic neural progenitors. *Neural Dev* 10, 18.

Zou, D., Chen, L., Deng, D., Jiang, D., Dong, F., McSweeney, C., Zhou, Y., Liu, L., Chen, G., Wu, Y., et al. (2016). DREADD in parvalbumin interneurons of the dentate gyrus modulates anxiety, social interaction and memory extinction. *Curr Mol Med* 16, 91–102.

**Curriculum Vita**  
Colleen Patricia McSweeney

**Education**

PhD	Candidate	8/2012-present	Penn State University, State College, PA
	Neuroscience		
B.S.	Psychology	8/2008-5/2012	Susquehanna University, Selinsgrove, PA

**Honors and awards**

2017-Gordon Conference-Inhibition in the CNS travel award  
2016-Received Penn State grant for undergraduate research, co-wrote with Jessica Vitale  
2016-2017--Graduate Adviser to the Huck Institute of the Life Sciences  
2016--J. Ben and Helen D. Hill Memorial Fund Award  
2012--Recipient of Penn State Eberly School of Science Homer F. Braddock Fellowship

**Publications**

1. **McSweeney, C.**, Deng, D., Jian, C., Zou, D., Shi, X., Vitale, J., Liu, L., & Mao, Y. An exon junction complex factor, RBM8a, is required for normal interneuron development. *Under review at Stem Cell Reports*
2. Deng, D., Lei, L., Jian, C., Zhou, Y., **McSweeney, C.**, Dong, F., Zhang, L., & Mao, Y. A short-term interruption of DISC1 function at the embryonic stage exhibits a long-term impact on adult behaviors and brain metabolism. *Oncotarget. Accepted*
3. Dong, F<sup>#</sup>, Jiang, J<sup>#</sup>, **McSweeney, C.**, Zou, D., Liu, L., Mao, Y. (2016). CTNNB1 deficiency in parvalbumin interneurons causes anxiety and social deficits, but enhances spatial learning memory. *Human Molecular Genetics*, PMID:27131348
4. Zou, D., Chen, L., Deng, D., Jiang, D., Dong, F., **McSweeney, C.**, Zhou, Y., Liu, L., Chen, G., Wu, Y., Mao, Y. (2016). DREADD in parvalbumin interneurons of the dentate gyrus modulates anxiety, social interaction and memory extinction. *Current Molecular Medicine*, 16(1), 91-102. PMID: 26733123.
5. Timbo W. Sriram, A., Reynolds, E.K., DeBoard-Lucas, R., Specht, M., Howell, C., **McSweeney, C.**, Grados, M.A. (2016). Risk Factors for Seclusion and Restraint in a Pediatric Psychiatry Day Hospital. *Child Psychiatry and Human Development*, doi:10.1007/s10578-015-0608-1, PMID: 26643416
6. Gilman, C., **McSweeney, C.**, and Mao, Y. (2014). The Applications of Pharmacogenomics to Neurological Disorders. *Current Molecular Medicine*, 14(7), 880-890. PMID:2510979
7. Zou, D<sup>#</sup>, **McSweeney, C<sup>#</sup>**, Sebastian, A., Dong, F., Zhou, Y., Deng, D., Wang, Y., Liu, L., Albert, I., Girirajan, S., & Mao, Y. (2015). A critical role of RBM8a in proliferation and differentiation of embryonic neural progenitors. *Neural Development*, 10:18. doi: 10.1186/s13064-015-0045-7. PubMed PMID: 26094033; PMCID: PMC4479087. (#, co-first author)
8. **McSweeney, C.** & Mao, Y (2015). Applying stereotactic injection technique to study genetic effects on animal behaviors. *Journal of Visualized Experiments*. (99): e52653, doi:3791/52653. PMID: 2599